Performance Improvement of Dense Dielectric Patch Antenna using Partially Reflective Surfaces

Muftah Mohamed Asaadi

A Thesis

in

The Department

of

Electrical and Computer Engineering

Presented in Partial Fulfilment of the Requirements

For the Degree of

Doctor of Philosophy (Electrical and Computer Engineering) at

Concordia University

Montréal, Québec, Canada

February 2019

CONCORDIA UNIVERSITY
SCHOOL OF GRADUATE STUDIES

This is to certify that the thesis prepared

By: Muftah Mohamed Asaadi

Entitled: Performance Improvement of Dense Dielectric Patch Antenna Using
            Partially Reflective Surfaces

and submitted in partial fulfilment of the requirements for the degree of

Doctor of Philosophy (Electrical and Computer Engineering)

Complies with the regulations of the University and meets the accepted standards with respect to originality and quality.

Signed by the final examining committee:

_____ Chair

Dr. Radu Grigore Zmeureanu

_____ External Examiner

Dr. Carlos Saavedra

_____ External to Program

Dr. A. Ben Hamza

_____ Examiner

Dr. A. Kishk

_____ Examiner

Dr. R. Paknys

_____ Thesis Supervisor

Dr. A. Sebak

Approved by: _____

Dr. Mustafa K, Mehmet Ali, Graduate Program Director

Tuesday, April 9, 2019 _____

Dr. Amir Asif, Dean

Gina Cody School of Engineering and Computer Science

ABSTRACT

Performance Improvement of Dense Dielectric Patch Antenna using Partially Reflective Surfaces

Muftah Mohamed Asaadi, Ph.D.

Concordia University, 2019

Recently, millimeter-wave (MMW) band is being considered as the spectrum for future wireless communication systems. Several advantages are achieved by utilizing the millimeter-wave range, including high gain with large available bandwidth, compact size, and high security. Nevertheless, attenuation loss may restrict wireless communication systems' transmission range. Meanwhile, printed antenna technology has gained the attention of antenna designers' due to its low profile and ease of fabrication. High-gain antennas are very desirable as a critical part of MMW systems. Designing millimeter wave antennas with high gain characteristics would be a significant advantage due to their high sensitivity to atmospheric absorption losses. Moreover, planar configurations are required in many applications, such as for wireless communication.

The main goal of this thesis is to design and propose state of the art designs of Fabry Pérot Cavity antenna (FPCA) designs with several types of superstrates to achieve high gain, wide bandwidth, and high efficiency to satisfy the requirements of today's advanced wireless communication systems. A dense dielectric patch (DD) antenna is used as the main radiator and designed to operate at 28 GHz. The thesis presents several contributions related to the design and analysis of FPC antennas using several types of superstrates.

The first research theme of this thesis has two parts. The first part presents a holey dielectric superstrate applied over a 2×2 dense dielectric square patch antenna array to enhance the gain, improve the bandwidth and efficiency, as well as to reduce the side lobe levels (SLLs). A dense dielectric patch replaces the metallic patch and is used as a radiated element. The measured results show a high gain of 16 dBi, with radiation efficiency of about 93 %, wide bandwidth of 15.3 %, and a reduced SLL. The second part focusses on a partially reflective surface (PRS) unit cell

composed of two thin perforated dielectric slabs. The effect of the thicknesses of the unit cell dielectric slabs is discussed in detail. An array of the proposed PRS unit cell is applied over a dense dielectric square patch antenna array to broaden the bandwidth and to enhance the gain as well. The measured results exhibit a 3 dB gain bandwidth of 27 % with a high gain of 16.8 dBi.

The second research theme presents an effective method to design a tapered superstrate of an FPC antenna with a DD patch element. This type of superstrate is designed to correct the phase above the superstrate to be almost uniform. The proposed single-layer perforated tapered superstrate is constructed by tapering the relative permittivity to be high in the center of the superstrate slab and then decrease gradually as it moves towards the edges. This tapered relative permittivity is then applied over a single DD patch antenna. The proposed antenna exhibits good performance in terms of the antenna gain and bandwidth. The antenna gain becomes flat and as high as 17.6 dBi. The antenna bandwidth is about 16 %, and the side lobe level of the antenna is very promising.

A third theme presents the implementation and design of a high gain dense dielectric patch antenna integrated with a frequency-selective surface (FSS) superstrate. A 7×7-unit cell is used to build the superstrate layer, and applied above the high DD patch antenna. A modified unit cell is proposed to generate a positive reflection phase with high reflection magnitude within the frequency design in order to broaden the antenna bandwidth. A bandwidth of 15.3 % with a high gain of 16 dBi is obtained.

Finally, a high gain linearly polarized (LP) substrate integrated waveguide (SIW) cavity antenna based on a high-order mode is implemented, fabricated, and tested. A TE440 mode is excited at 28 GHz. In this design, 4×4 slots are cut into the top metal of the cavity, where each slot is placed above each standing wave peak. These slot cuts contributed to a high gain of 16.4 dBi and radiation efficiency of about 96 %. The LP SIW cavity antenna was then integrated with a linear-to-circular polarization converter developed as a high gain circularly polarized (CP) SIW cavity antenna with high gain and high radiation efficiency of 16 dBi and 96 %, respectively.

Acknowledgements

I would sincerely like to extend my utmost gratitude to my supervisor, Prof. Abdel Razik Sebak for his patience, for being generous with his time and for countless great ideas and advices that assisted me to overcome the difficulties of research. The completion of this thesis would not have been possible without his significant support. I am truly indebted to him for his insightful comments and uncompromising attention to details.

Furthermore, I would like to thank the committee members, Prof. A. Kishk, Prof. R. Paknys, and Prof. A. Ben Hamza for their review of my thesis and their numerous constructive comments and feedback.

I would like to express sincere appreciation to all of my PhD colleagues for their help and friendship.

I would like to convey my thanks to my wife, sons, and daughters for their support and patience.

I would like to express a deep sense of gratitude to my family — my mother, father, sisters, and brothers, thank you all for your support, prayers, and inspiration.

Table of Contents

List of Tables

List of Figures

x

List of Symbols

Symbol	Definition
ε_r	Relative dielectric permittivity
σ	Electric conductivity
θ	Theta
D	Antenna Directivity
G	Antenna Gain
λ	Wavelength
λ_0	Free-Space Wavelength
Γ	Reflection Coefficient
ε_{eff}	Effective permittivity
ε_o	Permittivity of free space, 8.854×10^{-12} F/m
C	Speed of electromagnetic waves in a vacuum (2.99792458E8 m/s)
dB	Decibels
F_r	Resonant frequency
GHz	Gigahertz, 10^9 hertz
S11	Reflection coefficient expressed as an S parameter
Γ	Reflection Coefficient

List of Abbreviations

CP	Circular Polarization
MMW	Millimeter-Wave
TDMA	Time Division Multiple Access
W-CDMA	Wideband Code Division Multiple Access
HSPA	High Speed Packet Access
LTE	Long Term Evaluation
FM	Frequency Modulation
CDMA	Code Division Multiple Access
VOIP	Voice Over Internet Protocol
DRA	Dielectric Resonator Antenna
FPC	Fabry Perot Cavity
PRS	Positive Reflection Phase
EM	Electromagnetic
FSS	Frequency Selective Surface
SLL	Side Lobe Level
EBG	Electromagnetic Band Gap
PRP	Positive Reflection Phase
SIW	Substrate Integrated Waveguide
RGW	Ridge Gap Waveguide
FIT	Finite Integration Technique
CST MWS	Computer Simulation Technology Microwave Studio
HFSS	High Frequency Structure Simulator
LP	Linear Polarization
IEEE	Institute of Electrical and Electronics Engineers
BW	Bandwidth
DD	Dense Dielectric
CAD	Computer Aided Design
5G	Fifth Generation
FCC	Federal Communications Commission (U.S.)
FEM	Finite Element Method
LAN	Local Area Network
MIMO	Multi Input Multi Output

PCB	Printed Circuit Board
QoE	Quality of user experience
GSO	Geostationary Orbit
MSS	Mobile Satellite Service
LOS	Line of Sight
LTCC	Low Temperature Co-Fired Ceramic

Chapter 1 Introduction

1.1 Brief Overview of Millimetre Wave (MMW) Communications

The use of MMW technology in communications goes back several decades and has essentially been focused on military applications. The MMW region occupies the range of electromagnetic spectrum between 30 GHz and 300 GHz, which corresponds to wavelengths of from 10 mm to 1 mm [1]. Recent studies suggest that in (the likely) case of future wireless network congestion, MMW frequency spectrum in a range from 30 GHz to 300 GHz could be used as a possible solution [2]. With the explosive growth of mobile traffic demand, the contradiction between capacity requirements and spectrum shortage has become increasingly acute. The bottleneck of wireless bandwidth will become a key problem of fifth generation (5G) wireless networks [1]. In addition to the millimeter wave frequency range, MMW technology offers highly directional antennas, higher bit rates covering larger areas and lower infrastructure costs, all of which will contribute to the advancement of the future 5G network [4]. The MMW frequency range allows channel bandwidths to be expanded, thereby increasing the data capacity and thus helping to address the data overcrowding issue. At this frequency range, it is possible to exploit techniques such as a polarization converter, FSS (frequency-selective surfaces), metamaterials, massive MIMO (multiple inputs multiple outputs) and adaptive beamforming [5]. Moreover, radio signals have propagation characteristics that must be accounted for in the MMW spectrum usage.

While MMW has many attractive characteristics that make it a good candidate for future wireless communications, there are still many challenges, including its high atmospheric attenuation, free space loss, and low ability to penetrate hard materials. As a result, MMW signals cannot propagate over long distances, even under good weather conditions. In contrast, signals at lower frequencies have the ability to propagate for many miles and even penetrate easily through buildings. However, rain and humidity can affect signal performance and reduce signal strength. High-frequency wavelengths can be blocked by physical objects like buildings and trees, and thus millimeter waves travel by line of sight because of the short range of the propagating distance. There are many applications for MMW technology, such as point to point wireless communication, wireless home video, automotive radar, local area networks (LAN), and imaging systems [6].

1.2 Wave Propagation at Millimetre Wave Spectrum

The propagation mechanics of electromagnetic waves have been studied since 1901. There are four mechanisms for the over-the-horizon propagation of signals: diffraction, refraction, reflection and the transmission of surface waves. The transmission loss experienced by microwave systems is accounted by free space loss and can be calculated as:

$$FSL_{dB} = 92.4 + 20\log F + 20\log R \qquad (1.1)$$

where F is the frequency (GHz) and R is the line-of-sight distance between the transmitting and receiving antennas in (Km). Many other influential factors appear as the frequency increases toward the millimeter wave region. The propagation loss is dependent upon the operating frequency at higher frequencies, and so the signal propagation is much slower than at low frequencies. Moreover, atmospheric gasses such as water vapor and oxygen, diffraction, and blockage by foliage have a significant effect on signal propagation in the MMW spectrum. As shown in Fig. 1.1, intense oxygen absorption effect appears at the millimeter wave spectrum rather than at the lower frequencies. Foliage blockage has as much impact as atmospheric gases on the propagation of the signal at MMW bands. In terms of rain and snow, signal wavelengths are similar to the size of raindrops, leading to a scattering of the radio frequency signal. This scattering causes multipath interference as a result of multiple propagation paths. The reflection and scattering essentially increase the path loss with specific attenuation and time delays. Therefore, to compensate for all the aforementioned types of losses in future wireless communication, high directive antennas with wide bandwidth are strongly recommended[7].
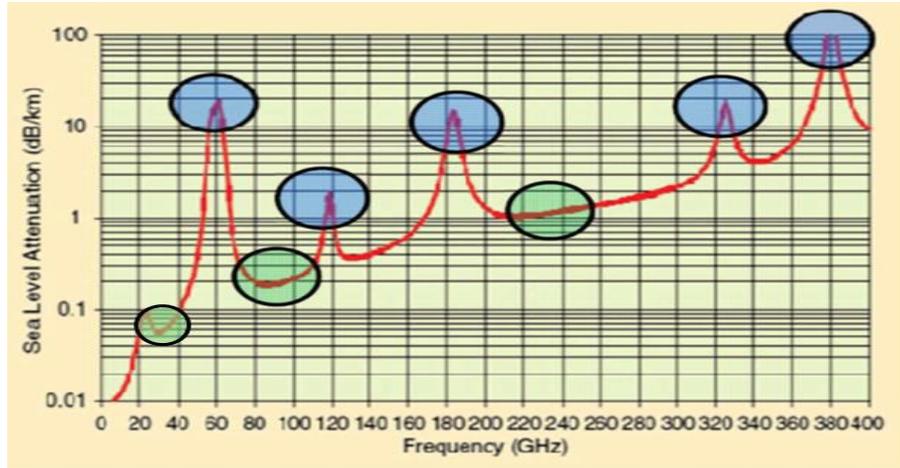
(a)
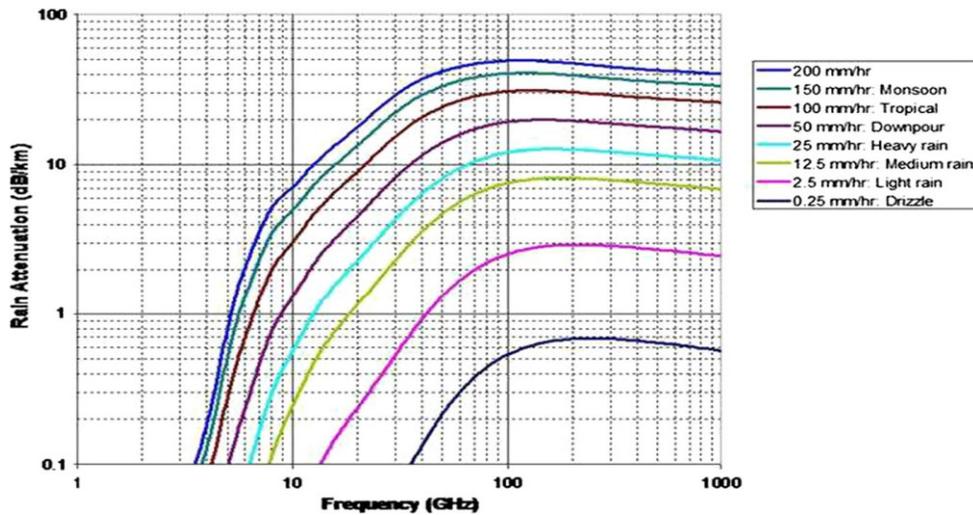
(b)

Figure 1.1: Atmospheric (a) and rain (b) attenuation curves for millimeter waves [2].

Fig. 1.1 (a) shows that atmospheric losses are much lower at 28 GHz than at 60 GHz, as millimeter waves traveling through the atmosphere are absorbed by molecules of oxygen, water vapor, and other gases. There is a 0.04 dB/Km to 0.07dB/km atmospheric loss at 28 GHz, which includes oxygen, normal water vapor, other gaseous atmospheric constituents and average rain, while in the MMW range there are low atmospheric losses in relatively transparent windows centered at 35, 94, 140 and 220 GHz [2], [8].

1.3 Evolution of Wireless Communication Systems

Wireless communications began to be developed and deployed in the early 1980's with the first generation, or 1G. Successive generations were then developed, both to compensate for the drawbacks of the former generation and to improve various aspects of wireless communication systems, including bandwidth. The development stages of wireless communication from 1981 to today are shown in Fig. 1.2, beginning with 1G networks which utilized analog technology for voice communication only. The 2G network system turned to digital modulation and Time Division Multiple Access (TDMA) or Code Division Multiple Access to offer data services. 3G networks, developed in the 2000's, provide high speed data transmission for both video and audio streaming using W-CDMA and HSPA technologies. The current generation is 4G, which uses LTE radio access technology to provide mobile internet access. Finally, the next generation of wireless communication, 5G, is planned to begin operation in the next few years [2].
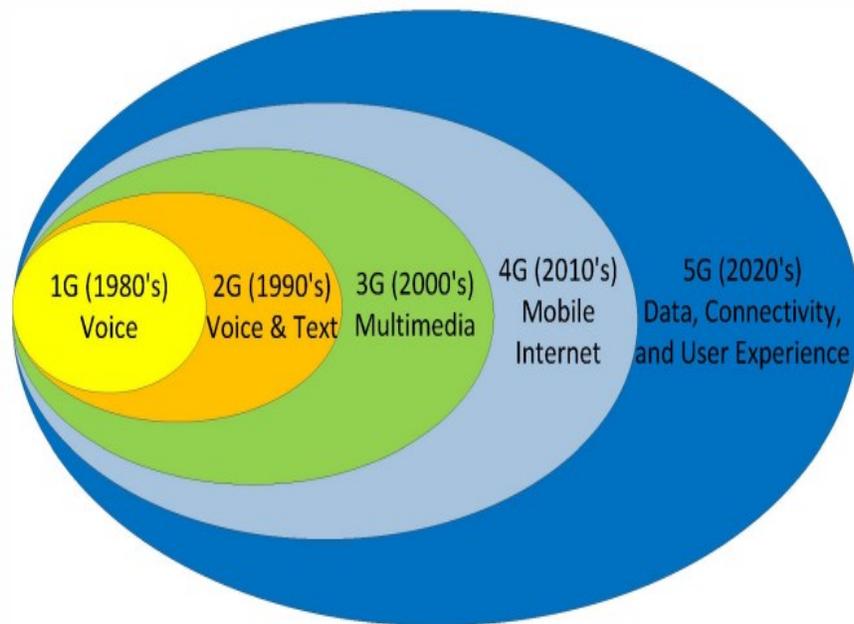
Figure 1.2: Evolution of wireless communications [9].

1.4 Future wireless communications (5G)

Given the current and projected use of wireless communications, there will be a high demand for next-generation systems. These will be expected to offer broad bandwidth, high speed, and low latency. Therefore, researchers and antenna designers are moving to use MMW spectrum as a good solution, thanks to its many advantages. The millimeter-wave region has several frequency bands that are considered as good candidates for future wireless communications such as 28, 38, 60 GHz [10], [11]. 5G wireless communication at 28 GHz and 38 GHz centered frequencies appear to be the most promising options in both indoor and outdoor environments [12]. Fig. 1.3 shows the most significant targets for future wireless communications.
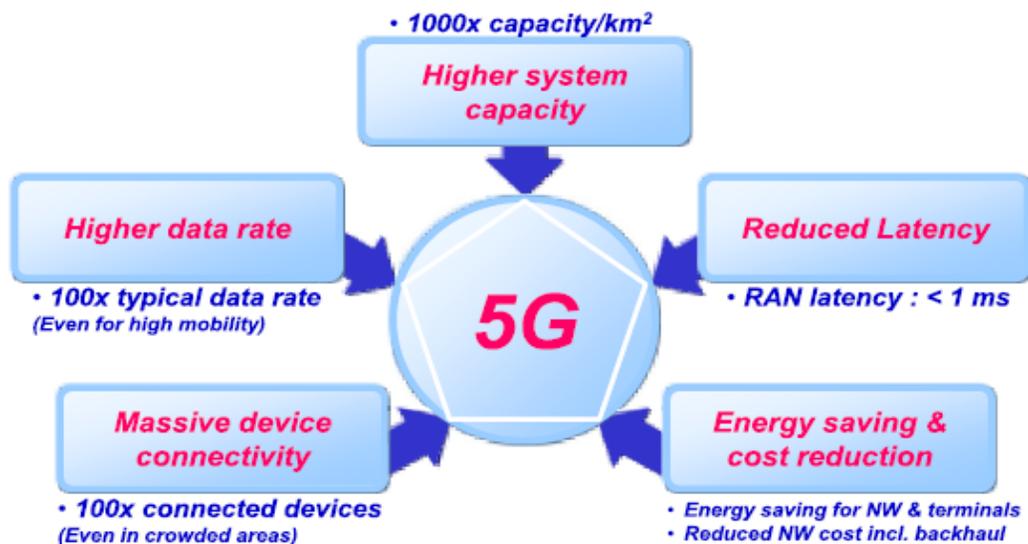
Figure 1.3: The most significant targets for 5G [13].

1.4.1 Why 28 GHz?

Working at MMW will provide a broad amount of spectrum which means high capacity and high data rates. In addition, the size of the antennas will get very small when the wavelengths reach millimeter waves [14]. It is not yet clear which MMW bands will be adopted first by 5G technologies. The 28 GHz band is a good choice, s supported and motivated by multiple reasons. First, the MMW range around 28 GHz is an extensively licensed and underutilized spectrum that has been shown to support cellular communications in the range of 500 meters. Second, compared to higher frequencies, the 28 GHz band is much more beneficial to multipath environments. In addition, it can be used for non-line-of-sight communications [15].

1.4.2 Future Wireless Communication Systems (5G) at the Ka-Band

The MMW band will be a key component in next-generation wireless communication systems (5G). MMW makes it possible to exploit additional spectrum to support greater data traffic for various multimedia services, such as broadband mobile and backhaul services. Detailed knowledge of the channel propagation characteristics in the ka frequency band is playing a crucial role in developing 5G wireless communications technology [16].

The number of mobile device users has been steadily increasing since the early 1980's, when the first-generation mobile communication system, based on analog Frequency Modulation (FM), was launched [17]. Over the years, as the development of wireless communication transformed from the 1st generation to its 4th generation incarnation, technologies such as Time Division Multiple Access (TDMA), High Speed Packet Access (HSPA), Code Division Multiple Access (CDMA), Voice Over Internet Protocol (VOIP), and Long-Term Evaluation have continued to evolve with each generation. The development of Fifth Generation (5G) communications has been driven by the increasing need for high speed reliable communications linked to the desire for significantly improved user experience. It has now been widely accepted that the capacity of 5G wireless communication systems should be much larger than the Fourth Generation (4G) Long Term Evolution (LTE) [18].

Due to the growing number of mobile devices and the increasing demand for better service quality, the next generation of mobile networks' issues are getting more and more attention from researchers. Fifth generation (5G) mobile communication networks could provide a flexible, reliable, and high-performance network architecture for wireless communication beyond 2020 [19].

By providing more spectra for future MMW cellular systems, future capacity demands could be met, while simultaneously incentivizing investments and technological developments that would ensure engineering competitiveness. Fig. 1.4 highlights the bands in this region with the highest potential
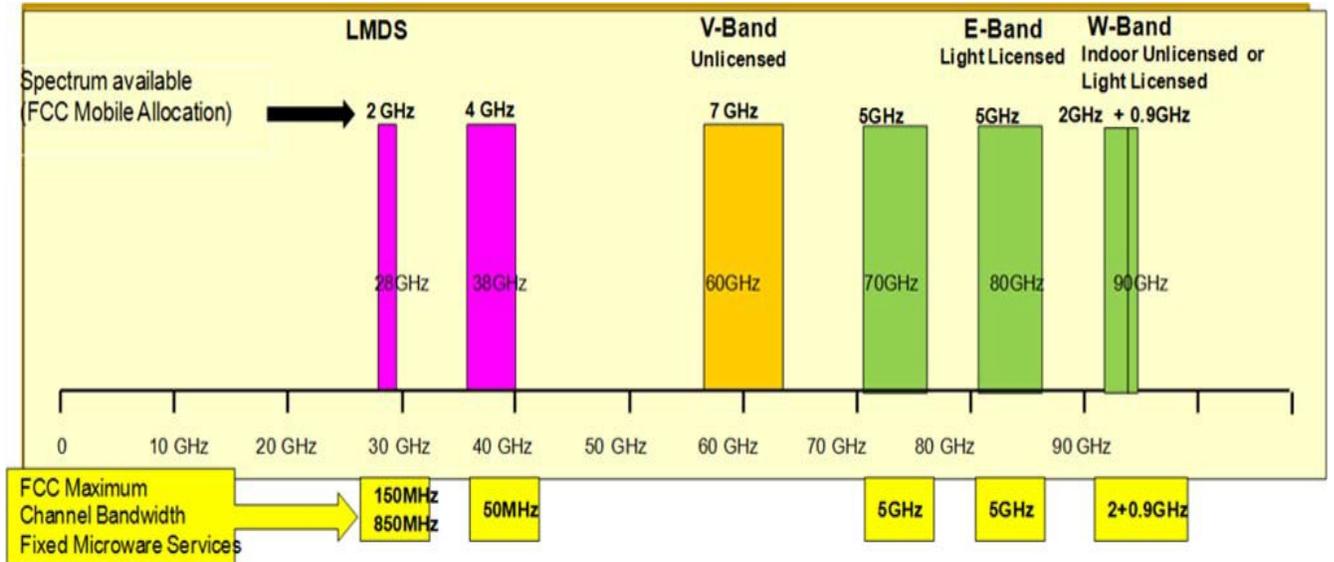
Figure 1.4: potential 5G spectrum above 20 GHz [5].

1.5 High Gain Antennas in MMW Communications

High gain antennas are vital components for many communication systems, such as radar, satellite, and mobile wireless communication systems. At the MMW spectrum, most of these applications suffer from attenuation difficulties. Consequently, MMW applications (5G) will face the increasing demands of high gain antennas to compensate for attenuation losses. Therefore, high gain antennas are required to overcome the propagation losses, free space losses, atmospheric attenuation, and multipath losses of MMW applications [20]. A brief review of dielectric resonator antenna (DRA) and Fabry-Perot Cavity (FPC) antennas that could provide high gain at the MMW spectrum is presented below.

1.5.1 Dielectric Resonator Antennas

Since the late 1980s, dielectric resonators have been investigated as the high Q element in microwave-circuit applications. Dielectric resonators are easier to integrate with planar circuits. Cylindrically shaped dielectric resonators are widely used, fabricated from materials with relatively high dielectric constants ($\varepsilon_r \geq 35$) for compactness. To prevent radiation and to maintain a high Q factor, dielectric resonators are also often enclosed in metal cavities, which is especially important for filter or oscillator designs. In 1980, Long, McAllister, and Shen studied dielectric resonators as radiating elements and tested the characteristics of dielectric resonator antennas (DRAs) with hemispherical, cylindrical, and rectangular shapes [21]. Dielectric resonator antennas

are utilized for MMW applications as broadside radiating elements because of their attractive advantages. The high radiation efficiency of dielectric resonator antennas (DRA) is considered to be a significant advantage over microstrip antennas.

A number of different antenna (DRA) shapes are reported in the literature. The possibility to have different dielectric resonator antenna shapes is itself an attractive characteristic, with a cylindrical [22], and a cubical [23] shape being possible, depending on the existing size and without affecting the radiation pattern characteristics. If the height of a dielectric resonator is significant, it results in a non-planar, high profile antenna structure. However, the dielectric resonator antenna can be made very thin for applications that need low profile antennas. The dielectric constant can be in the range of $80 \leq \varepsilon_r \leq 100$, and so the height of the DRAs should be between $0.025\lambda_o \leq h \leq 0.035\lambda_o$ [21].

A new kind of antenna element, the dense dielectric (DD) patch antenna, is introduced in [24]. A thin dielectric substrate of high permittivity can be used to replace the metallic patch. This high DD patch could be used as an array [25]. Fig. 1.5 shows an example of high dense dielectric patch antenna (a), and an array of dense dielectric patch antenna designed at 60 GHz (b).

(a)   (b)
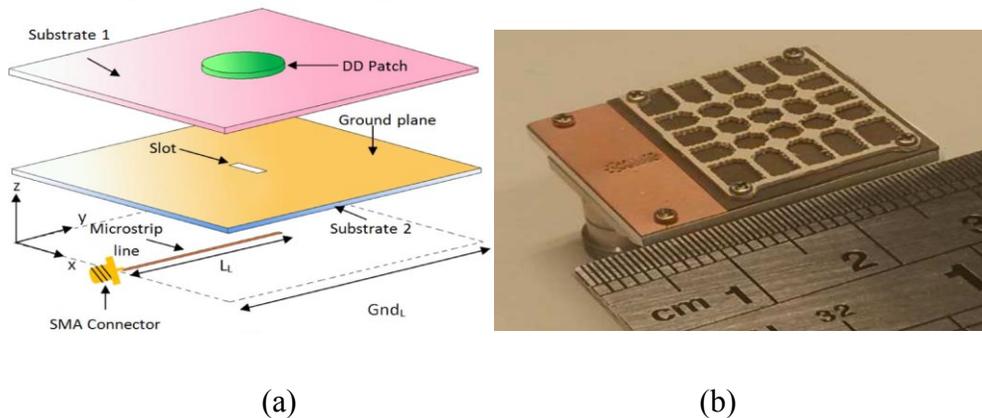
Figure 1.5: A single DD patch [24] (a), planar DD patch array [25] (b).

1.6 Fabry Perot Cavity antenna

High gain antennas can be achieved using different types of antennas, including reflector antennas, horn antennas, and antenna arrays. However, their bulk, heavy weight, feeding network losses as well as their fabrication complexity make these antennas unsuitable for millimeter wave applications [26]. The Fabry-Pérot Cavity (FPC) antenna (See Fig. 1.6) has therefore been

investigated to overcome these drawbacks. It consists of a grounded radiated source and a partially-reflected covered plate. There is a half-wavelength spacing between the main radiator, and the covered plate is behind the in-phase forward radiation. Its maximum high-directivity property can be achieved thanks to the multiple reflections between partially reflective surfaces and the ground plane [27]. The use of partially reflective surfaces was proposed by Trentini in 1953 when he discovered that these surfaces have the ability to enhance the directivity when placed in front of the antenna.
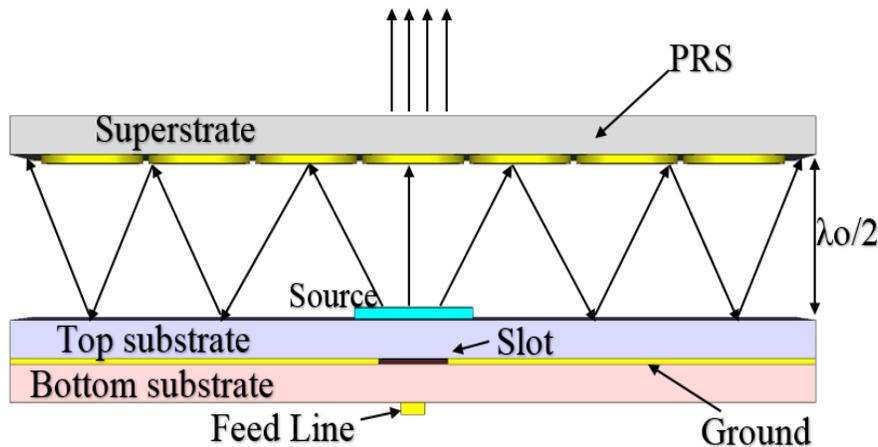
Figure 1.6 Schematic diagram of a PRS Fabry Perot Cavity antenna [109].

Trentini was the first to investigate the concept of an FPC antenna and proved that the directivity of a waveguide aperture in the ground plane could be increased by using several types of partially-reflective surfaces (PRSs) through the multiple reflections between the ground plane and the PRS. In order to achieve constructive interference of the waves bouncing between the PRS and the ground, the cavity distance should be a multiple of a half wavelength at the desired operating frequency [28].

1.6.1 Periodic Structures

A structure is defined as periodic when it can be designed by an infinite number of the same basic unit, called a unit cell, and it can be a 1-D, 2-D or 3-D structure. Periodic structures are considered as the traditional concept in the electromagnetic (EM) field. The periodicity of a structure adds some features for the wave propagation within. Frequency selective surfaces (FSSs) are the most popular type of periodic structures as shown in Fig. 1.7. An FSS can be used as a frequency filter [29] and as a lens [30]. A dielectric superstrate is used to cover the antenna element, which can be

a microstrip patch, slot, or a DRA, to enhance the directivity in the broadside direction. Single and multiple stacked layers have been used to improve the antenna performance in terms of gain, bandwidth, and side lobe levels [31].

(a)   (b)
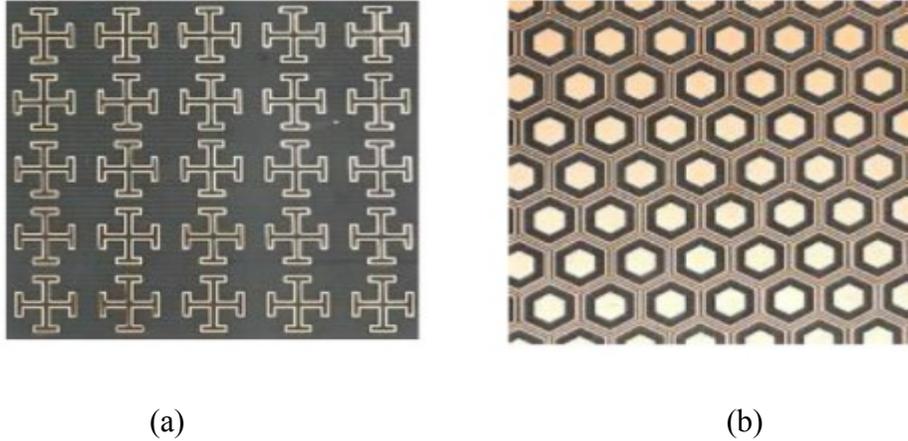
Figure 1.7: Schematic of different periodic stuctures: Jerusalem metal ring (a), and hexagon patch ring (b) [32].

1.7 Motivation

Future wireless communication systems or 5G, a new generation of mobile wireless technology, has been attracting the attention of many research institutes around the world, as this new technology will have the ability to deliver higher data rates of up to 10 Gbps, along with orders of magnitude greater capacity and lower latency than today's wireless systems. Enormous research and development have been invested recently in antenna design and optimization that could efficiently work in the Ka-band, which is from 26.5 GHz to 40 GHz. The MMW spectrum is a good candidate for 5G wireless communications as it offers the ability to provide access to a wide spectrum with small-sized high directive antennas. [33], [34].

Fabry-Pérot cavity (FPC) antennas have been widely used, as their attractive advantages include their simple configuration and low profile, as well as their ability to provide high gain; this last property makes them particularly well-suited to be used in high gain millimeter wave antennas [35]. The antenna superstrate, whether it is dielectric or FSS, plays a key role in enhancing gain, broadening the bandwidth, and decreasing side lobe levels, which is a simple means compared to using arrays for instance. A radiated source, the dense dielectric (DD) patch antenna, was introduced as an antenna that uses a dielectric material with very high permittivity to replace the

metallic patch of a conventional microstrip antenna. Designing a compact, small MMW antenna with excellent characteristics in terms of high gain, bandwidth, efficiency, and radiation patterns has become essential in order to compensate for the high attenuation of MMW systems and thereby increase the communication distance between the source and the destination. To sum up, since MMW applications (the future applications for 5G) need high gain antennas to compensate for the attenuation losses, and broad bandwidth to match the high data rates, a combination of a high dense dielectric patch as a radiated source and a well-designed superstrate (dielectric or FSS) could be a promising approach. Therefore, the significant targets of this work are gain enhancement and bandwidth improvement using partially reflective surfaces for either dielectric or FSS superstrates.

1.8 Objectives

Wireless communication systems are in high demand for fifth generation (5G) millimeter wave (MMW) applications. Some of the most desired characteristics of MMW systems are their low profile, high gain, compact size, broad bandwidth, and high efficiency. Highly directional antennas are needed to compensate for the signal attenuation that occurs due to the high propagation loss caused by atmospheric absorption. Moreover, the high data rates for most MMW applications require a wide bandwidth. Therefore, most high frequency applications need to have high gain, high efficiency, and wide bandwidth antennas.

The main purpose of this work is to investigate and develop high dense dielectric patch antennas for millimeter wave applications, employing different techniques to meet the future wireless communication requirements. The specific objectives are listed in the following points:

(1) Improving the performance of the Fabry-Pérot cavity (FPC) antenna in terms of gain, bandwidth, radiation efficiency, and side lobe levels by utilizing a single layer perforated dielectric superstrate and a high dense dielectric patch array as radiated elements.

(2) Broadening the FPC antenna bandwidth while maintaining high gain performance using a partially reflective surface composite of two thin perforated dielectric slabs.

(3) Enhancing the antenna gain and improving the side lobe levels by designing a flat tapered dielectric superstrate with non-uniform permittivity to correct the phase distribution over the superstrate. Also, this tapered superstrate is designed to be used to tilt the antenna beam without using a phase shifter.

(4) Improving the gain of the FPC antenna by designing a partially reflective surface FSS superstrate, and addressing the limited bandwidth issue of this antenna by expanding the 3-dB gain bandwidth using a positive reflection phase FSS superstrate. In addition, a simple design of linearly and circularly millimeter wave antennas is targeted, employing a linear-to-circular polarization converter.

1.9 Thesis Outline

This thesis is organized into seven chapters including this introduction chapter (chapter 1).

Chapter 2 provides a literature review and a brief history of the Fabry-Pérotcavity (FPC) antenna, as well as different practical applications.

Two FPC antennas based on partially reflective surfaces' perforated dielectric superstrates are presented in chapter 3. The goal of this chapter is to enhance gain and expand the 3-dB gain bandwidth. A discussion about the effects of the permittivity and the thickness of the superstrate on the antenna performance is also presented.

Chapter 4 presents a flat tapered dielectric superstrate designed to correct the phase distribution in order to enhance the antenna gain and decrease the side lobe levels. Beam tilting without phase shifters is also presented in this chapter.

Chapter 5 describes a high dense dielectric patch antenna integrated with a frequency selective surface (FSS) superstrate, designed to enhance the antenna gain and expand the 3-dB gain bandwidth. Two different partially reflective surface unit cells are designed and evaluated. These are then applied over the dense patch antenna to achieve the targeted results.

An example of a circularly polarized millimeter wave antenna is discussed in chapter 6. A simple approach is utilized to convert the polarization of the substrate integrated waveguide (SIW) cavity antenna from linear to circular polarization while maintaining the high gain characteristic.

Chapter 7 concludes the thesis and suggests promising future work.

1.10 Contributions

1- **M. Asaadi** and A. Sebak, "High-Gain Low-Profile Circularly Polarized Slotted SIW Cavity Antenna for MMW Applications," in *IEEE Antennas and Wireless Propagation Letters*, vol. 16, no. , pp. 752-755, 2017.

2- **M. Asaadi** and A. Sebak, "Gain and Bandwidth Enhancement of 2×2 Square Dense Dielectric Patch Antenna Array Using a Holey Superstrate," in *IEEE Antennas and Wireless Propagation Letters*, vol. 16, no. , pp. 1808-1811, 2017.

3- **M. Asaadi**, I. Afifi and A. Sebak, "High Gain and Wideband High Dense Dielectric Patch Antenna Using FSS Superstrate for Millimeter-Wave Applications," in IEEE Access, vol. 6, pp. 38243-38250, 2018.

4- **M. Asaadi**, M. Zaid, and A. Sebak, "High Gain of Low Profile High Dense Dielectric Patch Antenna using Tapered Dielectric Superstrate," IEEE Trans. Antennas Propagat., 2019, **submitted.**

5- **M. Asaadi** and A. Sebak, "Broadside high gain H-plane substrate integrated horn antenna for future 5G applications," *2016 IEEE International Symposium on Antennas and Propagation (APSURSI)*, Fajardo, 2016, pp. 1491-1492.

6- **M. Asaadi** and A. Sebak, "High gain high dense dielectric patch antenna with a holey superstrate for 5G applications," *2017 International Conference on Electromagnetics in Advanced Applications (ICEAA)*, Verona, 2017, pp. 1109-1111.

7- **M. Asaadi** and A. Sebak, "High gain low profile slotted SIW cavity antenna for 5G applications," *2016 IEEE International Symposium on Antennas and Propagation (APSURSI)*, Fajardo, 2016, pp. 1227-1228.

8- **M. Asaadi** and A. Sebak, "Circularly polarized high gain low profile slotted SIW cavity antenna," *2016 17th International Symposium on Antenna Technology and Applied Electromagnetics (ANTEM)*, Montreal, QC, 2016, pp. 1-2

9- **M. Asaadi**, A. Beltayib, and A. Sebak, "High Gain High Dense Dielectric Patch Antenna Using FSS Superstrate for Millimeter-Wave Applications," *2018 18th International Symposium on Antenna Technology and Applied Electromagnetics (ANTEM)*, Waterloo, ON, Canada, 2018, pp. 1-2.

10- A. Beltayib, **M. Asaadi**, Z. Briqech and A. Sebak, "A beam deflector based on gradient refractive index metamaterial," *2017 International Conference on Electromagnetics in Advanced Applications (ICEAA)*, Verona, 2017, pp. 1134-1136.

Chapter 2 Literature Review

This section presents a literature review of Fabry-Pérot Cavity (FPC) antenna, its radiated sources and its superstrate layer, followed by an overview of un-printed dielectric slabs and frequency selective surfaces (FSS). A brief history and background of the FPC antenna and its use with several types of superstrates is then presented.

2.1 FabryPérotCavity Antenna

Researchers have been motivated to study the Fabry-Pérot Cavity (FPC) antenna for several decades thanks to its attractive characteristics. It consists of a grounded radiated source and a partially-reflective covered plate. There is a half-wavelength spacing between the main radiator and the covered plate behind the in-phase boresight radiation. The first application of an FPC structure to enhance the gain of a boresight antenna was in 1956 [28]. More studies were done in the late 80s [36, 37], where the dense, quarter wavelength and dielectric sheets replaced the partially reflective surface (PRS) while maintaining a half wavelength spacing between the radiator source and the superstrate. In [38], many layers of a dielectric sheet were proposed to cover the radiated element. Subsequently, the electromagnetic band gap (EBG) was investigated and utilized to replace the top reflective superstrate [39, 40]. Researchers determined that metamaterial can be designed to provide a high impedance with no reflection coefficient phase delay to replace the ground plane in order to decrease the gap distance between the antenna source and covered plate [41] and that zero-index metamaterial can be implemented to enhance antenna gain [42].

Fabry Pérot Cavity (FPC) antennas are considered to be good candidates for a wide range of applications in microwave and millimeter wave communications because of its planar configuration and simple design. Also, it is a potential to avoid using bulky antennas such as horns to achieve high gain [43]. This thesis investigates high gain and wide band high dense dielectric patch antennas with several superstrates. Both FPC antennas with different dielectric slab superstrates and frequency selective surfaces (FSS) covering the high dense dielectric patch antenna are evaluated.

2.1.1 FabryPérotCavity Radiated Source

Since the FPC was first introduced, many types of radiated sources have been used to excite FPC antennas. They can be excited by a single source or by multiple sources located inside the resonator, such as a microstrip patch [44], a dielectric resonator antenna (DRA) [45], or a slot in the ground plane [46]. Recently, a new kind of low-profile patch was used as a radiated element. A thin high dense dielectric patch can replace the metallic patch to realize many attractive advantages, such as low profile, wideband, high radiation efficiency [24], [47].

2.1.2 Unprinted Dielectric superstrate

Superstrates are the significant parameters in designing FPC antennas. They work as a lens to enhance the antenna gain and play an important role in obtaining the highest broadside gain. Superstrates also have the ability to determine the gain bandwidth of an antenna. Superstrates are defined as printed and un-printed dielectric slabs. One of the earlier studies on dielectric layers covering an antenna was performed by Y. Sugio et al. at the Setsunan University, Osaka, Japan in 1983 [48]. Different types of dielectric superstrates covering Fabry Pérot (FP) resonator were investigated by Jackson [36], Thevenot [49], and Fangming Zhu et al. [50]. These can be single or a number of stacked dielectric slabs and frequency selective surfaces, as in [51]. In an un-printed dielectric superstrate, the electrical thickness of each slab must be a quarter wavelength in order to increase the antenna gain. The permittivity and dielectric slab thickness have to be selected appropriately. The antenna gain can be enhanced as the number of superstrate layers is increased. The effect of the superstrate on the antenna gain bandwidth cannot be ignored, as the gain bandwidth can be increased by using multiple superstrates above the radiating source [52].

2.2 Frequency Selective Surfaces (FSSs)

Frequency Selective Surfaces (FSSs) are planar periodic structures of identical patches or apertures of conducting elements that reiterate periodically in a one- or two-dimensional array on a dielectric substrate layer. FSSs have many applications in several sectors because of their unique properties, leading to their use in reflector antennas, aerospace, medical, and microwave communications fields. High performance low-observable antennas are required in strategic areas. These qualities can be acquired by combining an FSS structure with a planar antenna, where the FSS can be acting

as a superstrate or as the high impedance ground plane of an antenna. Integrating an FSS with an antenna enhances both its gain and its bandwidth [53].

2.2.1 FSS Background and Applications

Frequency Selective Surfaces (FSSs) have been known since 1919. [54]. Marconi and Franklin investigated and studied a parabolic reflector made using half-wavelength wire sections. Their contribution is considered to be a pioneering effort in this field [55]. Due to the multiple advantages of FSSs that are especially useful for military applications, the use of FSSs has increased rapidly since the 1960s [56]. Based on their reflection and transmission coefficients on the frequency of operation and polarization, contributing to their usage in a range of applications [57]. FSSs have been applied in many areas, such as in dual or metallic radomes [58], phase screens for beam steering [59], dual-band arrays [60] and absorbers [61].

FSSs take different shapes and structures. They can be planar of two dimensional (2-D) periodic arrays of metallic elements or apertures. Even though FSSs can take different shapes, conventional FSSs have similar operation mechanisms that can be explained by the phenomenon of resonance. When a plane wave is incident to the array of elements on a planar surface, the elements of the periodic surface resonate at frequencies where the effective length of the elements is a multiple of the resonance length, $\lambda/2$ [62]. These elements have a certain phase delay. Therefore, the scattered radiation of each single element will add up coherently. Marconi and Franklin's parabolic reflector provides such an arrangement of planar elements. The resonance of an FSS is determined based on how the FSS surface is exposed to the EM wave. Some FSSs with a particular shape have the ability to provide a total reflection, such as a patch FSS; while an aperture FSS can exhibit a total transmission at the resonance frequency and act as a Partially Reflective Surface (PRS) at frequencies near resonance.

2.2.2 Types of Frequency Selective Surfaces (FSSs)

There are many types of FSS elements, each with its unique transmission/reflection characteristics, sensitivity to oblique angle of incidence, polarization type, and bandwidth. These are classified according to their shape and structure into four groups, as shown in Fig. 2.1 [63-65].

16
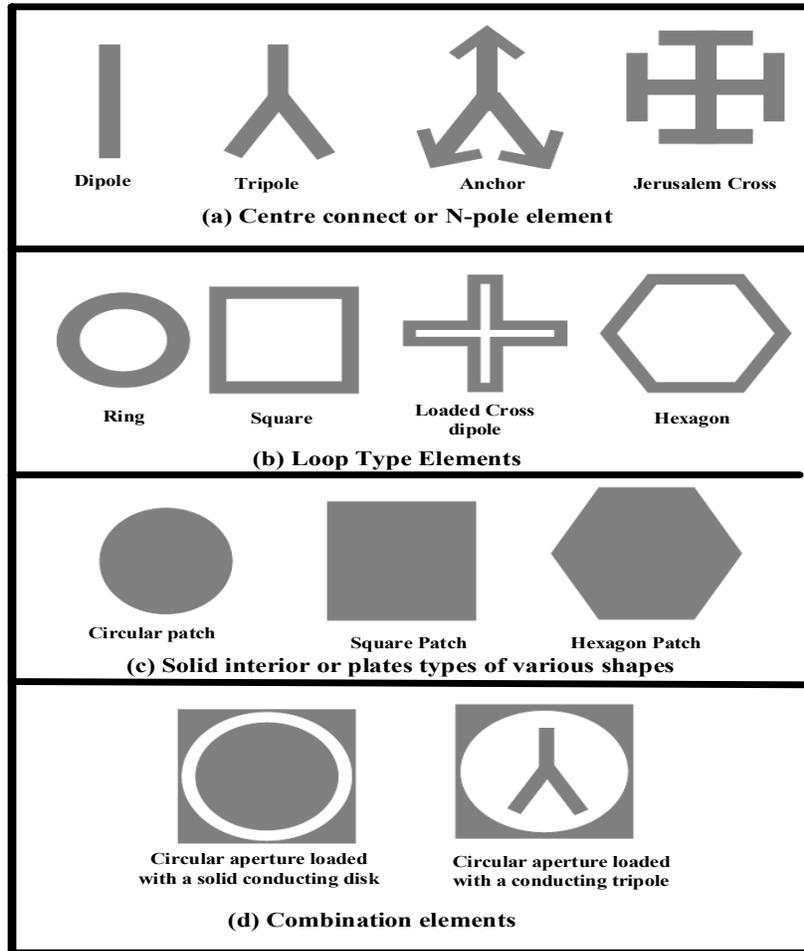
Figure 2.1: Some popular FSS elements, classified into four categories [64], [65].

Modern wireless communication systems need highly directive antennas with a wide operational frequency range due to the ever-increasing demand for greater data capacity. Designing high gain and broadband FPC antennas thus remains an important challenge. This thesis investigates, develops, and improves the performance of FPC antennas in terms of gain, bandwidth, and radiation pattern.

2.3 Analytical Model of the Fabry-Pérot Cavity Antenna

Several analytical models have been used to explore the radiation behavior of Fabry-Pérot Cavity (FPC) antennas, including the leaky wave model [66], transmission line model [52], ray-tracing approximation [67,28], and the electromagnetic band gap (EBG) defect model [68]. However, these models are mathematically complicated. A less-complicated method, based on the periodic analysis property and incorporating a superstrate reflection model, was therefore developed and investigated [69]. The solutions for electromagnetic fields and waves are key to investigating the radiation performance of antennas as well as that of microwave devices and components. Such solutions are based on Maxwell's equations, either in the time or frequency domain, subject to proper boundary conditions [26], [70]. Maxwell's equations are applied under the appropriate boundary conditions to obtain a solution [26]. Many commercial software packages such as CST MWS, Ansoft HFSS, and FEKO have been investigated and utilized to support the foundations for full-wave numerical analysis methods. In this thesis, all of the FPC antenna designs were simulated and carried out using the full-wave CST software package.

2.4 High Gain Low Profile of High Dense Dielectric Patch Antenna using a Holey Superstrate

Wireless communication systems are in high demand for the development of future fifth generation (5G) millimeter wave (MMW) applications. Some of their attractive characteristics are especially desirable in millimeter wave systems, including low profile, high gain, compact size, broad bandwidth, and high efficiency [71]. Highly directional antennas are needed to compensate for the signal attenuation due to high propagation loss caused by atmospheric absorption [25]. The high data rates for most MMW applications need a wide bandwidth. Most high frequency applications, therefore, need high gain, high efficiency, and wider bandwidth.

Dielectric resonators were investigated in the late 1960s, and have been used as high Q elements in microwave circuits such as filters and oscillators. They have been used as dielectric (DR) antennas since the 1980s [72]. A new kind of antenna element, the dense dielectric (DD) patch antenna, was developed more recently [24]. A thin dielectric substrate of high permittivity is used to replace the metallic patch in [73]. As reported in [74], the radiation efficiency of DR antennas is generally better than that of microstrip antennas. The FPC antenna is considered as a potential

replacement for bulky antennas such as reflectors and horns thanks to its - planar configuration and simple design, among its other advantages.

To design a PRS as an efficient part of an FPC antenna with a strong reflectivity, the PRS permittivity should be greater than one, with the relative dielectric permittivity $\varepsilon_r \gg 1$, the permeability $\mu_r \gg 1$ and a large area of $25\text{-}36\lambda_0^2$. However, this antenna has a narrow band due to the highly selective cavity (high Q-factor) [68], [75]. A dielectric superstrate was used with different ground plane types which are perfect electric conductors (PECs), perfect magnetic conductors (PMCs), and artificial magnetic conductors to produce an FPC antenna. That work achieved a directivity of about 15 dBi [76]. Another work applied a conventional superstrate with high permittivity $\varepsilon_r = 10.2$ over a 1×4 circular DD patch to improve the antenna performance. However, the antenna gain was only about 16 dBi, the 3dB gain bandwidth was 10.7 %, and the side lobe level was around -10.9 and -11.6 dB in the E and H planes, respectively [77].

A U-slotted patch antenna fed a single layer frequency selective surface (FSS) superstrate with dissimilar sized square patch was designed for broad bandwidth applications in [78]. However, its bandwidth is limited to 7.99 % to 12.2 % with an efficiency of 69.1 %. In [79], an FSS layer is applied above a microstrip patch antenna to enhance the antenna gain. The corresponding structure is not flat, is bulky and has two air gaps between the layers. A microstrip patch antenna with a superstrate layer was designed at 60 GHz to improve the antenna gain [80]. However, it resulted in an impedance bandwidth of 6.8 %, and the side lobe levels (SLL) were high.

Gain enhancement of a microstrip patch antenna using a holey superstrate is reported in [81]. The antenna gain is about 6.9 dBi, and the antenna bandwidth is 3.8 %. Several approaches have been investigated to improve antenna bandwidth while maintaining high gain performance. Several examples of exploiting partially reflective surfaces (PRSs) with positive phase gradients using dielectric superstrates can be found in the literature. Two dielectric substrates with the same thickness, a quarter of the dielectric wavelength, were applied above the metallic patch antenna to enhance the antenna gain and the bandwidth [82]. However, the antenna gain is not very high, and the bandwidth is quite narrow. Another approach applied two dielectric superstrates above a waveguide antenna to broaden the antenna bandwidth. However, in that effort, the two dielectric superstrates are thick, realizing a 3 dB gain bandwidth of 17.9% [83]. Meanwhile, using three dielectric slabs successfully improved antenna performance, achieving a 3 dB gain bandwidth of

22% and a peak gain of 18.2 dBi [84]. Another approach improves the antenna bandwidth using frequency selective surface (FSS) superstrates, so they do not have to respect the quarter dielectric wavelength thickness of the superstrate. The three open cavities formed by three periodic partially reflective surfaces (PRSs) applied above a slot fed by a waveguide to enhance the bandwidth. However, a 3 dB gain bandwidth of only about 15 % was achieved [85]. In [86], two layers of FSS superstrate based on a PRS covered a single slot antenna fed by a ridge gap waveguide in an effort to broaden the bandwidth. The composite unit cell was designed to provide a positive reflection phase over a particular frequency. However, the 3 dB gain bandwidth is only 12.2 %. Thicker substrates with thicknesses of either $\lambda d/4$ or $\lambda d/2$ (where λd is the dielectric wavelength) have been used as PRS surfaces to achieve a positive refection phase. However, at some frequencies, these thicknesses are not available.

In this thesis, a holey dielectric superstrate is applied over a 2×2 high dense dielectric square patch antenna to enhance the antenna gain, improve bandwidth and efficiency, and to reduce the SLL. This antenna is designed to meet several of the MMW applications' needs in terms of antenna size, gain, bandwidth, SLL, and efficiency. The standard metallic patch is replaced by a high dense dielectric (DD) patch with a relative permittivity of 82. Aperture feeding technique is used to feed 2×2 DD patches. A number of uniform circular holes are drilled through a dielectric superstrate layer to reduce the permittivity and to improve the antenna impedance bandwidth. This design provides higher gain, wider bandwidth, low side lobe level, and high radiation efficiency.

A simulated design of a thin dual layer PRS to broaden the bandwidth of a high dense dielectric patch antenna array is also presented in this thesis. The antenna bandwidth will increase as the reflection phase of the PRS superstrate increases with the frequency, and when the phase resembles the optimum phase. A PRS unit cell composed of two thin dielectric substrate layers with different permittivities and thicknesses is utilized to provide a positive phase gradient over a certain frequency band. The PRS is applied over the DD patch antenna array to improve the antenna bandwidth. This work shows that the thickness of each slab of the PRS unit cell could be less than $\lambda d/4$, and that the PRS works efficiently to enhance the antenna performance, as will be demonstrated later.

20

2.5 Performance Improvement of High Dense Dielectric Patch using a Tapered Superstrate

Wireless communication systems are in high demand for future fifth generation (5G) millimeter wave (MMW) applications. Modern communication systems require compact size and light weight with good performance. The need for wide gain bandwidth has been increasing throughout the development of wireless device technology. Meeting this growing need for high bandwidth is a difficult problem in the low frequency spectrum. Therefore, researchers have begun to investigate and exploit the millimeter-wave available around 30 GHz [87]. Moving to the millimeter-wave spectrum offers a solution to several 4G issues, including low data rate [88].

While the bandwidth is a significant feature for future wireless communications, the antenna gain is also very important. Due to the high attenuation at high frequencies caused by atmospheric loss, free space loss, and vapor loss, high gain antennas are a requirement for millimeter-wave applications [87]. Fabry-Pérot Cavity antennas (FPCA), also known as Resonant Cavity antennas (RCA), are considered to be good candidates for millimeter-wave wireless communications. They have attracted significant attention as they provide high-gain performance, wide bandwidth, high efficiency, and a low-complexity feeding network [89]. Furthermore, the excitation of this type of cavity antenna may be accomplished by one or many types of radiated sources such as slots, patches, or dipoles.

Dielectric resonator antennas (DRAs) have been deployed since the 1980s. Dielectric resonators were investigated for their use in industry beginning 1960 and used as high Q elements in microwave circuits [72]. Recently, a thin high dense dielectric (DD) patch with high permittivity was used to replace a metallic patch [90], and [91]. Many significant characteristics such as their low profile, high radiation efficiency, and wide bandwidth make this new type of patch a good candidate to excite FPC antennas for millimeter-wave applications. However, FPC antennas have a narrow operational bandwidth with high gain performance, while the high data rates for most MMW applications need a wide bandwidth. Therefore, most high frequency applications need high gain, high efficiency, and a wide bandwidth [91].

When FPC antennas were first investigated, they offered a narrow performance band with a bandwidth of about 3% [92]. More recently, many FPC antennas have been reported to offer enhanced gain and expanded bandwidth. A 2×2 dense dielectric patch antenna as a radiated source was used to feed a perforated superstrate to enhance the gain and to improve the bandwidth [93].

However, this approach may need more space for the array source, increasing the overall antenna dimensions as well as the feeding network complexity and the losses. In [79], a frequency selective surface (FSS) was used to enhance the antenna performance in a multilayer antenna with two air gaps. While this improved the antenna gain, the bandwidth was only moderate. An FPC antenna incorporating multi-layer superstrates integrated with the input reflection phase technique successfully broadened its bandwidth and enhanced its gain [94].

Beam-switching antenna systems, one of the smart antenna technologies, have received much interest in recent wireless communication systems research. They offer many significant advantages including energy savings, reduced multipath fading, and making antennas more flexible [95] [96].

An FPC antenna can be utilized to steer the antenna beam in the broadside direction in a simple way without using active phase shifters. An unequally-extended frequency selective surface (FSS) is required to steer the antenna beam. However, this approach incurs the disadvantage of large side lobe levels (SLL) proportional to the angle of scanning [97]. Mechanical scanning is achieved in [98] by rotating a conventional dielectric slab placed above an array of dielectric resonators.

There are many approaches that help in designing antennas with tilted beams at particular frequencies. In [99], a broadside antenna with a maximum tilt of 20° was achieved by changing the capacitance of the PRS. A PRS with a varactor diode was used to steer the antenna beam with $\pm 7^o$ [100]. A phase shifter was utilized to excite the PRS over a two-patch antenna array [101]. This antenna beam was scanned from -10° to $+10^o$ with a 13 dBi gain. Another approach used a reconfigurable PRS excited by a phased array to steer the antenna beam, with consistent beam steering from -15° to 15° achieved with a 12 dBi gain [102]. A metasurface superstrate with different effective refractive index regions was applied over a microstrip patch antenna to tilt the beam, producing a maximum beam tilt of 27° in the E-plane with a maximum gain of 8.4 dBi [103].

In this thesis, a single unprinted dielectric tapered superstrate is proposed to improve the antenna performance in terms of gain, wideband, and sidelobe levels (SLLs). A low profile high dense dielectric (DD) patch antenna with a relative permittivity of 82 is used to excite a resonant cavity antenna instead of using a microstrip patch antenna. An aperture feeding slot is used to couple the DD patch antenna. A single unprinted tapered dielectric layer is designed and placed above the DD patch antenna to enhance the antenna gain towards the broadside direction, broaden the

bandwidth and reduce the side lobe level. This tapered dielectric layer is designed to compensate for the phase along the superstrate by making the permittivity of the single slab superstrate high in the center and decreasing it gradually toward the edges. Drilling holes in the dielectric substrate can alter the effective dielectric constant to match the required permittivity in each zone. This antenna meets some of the needs of MMW applications, particularly in providing higher flat gain, wider bandwidth, low side lobe levels, and high radiation efficiency. Beam steering is also targeted by using this proposed superstrate. A good performance in terms of the tilting angle, gain, bandwidth, and side lobe levels is achieved.

2.6 High gain and Wideband of Dense Dielectric patch Antenna based on FSS Superstrate

Future wireless communication systems require wider bandwidth, higher speed, and low latency. The millimeter wave (MMW) band has therefore been selected for its ability to provide all of the next generation's requirements. High gain wideband antennas capable of working in the MMW spectrum are also required [80]. Due to the high attenuation in the atmosphere and the low output power of MMW solid state sources, MMW applications require antennas with high gain in order to compensate for the expected losses [104]. Dielectric resonators were investigated in the late 1960s, and have been used as high Q elements in microwave circuits such as filters, and oscillators. Moreover, dielectric resonators have been used as dielectric resonator antennas (DRAs) since the 1980s [75].

More recently, a new kind of antenna element, the dense dielectric (DD) patch antenna, has been introduced [24]. This advance allows a thin dielectric substrate of high permittivity to replace the metallic patch. In [93], a perforated superstrate was used to enhance the antenna gain as well as to improve the bandwidth. This antenna's radiated elements were 2×2 DD patch arrays. A highly reflective metamaterial surface was used as a superstrate over the antenna patch in [105], with a gain of about 12.5 dBi, and 3 dB gain bandwidth of about 10%. The linearly polarized antennas reported in [106] and [107] only offer low gain, and they use bulky multi-FSS layers. In [108], three layers of FSS superstrate were applied over a microstrip patch antenna to enhance the antenna performance, realizing an antenna gain of about 14.2 dBi, but with low radiation efficiency. A high-gain circularly polarized dielectric resonator antenna is reported in [109]. It uses an FSS superstrate to enhance the antenna gain, achieving a high gain of about 15.5 dBi.

An important drawback of the electromagnetic band gap (EBG) resonator antennas is the narrow frequency bandwidth due to their naturally narrowband resonant cavity. Several methods to improve the bandwidth have been published. A reconfigurable wide band partially reflective surface (PRS) antenna was implemented in [110] to function throughout a broad frequency range. In [111], the bandwidth of an EBG resonator antenna is improved up to 13.2 % by using a slot antenna array. However, the antenna structure and fabrication in both [110] and [111] are complicated, which is not a good match with the simplicity of the EBG resonator antenna. Based on the analysis in [51], a wideband EBG resonator antenna can be achieved if the reflection phase of the PRS increases linearly with frequency. Utilizing that observation, PRSs with positive reflection phase gradients were implemented using two dielectric slabs with an air gap spacing to produce wideband EBG resonator antennas [112]. Another approach utilized a dual-layer PRS to provide a positive phase gradient with a 2-D unit cell, the unit cell composed of two different FSSs [86]. A single layer of a PRS was applied over an inset-fed microstrip patch antenna to improve the antenna bandwidth and gain. The resulting antenna gain and bandwidth were 16 dB and 8.3%, respectively [113]. A PRS was directly placed over a fully reflective ground plane with a two-element patch array employed as a feeder. Its 3 dB gain bandwidths of 12.5% and 14.6% were obtained with peak realized gains of 15.1 and 14.8 dBi for the horizontal polarization (HP) and vertical polarization (VP), respectively [114].

In this thesis, two FSS superstrates, a highly reflective FSS superstrate and a superstrate with a positive reflection phase, are investigated, fabricated, and tested. High reflective unit cells are placed above a square dense dielectric (DD) patch antenna to enhance the antenna gain. A set of highly reflective unit cells is put over the DD patch as a superstrate layer to act as a lens to improve the antenna gain. A set of 7×7 unit cells with the positive reflection phase (PRP) feature are then applied over the same DD patch antenna to broaden the antenna's bandwidth.

2.7 Substrate Integrated Waveguide (SIW) Cavity Antennas

SIW cavity antennas are high performance broadband interconnect with excellent immunity to electromagnetic interference, suitable for use in the microwave and millimeter-wave applications. They are very low cost compared to classic milled metallic waveguides, as they may be developed using an inexpensive printed circuit board (PCB) fabrication techniques. The SIW cavity resonator design was first presented in [115], and later in [116]. Using the SIW technique, the general type

of bulky size, cavity can be replaced by a planar type of cavity resonator. Attractive system performances can be achieved by using SIW cavity resonators, especially given their ease of integration compared to the commonly-available planar PCB microwave resonators. Designing microwave oscillators with very low phase noise and compact high-gain antennas become easier due to the high-quality factor of waveguides based on SIW cavity resonators [117]. The advantages of the SIW approach are due to the antenna's planar form, its strength of construction, high power operation capability, high efficiency, small thickness, and light weight. The continuing progress in the development of such antenna arrays is essentially related to increase both their operating frequency and their bandwidth [118].

There are many techniques for enhancing antenna gain. For instance, array antennas that involve several radiated elements feeding simultaneously with a feeding network [26]. However, the losses from the feeding network and the mutual coupling phenomenon may degrade antenna performance [119]. In addition to array antennas, other means can be used to enhance the antenna gain and avoid a feeding network. A high gain of about 12 dBi at 31 GHz was obtained using a disc patch loaded by a metallic conical horn. However, this antenna has a relatively high profile and may not fit into MMW systems [120]. In [121], a hybrid resonator antenna was designed to increase the antenna gain. This antenna achieved a high gain of 11.9 dBi.

Circularly-polarized (CP) antennas have been widely used and are in high demand for many wireless communication systems, as they have several attractive benefits compared to linearly-polarized antennas [122]. A 4×4 U-slot circularly-polarized high gain patch antenna array was designed on low temperature co-fired ceramic (LTCC) at 60 GHz in [123]. However, it requires a feeding network, along with the associated losses. In [124], circular polarization with 12 dBi gain is achieved by implementing a 2×2 right-hand circularly polarized planar array. A subsequent effort using a 2×2 dual polarized patch array realized a gain of about 12.35 dB in [125]. However, this array requires dual feeding, which is rather complex. In [126], a 4×4 antenna array was designed on an LTCC ceramic, fed with a SIW for an antenna gain of about 12.5 dB. There are other approaches which can be used to achieve circular polarization, e.g., dielectric resonator antennas [127], helical antennas [128], and crossed dipole antennas [129]. All of these types of antennas suffer from several drawbacks, such as a non-planar profile, feeding network complexity, multiple layers, and low gain. A high gain CP antenna array is implemented in [130], but it has the complexity of multiple layers and an SIW feeding network. An X-shaped slot cut into the top

of a circular SIW cavity fed by a rectangular SIW waveguide is implemented in [131]. However, the gain is only about 6.7 dBi. In [132], circular polarization is achieved by using a polarization converter. The SIW cavity antenna is fed by a coaxial cable probe. The single feed allows a reduction in the complexity, weight, and losses for arrays, all of which are desirable in many MMW applications [133].

In this thesis, a high gain low profile circularly polarized SIW slotted cavity antenna is studied with the objective of overcoming some of its limitations in terms of size, feeding, and performance. A feeding network can be avoided when the implemented antenna is fed with a coaxial probe. The SIW technique is used to build the cavity in a single-layer substrate. The antenna polarization is changed from linear to circular polarization using a single-layer polarization converter which is placed efficiently above the SIW cavity antenna. High order modes (TE_{440}) is excited. This design provides both right- and left-hand circular polarization, as well as linear polarization, in addition to high gain and high radiation efficiency.

Chapter 3 High Gain Wide-Band Fabry-Pérot Cavity Antenna Based on a Dielectric PRS

3.1 Introduction

High gain and broadband antennas have been in the center of interest for various millimeter-wave (MMW) wireless applications. Several types of antennas have the ability to provide high gain radiation at high frequencies, such as reflector and array antennas. However, reflector antennas are bulky, and array antennas suffer from structural losses due to their feeding network/circuitry (especially for high-gain arrays that require a large number of elements). On the other hand, planar Fabry-Pérot cavity (FPC) antennas are known for their ability to produce highly-efficient directive radiation pattern [66], [134].

This chapter presents a perforated PRS superstrate and evaluates the effect of PRS permittivity on the FPC antenna performance. The limitation of the 3-dB gain bandwidth is one of the critical disadvantages of FPC antennas. Therefore, a unit cell composed of two thin dielectric slabs is investigated to expand the 3-dB gain bandwidth of the antenna, and the effect of the slab thickness on bandwidth gain is evaluated.

3.2 High gain low profile of High dense dielectric patch antenna using a holey superstrate

Gain enhancement and bandwidth improvement of a 2×2 square dense dielectric patch antenna using a holey superstrate is proposed. This aperture-coupled antenna is fed by a conventional power divider. A dielectric superstrate layer is utilized to enhance the antenna gain. Drilling a set of identical circular holes in the superstrate layer both improves the antenna's bandwidth and decreases the side lobe level. The proposed antenna was fabricated and tested. The prototype produces an impedance bandwidth of 15.35%, from 26.5 GHz to 30.8 GHz. The proposed antenna exhibits a flat measured gain of about 16 dBi over all the bandwidth, with a high simulated radiation efficiency of 92%. Furthermore, the side lobe levels are -15.8 dB and -21 dB in the E- and the H-plane, respectively.

To expand the antenna 3-dB gain bandwidth of the prototype antenna, a partially-reflective surface (PRS) of two thin perforated dielectric layers is proposed. This PRS is placed on a 2×2 high dense dielectric patch antenna array. The antenna is excited by an aperture coupling technique. This PRS

of two thin perforated dielectric substrate layers is designed to create a positive reflection phase gradient with high reflection to improve the antenna bandwidth and gain. A set of identical circular holes drilled in the PRS superstrate layers successfully alters the permittivity of the dielectric superstrate. As well known, the thickness of the conventional superstrate should be equal to one-quarter of the dielectric wavelength. However, in the proposed PRS of two thin perforated dielectric substrate layers has a thickness less than the quarter dielectric wavelength and provided good performance. The proposed antenna with this PRS yields a 3 dB gain bandwidth of 27 %, from 29 to 38 GHz. The proposed antenna also exhibits a high gain of about 16.8 dBi over all the bandwidth, with a high simulated radiation efficiency of 93.3%. Its side lobe levels are below −12 and −15 dB in the E- and the H-plane, respectively.

3.3 Design Methodology of the Fabry-Pérot Cavity Antenna with a Dielectric Superstrate

The proposed antenna design began with the design of a single patch element, a dense dielectric patch antenna with high performance in terms of gain and bandwidth. The next step was to make an array out of this single element. Two dielectric substrates were chosen for the antenna design: Rogers Duroid 6002 substrate as a top substrate underneath the DD patch, and Rogers RT 3010 as the bottom substrate for the feed line. The aperture feeding technique is used to feed the antenna, which is fed by etching the slot in the common ground plane directly under the radiated patch. Upon constructing the single element, a 2×2 DD patch array is designed with that single element to enhance the gain even further. A feeding network was designed to excite all the radiated elements. A perforated dielectric slab was designed as a superstrate and placed over the antenna array to enhance the antenna's performance. The dielectric superstrate's thickness was a quarter of the dielectric wavelength. The proposed antenna was designed and simulated using the CST software package.

3.4 DD patch antenna array with a conventional superstrate

3.4.1 Antenna Design and Configuration

The geometry of a 2×2 square DD patch antenna array with a conventional superstrate is illustrated in Fig. 3.1. The square DD patches are very low profile with a length Lp=4.1 mm and a height Hp=0.15 mm, with a relative permittivity of 82. The DD patches are designed on a Rogers Duroid 6002 substrate (top layer) with thickness h_1=20 mil, (ε_r=2.94 and tanδ=0.0009). The bottom

substrate is a Rogers RT 3010 with the same thickness as the top substrate. The two substrates have the same length and width (L=W= 20 mm). A 50 Ω conventional power divider is located on the bottom side of the bottom substrate. The aperture coupling feed method is used to excite the 2×2 DD patch antenna array. The coupling slot in the common ground plane between the two layers has a length L_s=2.55 mm and width W_s=0.25 mm. A superstrate dielectric layer with a relative permittivity of 10.2 and thickness h_s =0.64 mm is designed and applied over the 2×2 DD patch antenna array at a distance d=5.32 mm above the DD array.
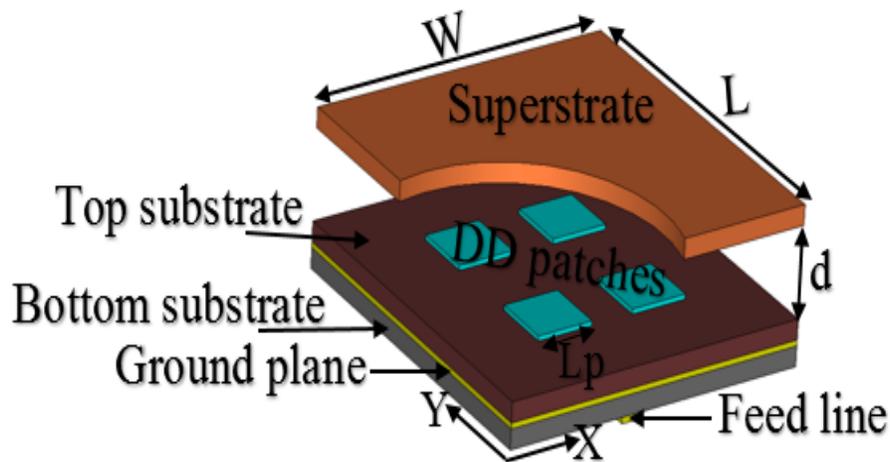
Figure 3.1: Geometry of the 2×2 DD patch antenna array: side view. Superstrate is partly removed to show the patches under it [93].

3.4.2 Simulated Results

The implemented antenna is simulated using the CST software package. The simulated reflection coefficient of the antenna is illustrated in Fig. 3.2. The DD patch antenna array with a conventional superstrate shows a good matching with about a 7.1 % bandwidth.
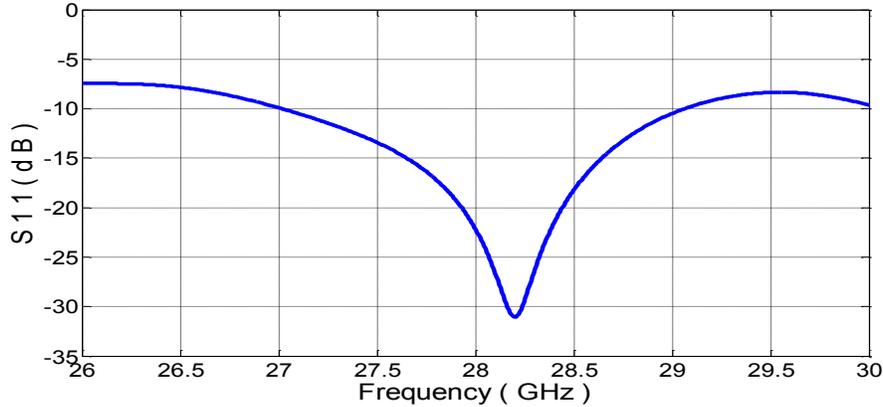
Figure 3.2: Reflection coefficient of the simulated 2×2 DD patch antenna array with a conventional superstrate [93].

Fig. 3.3 illustrates the simulated E- and H-plane patterns at 28 GHz with side lobe levels of -14.5 dB and -15.8 dB, respectively.
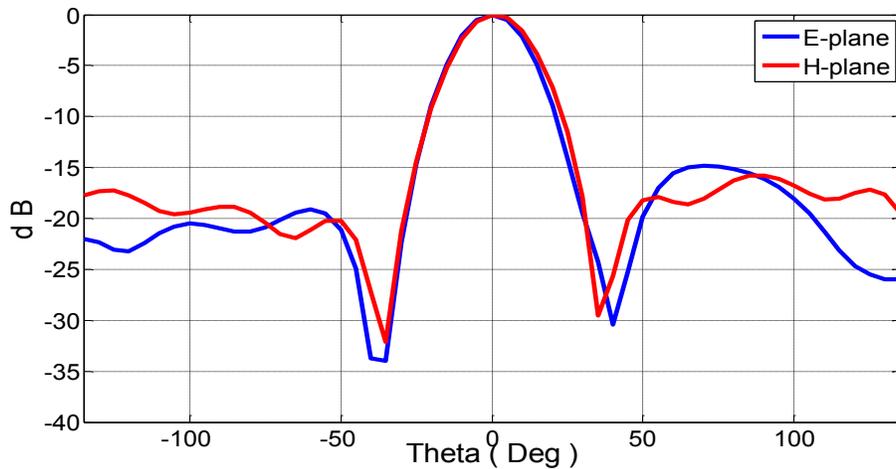
Figure 3.3: E- and H-plane radiation patterns of the simulated 2×2 DD patch antenna array with a conventional superstrate [93].

3.5 Dense Dielectric Patch Antenna Array with a Holey Superstrate

3.5.1 Principle and Antenna Design

As is well known, a Fabry-Pérot cavity (FPC) antenna is built from two reflectors, a partially reflective surface (superstrate cover) and the ground plane. The air gap distance between the two reflector plates should be close to a multiple of a half wavelength ($\lambda_0/2$) in order to enhance the antenna directivity by means of in-phase waves. Therefore, when the waves radiated by the antenna

source, which is a dense dielectric patch in our proposed design, towards the partially reflective surface, a perforated dielectric slab in this work, the PRS plate reflects the waves back, and then the ground plane re-radiates all the waves to the broadside direction. Thus, maximum directivity can be achieved using a strong superstrate reflectivity. However, high superstrate reflectivity results in a high Q-factor, which will lead the FPC antenna to provide a high directivity with a narrow-band (See Chapter 2.3). Therefore, a perforated dielectric superstrate is proposed here, as it reduces the slab permittivity while decreasing the superstrate reflectivity, and therefore dicreasing the Q-factor. This results in enhanced antenna bandwidth as well as improved sidelobe levels.

(a)   (b)

(c)
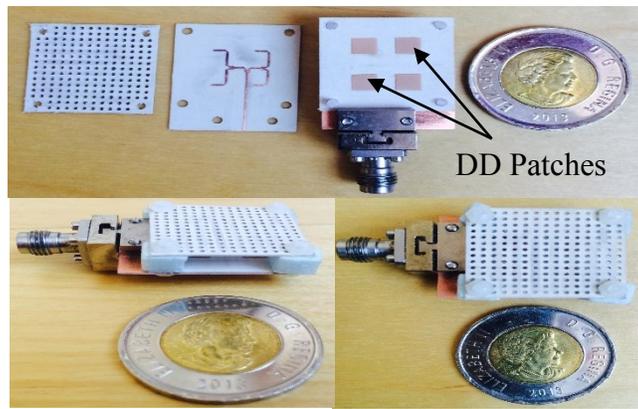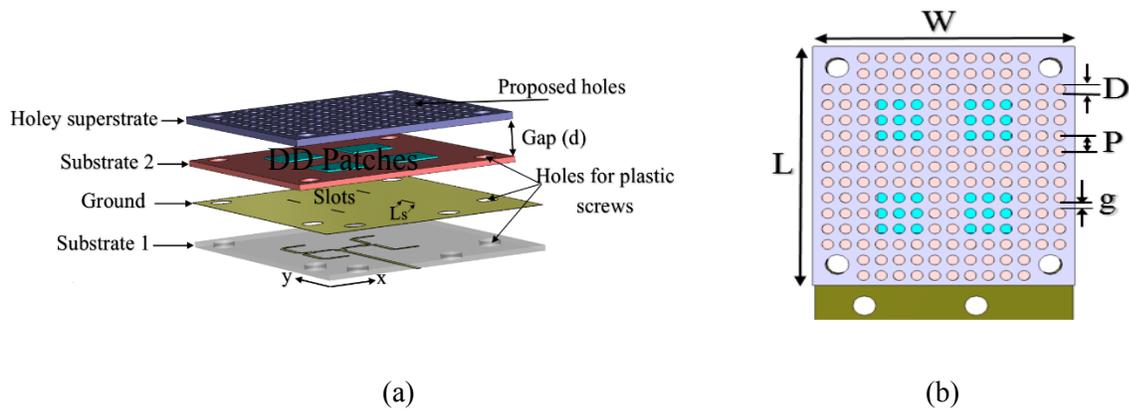
Figure 3.4: Geometry of the proposed antenna: (a) side view, (b) top view, and (c) photographs of the antenna prototype [93].

Fig. 3.4 shows the configuration of the implemented DD patch antenna array. Using the same size of the above DD square patch antenna array, a 2×2 identical dense dielectric square patch antenna array with a holey superstrate is proposed. A simple conventional feeding network is designed to feed the proposed DD patch array. The dielectric substrate layer is perforated by a set of identical periodical circular holes of diameter D (with period P) placed along the x and y-axes. The antenna layers with DD patches together with top and side views of the fabricated prototype are shown in the same figure. Furthermore, plastic screws and foam material are used to maintain a gap (d) between the antenna and the superstrate. Drilling holes on the dielectric layer alters the effective permittivity of the material. The effective relative permittivity of the holey superstrate layer is calculated as given below [138]:

$$\varepsilon_{eff} = \varepsilon_r * \left(1 - \frac{\pi}{2} * \left(\frac{D}{D+g}\right)^2\right) + \frac{\pi}{2} * \left(\frac{D}{D+g}\right)^2 \tag{3.1}$$

Fig. 3.5 illustrates the dependence of the calculated effective permittivity on the hole diameter (D). The optimized antenna parameters are listed in Table 3-1.
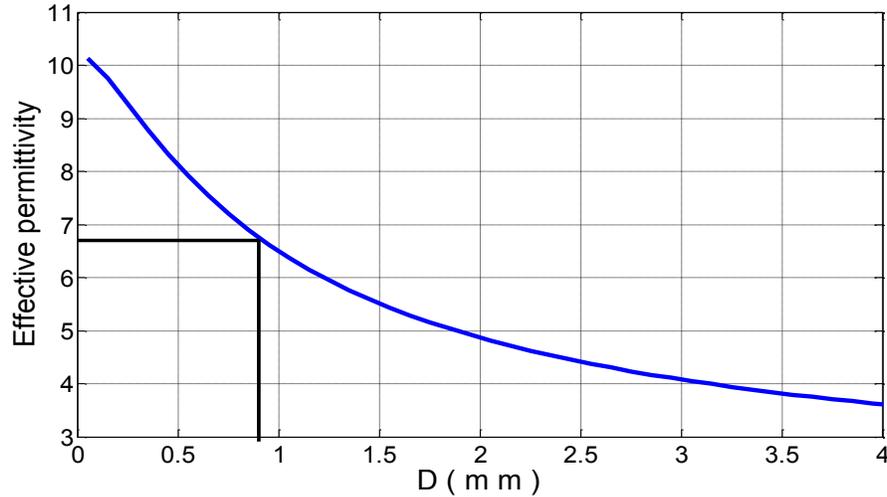
Figure 3.5: Calculated effective permittivity of the superstrate layer [93].

Table 3-1: The optimized parameters of the proposed antenna.

Parameter	Values (mm)	Parameter	Values(mm)
L	24	L_s	2.55
W	22	d	5.4
P	1.56	Slot width	0.15
D	0.9	g	0.66

A parametric study was conducted to study the effect of the hole diameter D on the performance of the proposed antenna. As can be seen from Figs. 3.6 and 3.7, as D increases, a good impedance matching, and a flat gain is obtained, along with a reduction in the side lobe levels. In addition, the size of the drilled holes also has a significant effect on the antenna resonance and gain, as well as on the effective permittivity of the superstrate. Holes drilled in the superstrate with ε_r=10.2 resulted in an effective permittivity of about 6.7. That result allowed for an antenna resonance frequency at 28 GHz and flat gain of 16 dBi, along with a 15.35 % bandwidth. Moreover, it was found, but not shown here, that the gap d between the antenna and the superstrate has a significant effect on the resonance of the antenna, and less effect on the antenna gain. As d increases, the resonance frequency is shifted downwards, and vice versa.

3.5.2 Antenna Array with a holey superstrate performance

To verify the simulated results, a 2×2 square DD patch array antenna with a perforated superstrate was fabricated and tested. Fig. 3.8 shows the simulated and measured reflection coefficients of the proposed antenna. They exhibit a wider bandwidth of 15.35 % from 26.5 GHz to 30.8 GHz. It can be observed that there is a frequency shift between the measured and the simulated results considering the manufacture rated value (at 10 GHz) of the relative permittivity for all layers. However, at MMW frequencies, the value of ε_r is typically different, which may contribute to the shift in the resonance frequency [139].
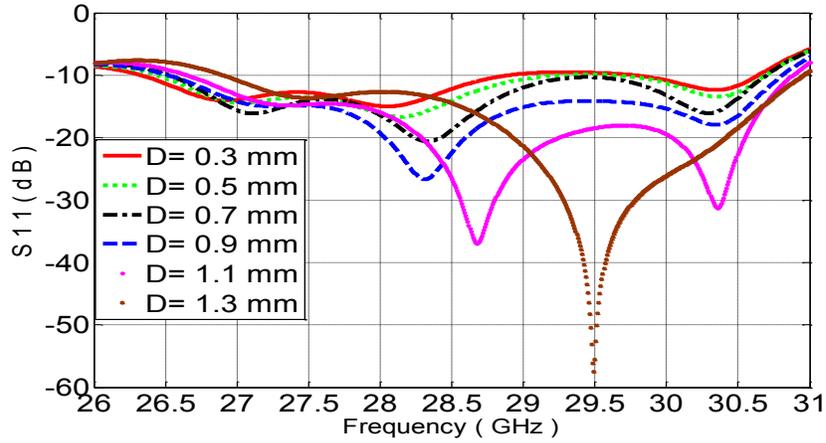
Figure 3.6: Simulated reflection coefficient of the antenna considering the effect of varying the diameter of the holes on the superstrate layer [93].
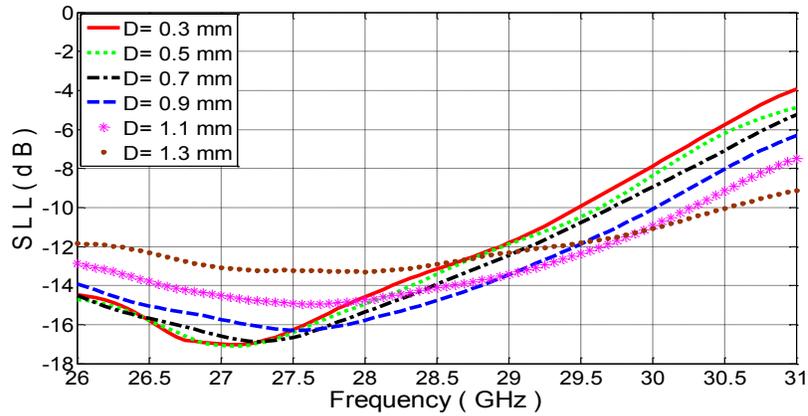
(a)
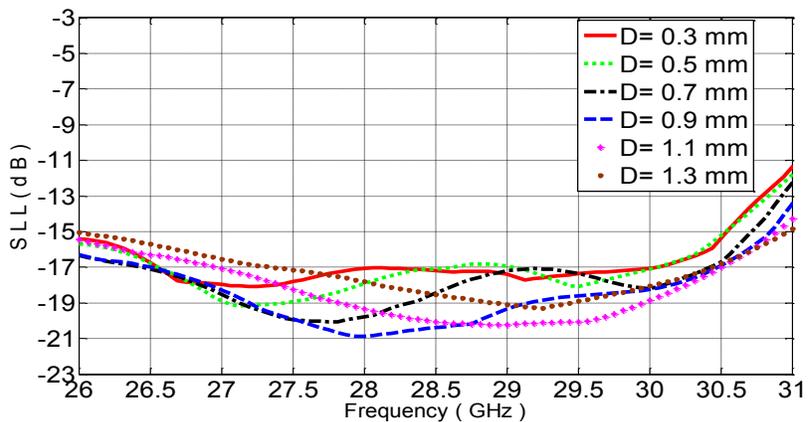
(b)

Figure 3.7: Simulated side lobe level in the E-plane (a) and in the H-plane (b) of the proposed antenna considering the effect of varying the diameter of the holes on the superstrate layer [93].
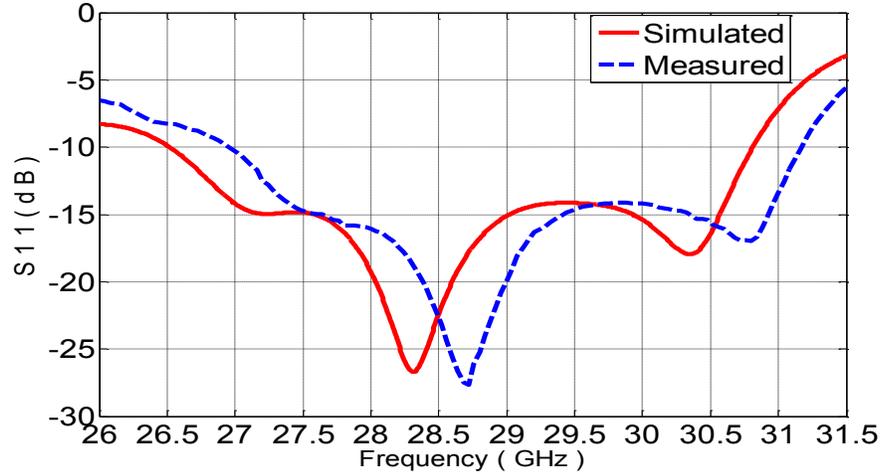
Figure 3.8: Measured and simulated reflection coefficients of the proposed antenna [93].

The simulated and measured gain and the simulated radiation efficiency of the implemented array with a holey superstrate are depicted in Fig. 3.9. The gain and radiation efficiency of the 2×2 DD patch antenna array with a conventional superstrate is also introduced in the same figure for comparison. The magnitudes of the E-field distribution of both antennas are illustrated in Fig. 3.10. Both the measured and simulated results of the antenna gain are in good agreement. An almost-flat gain is achieved over the band where the peak gain about 16 dBi. The simulated radiation efficiency of the antenna is almost 92 % over the bandwidth. As shown in Fig. 3.10, flat radiation efficiency is achieved.
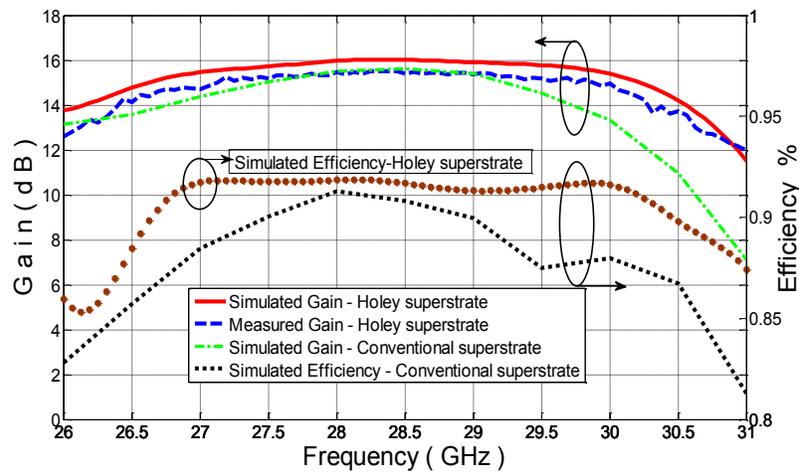
Figure 3.9: Simulated and measured gain and simulated radiation efficiency of the implemented antenna compared to the DD patch array with a conventional superstrate [93].

35
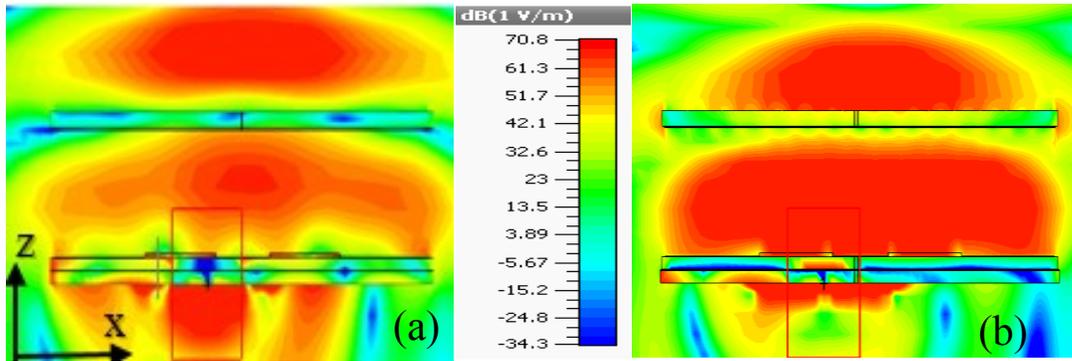
Figure 3.10: Magnitude of the E-field distribution of DD patch antenna array with a conventional superstrate (a) and with a holey superstrate (b) at 28 GHz [93].

Fig. 3.11 shows the simulated and measured radiation patterns of the proposed square DD patch antenna array at different frequencies. The antenna has good radiation patterns. The side lobe levels are about -15.4 dB, -15.8 dB, -13.3 dB, and -9.9 dB in the E-plane radiation pattern at frequencies 27 GHz (not shown here), 28 GHz, 29 GHz, and 30 GHz, respectively. Furthermore, in the H-plane the SLLs are about -18.2 dB, -21 dB, -19.1dB, and -18.5 dB at frequencies 27 GHz (not shown here), 28 GHz, 29 GHz, and 30 GHz, respectively.
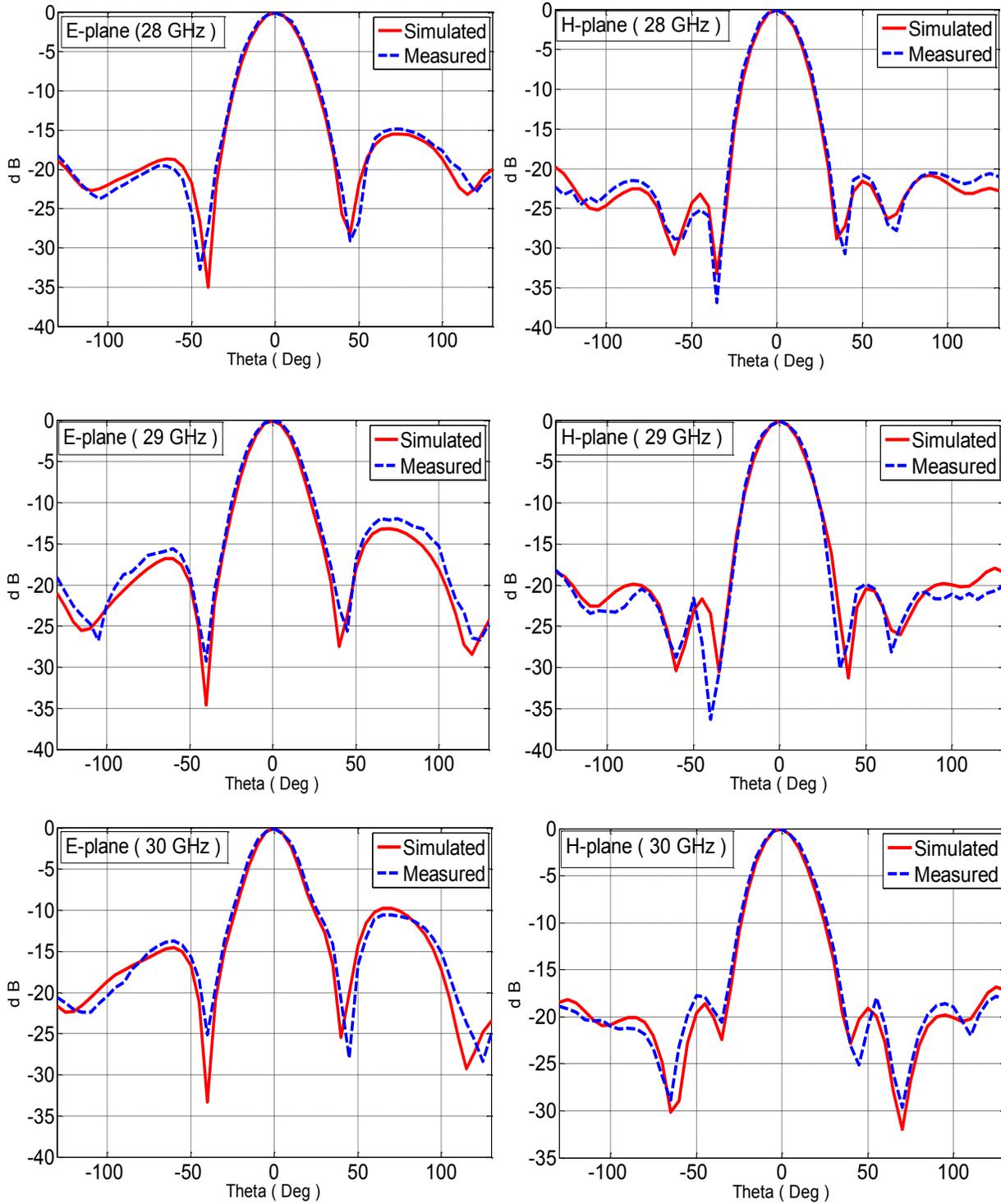
Figure 3.11: Simulated and measured radiation patterns of the DD patch antenna array with a perforated superstrate [93].

3.6 Dense Dielectric Patch Antenna Array with a PRS composed of Two Thin Perforated Dielectric Slabs

The use of millimeter-wave (MMW) frequencies for future wireless communications (5G) has become a very popular research area for antenna designers due to the narrow spectrum below 6 GHz bands and 5G's need for higher data rate, high speed, and low latency [4]. Several types of antennas have been used to provide the level of performance needed to meet 5G requirements. Fabry-Pérot cavity (FPC) antennas have been widely utilized for their ability to broaden the antenna bandwidth while obtaining high directivity [28], [140].

The FPC antenna presented earlier in this chapter is based on a perforated single layer highly reflective PRS. The antenna result was a moderate gain and bandwidth. In this approach, the single layer perforated superstrate provides just one resonance where the reflection phase of the superstrate decreases with the frequency. The reflection phase intersects with the optimum phase at only one point, and so the antenna bandwidth is only 15.35%. The narrow band issue could be addressed by introducing a PRS composed of two thin perforated dielectric slabs.

A partially reflective surface (PRS) of two thin perforated dielectric substrate layers is therefore proposed and designed to create a positive reflection phase gradient with high reflection to improve the antenna bandwidth and gain. A set of identical circular holes drilled in the PRS superstrate layers plays a significant role in altering the permittivity of the dielectric superstrate. The thickness of the two superstrates could be different and also could be the same as will be shown later in our design. In the literature, the thickness of the conventional superstrate should be equal to one-quarter of the dielectric wavelength. However, in the proposed design, a PRS of two thin perforated dielectric substrate layers is utilized as a superstrate to broaden the bandwidth and to enhance the antenna gain. The antenna is excited by an aperture coupling technique. The proposed antenna yields a 3 dB gain bandwidth of 27 % from 29 to 38 GHz and a high gain of about 16.8 dBi over all the bandwidth, with a high simulated radiation efficiency of 93.3%. Furthermore, the side lobe levels of the proposed antenna are below −12 and −15 dB in the E- and the H-plane, respectively.

3.6.1 Design Methodology of the Implemented antenna

The design methodology of this proposed antenna is similar to the methodology presented in section 3.3. However, the partially reflective surface (PRS) that covers the DD patch array in this design is built from two thin perforated dielectric substrates. The bottom slab is constructed from a Rogers RO 3006 with $\lambda d/6$, and the top layer is made from a Rogers RO 3010 with the same thickness of the bottom substrate. Initially, the distance between the two slabs was $\lambda_0/2$ when the dielectric slab thickness was $\lambda d/4$. This distance was optimized to compensate for the decrease of the slab thickness. The CST software package simulator was used to design and simulate the proposed antenna.

3.6.2 Design of a PRS with a Positive Phase Gradient

This section presents the design of the unit cell of the PRS to be used as a superstrate of the DD patch antenna array. The composed unit cell dimensions are selected carefully to achieve a positive gradient in the reflection phase response where the positive phase gradient is required to broaden the antenna bandwidth. The unit cell is composed of two thin unprinted perforated dialectic slabs, as illustrated in Fig. 3.12. They are perforated to control the effective permittivity of the two substrates. As is common knowledge, a conventional dielectric superstrate should have a thickness of $\lambda_d/4$, and should be located at $\lambda_o/2$ above the antenna to achieve the goals of enhancing the gain or of broadening the bandwidth. However, in this proposed design, two thin dielectric substrates are used to build the PRS superstrate. Therefore, to compensate for the thickness, the height h_{c1} is added to $\lambda_0/2$ between the two layers of the PRS. A specific air gap thickness (h_{c1}) is added to the $\lambda_0/2$ between the PRS superstrate and the antenna elements. The unit cell was designed and simulated using the full-wave electromagnetic simulation tool CST software package.
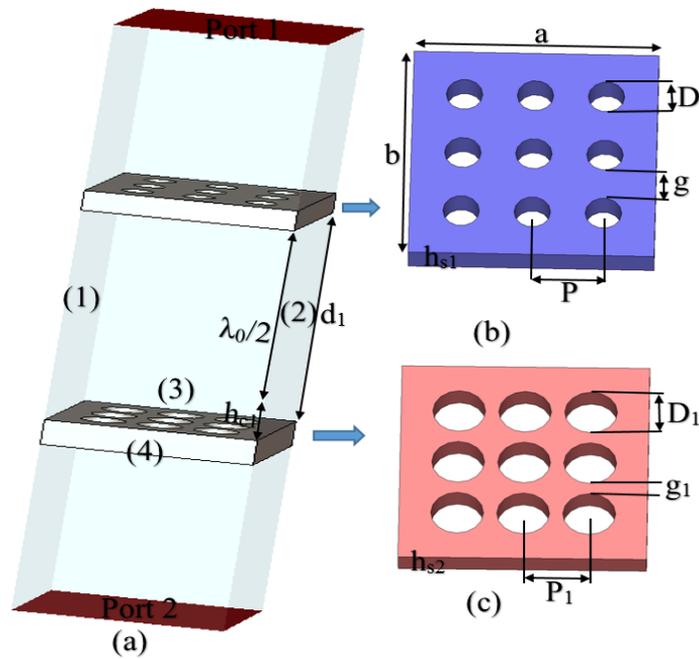
Figure 3.12:   Geometry of the proposed unit cell: Characterization model of the unit cell (a), top substrate (b), and bottom substrate (c).

Periodic boundary conditions can be applied to the four side walls of a unit cell, as shown in Fig. 3.12(a). Boundaries 1 and 3 are set as perfect electric conductors (PEC), and boundaries 2 and 4 are set as perfect magnetic conductors (PMCs).

The effective permittivity of the top substrate is 8, and the permittivity of the bottom substrate is 4. Fig. 3.13 illustrates the dependence of the calculated effective permittivity on the hole diameter (D, D_1).
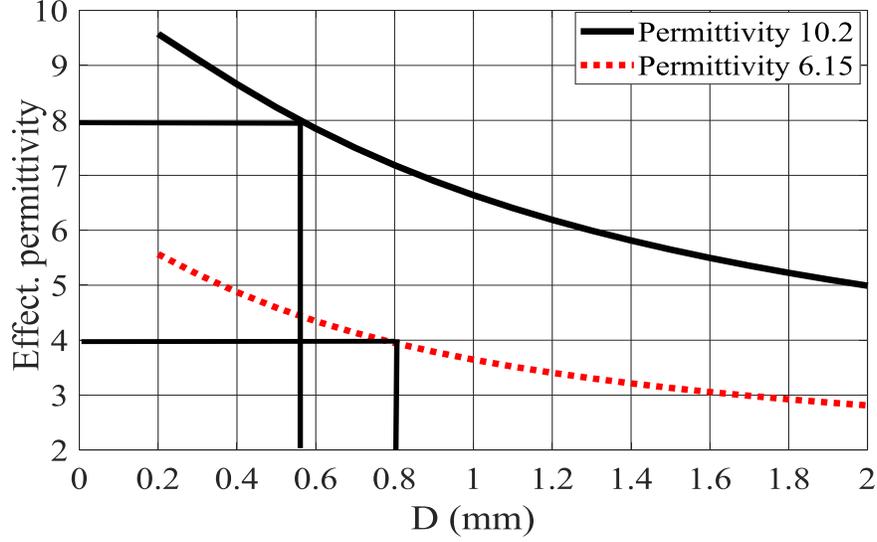
Figure 3.13: Calculated effective permittivity of the PRS slabs.

When the PRS is applied at the resonant distance d from the radiated antenna, the gain of the antenna is significantly enhanced. The rays released by the radiating antenna are reflected multiple times between the PRS and the ground plane, and with decreasing amplitudes. As a result, constructive interference occurs, and the antenna directivity is enhanced when the resonance distance d (air gap) is equal to [86]

$$d = \frac{\lambda}{2} * \left(\frac{\Phi}{2\pi} + 0.5 \right) + N * \left(\frac{\lambda}{2} \right) \qquad (3.2)$$

where Φ is the reflection coefficient phase of the PRS, λ is the free space wavelength, and N is the resonant mode order. The ground plane and the PRS are assumed to be of infinite size. Equation (3.2) can be written as:

$$\Phi = \frac{4\pi d}{c} * f - (2N - 1)\pi \qquad (3.3)$$

where f is the frequency and C is the speed of light in a vacuum. The optimum phase of the PRS can be achieved by using equation (3.3). This optimum phase indicates that high gain and wide bandwidth can be obtained by utilizing a PRS that has a reflection phase which increases with frequency.

The proposed unit cell is constructed of two thin dielectric substrates with different permittivities. The top dielectric substrate is a Rogers RO 3010 (εr = 10.2 and $\tan\delta$ = 0.0023) with effective

permittivity of about 8 and thickness h_{s1} = 20 mils and the bottom substrate is a Rogers RO 3006 (εr = 6.15 and tanδ = 0.0009) with effective permittivity of about 4 and thickness h_{s2} = 20 mils. The optimized dimension values are given in Table 3-2. The implemented unit cell was simulated using the CST software package, where a plane wave is normally incident on the bottom face of the bottom substrate. Fig. 3.14 shows the magnitude and phase of the reflection coefficient of the proposed unit cell.

Table 3-2: The proposed unit cell's optimized parameters.

Parameter	Values (mm)
a	4.7
b	4.7
P	1.36
D	0.7
g	0.66
P_1	1.25
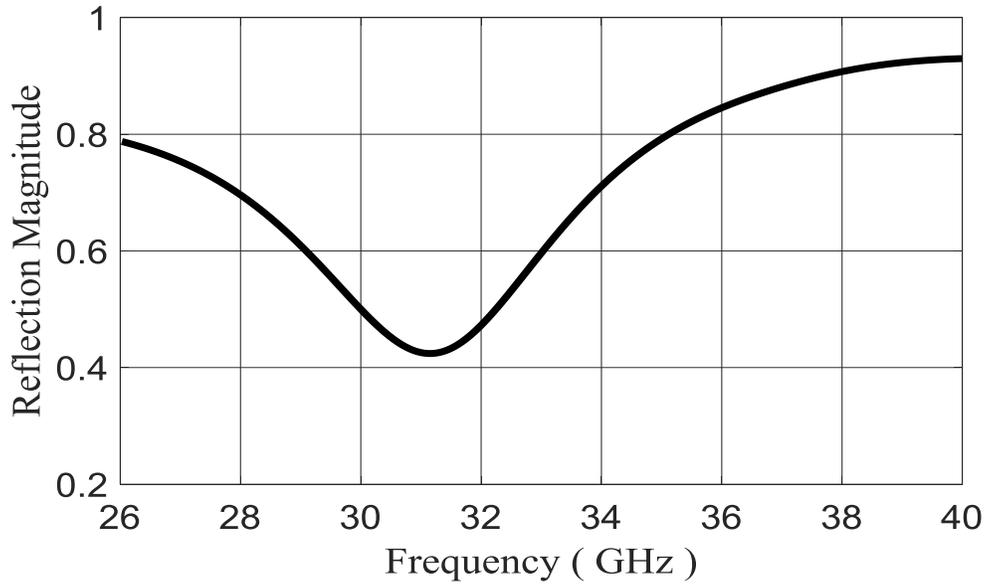
(a)
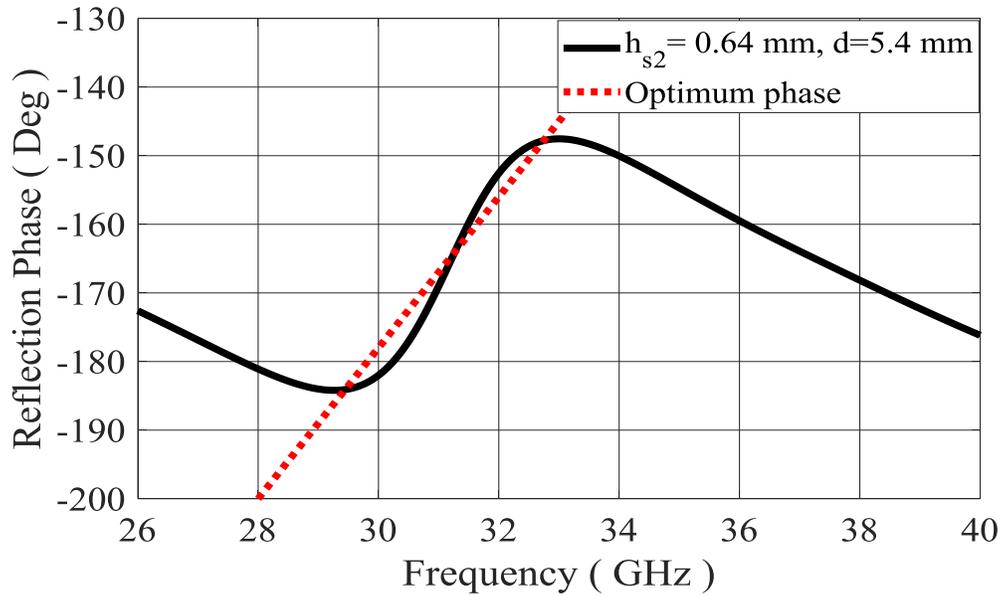
(b)

Figure 3.14:   The magnitude (a), and reflection phase (b) of the proposed unit cell.

A parametric study was conducted to evaluate the effect of the bottom substrate thickness h_{s2} of the proposed unit cell on the unit cell performance. Fig. 3.15 shows the effect of altering the bottom substrate thickness of the unit cell from one quarter dielectric wavelength to smaller thicknesses on the PRS performance. The thicknesses $\lambda_d/4$=0.8 mm, $\lambda_d/6$= 0.64 mm, and $\lambda_d/9$= 0.36 mm of the bottom dielectric substrate were considered to determine the effect of the

superstrate thickness. It is clear that the results from cases $\lambda_d/6$ and $\lambda_d/4$ show almost the same behavior in terms of the reflection magnitude and reflection phase. The thickness $\lambda_d/9$ provides a positive reflection phase where the reflection phase increases with a frequency within the desired band. The $\lambda_d/6$ thickness was selected for the proposed unit cell. That substrate was perforated to obtain a relative permittivity of 4 at the designed thickness. A compensation height, h_{c1}, was added to the air gap d_1, which is equal to $\lambda_0/2 + h_{c1}$ as the bottom substrate thickness is decreased. With the $\lambda_d/6$ thickness of the bottom substrate, $h_{c1} = 0.7$ mm was added, where h_{c1} is zero in the case of $\lambda_d/4$. d_1 is the overall height between the two thin substrates of the proposed unit cell. The compensation height h_{c1} is inversely proportional to the bottom substrate thickness. The same procedure was conducted between the top substrate and the radiating source, the DD patch array.
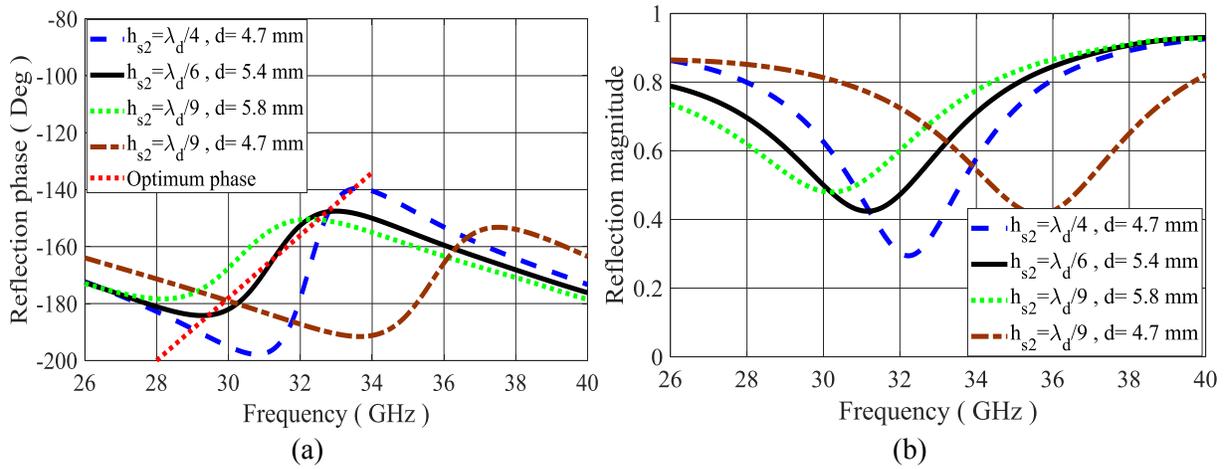
Figure 3.15:   Effect of changing the bottom substrate thickness of the proposed unit cell on the PRS performance: reflection phase (a), and reflection magnitude (b).

3.6.3 Antenna Design
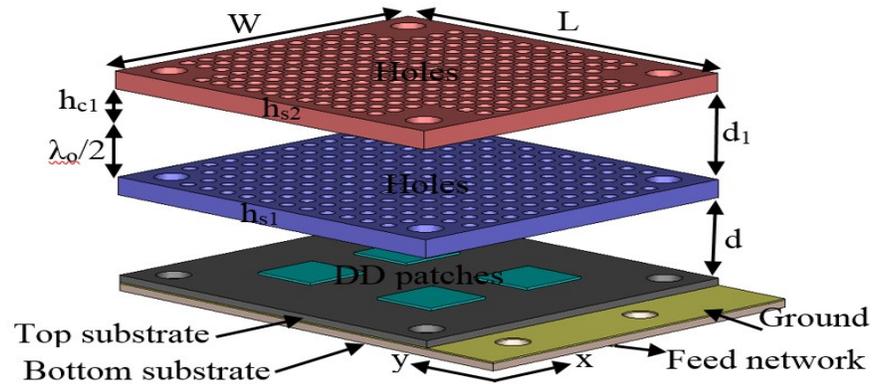
Figure 3.16: Geometry of the proposed antenna: side view.

Fig. 3.16 shows the wideband-high gain of a 2×2 high dense dielectric patch array antenna with two thin PRS superstrate layers. The proposed PRS superstrate is applied over the DD patch array at a distance d= 5.7 mm. The optimized parameters are listed in Table 3-3.

Table 3-3: The optimized parameters of the implemented antenna.

Parameter	Values (mm)
L_p	3.8
H_p	0.15
L	19
W	18
L_s	2.1
W_s	0.14

3.6.4 Antenna Results

The proposed antenna was simulated using the CST software package. The simulated reflection coefficient of the antenna is depicted in Fig. 3.17. A 3-dB gain bandwidth of 27 % from 29 GHz to 38 GHz was achieved. The simulated gain and radiation efficiency of the implemented array with a thin PRS superstrate are depicted in Figure 3.18. The antenna's highest gain was 16.8 dBi.
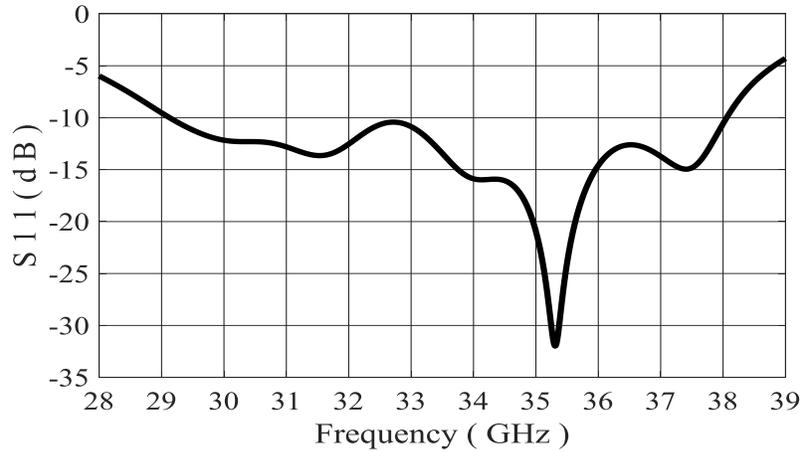
Figure 3.17: Simulated reflection coefficient of the proposed antenna with a thin PRS superstrate.

(a)   (b)
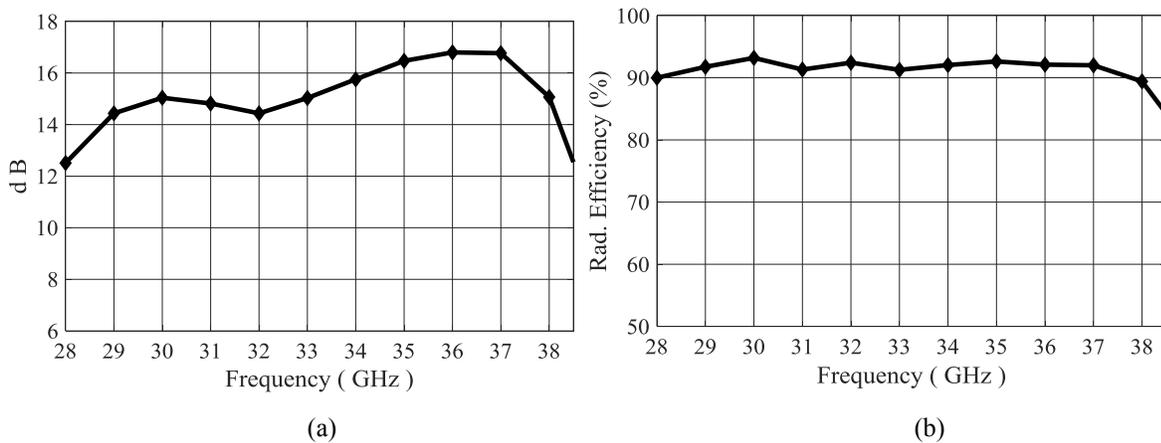
Figure 3.18: Simulated gain (a), and radiation efficiency (b) of the proposed antenna with a thin PRS superstrate.

Fig. 3.19 shows the simulated radiation pattern of the proposed DD patch array with a thin PRS superstrate at different frequencies. The antenna produces good radiation patterns. The SLLs are about −18, −13.5, −14.9, and −12 dB in the E-plane radiation pattern at frequencies 29.5, 32, 35, and 37, respectively, and close to −17, −18, −21, and −15 dB at frequencies 29.5, 32 35, and 37 GHz, respectively in the H-plane. 3D images of the radiation patterns at 30, 33, and 36 GHz are shown in Fig. 3.20.
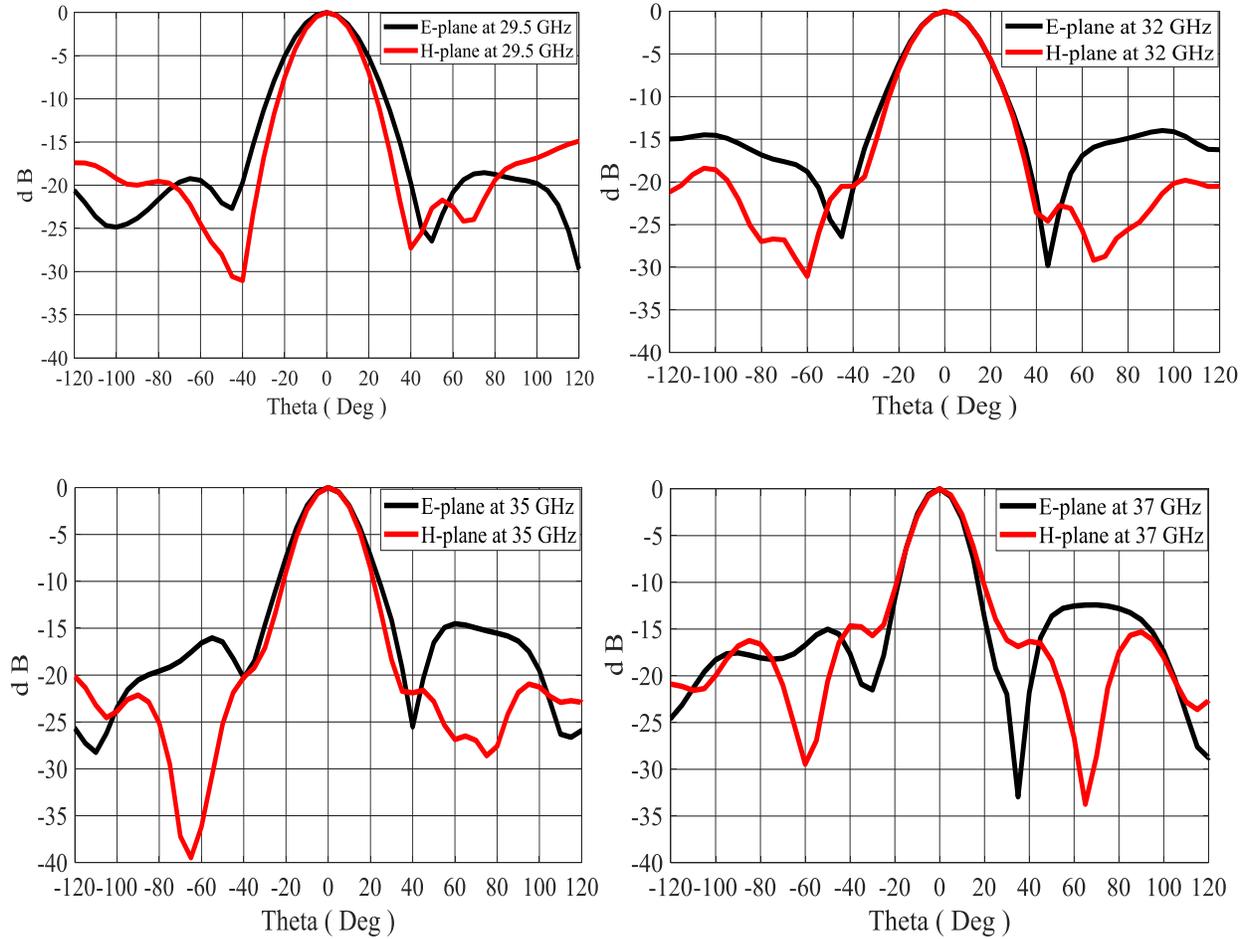
Figure 3.19: E and H-plane radiation patterns of the proposed antenna with a thin PRS superstrate at different frequencies.
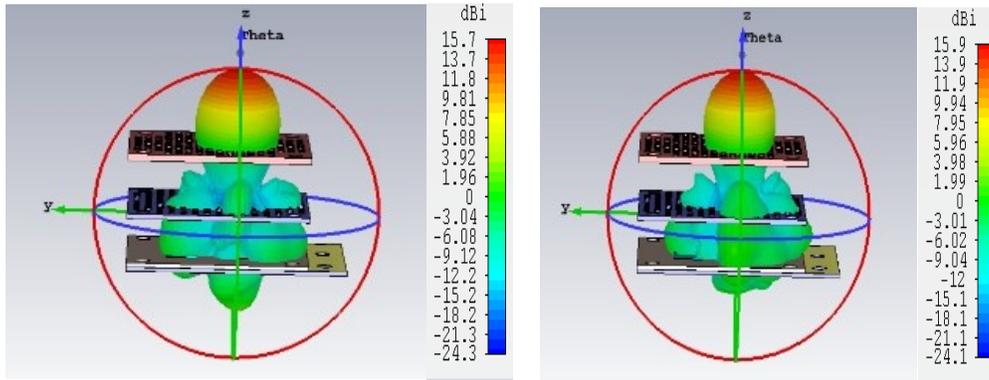
(a) at 30 GHz

(b) at 33 GHz
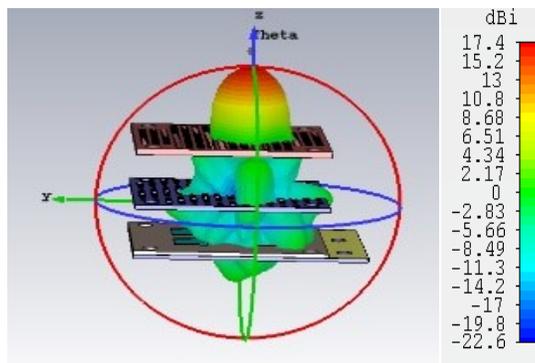
(c) at 36 GHz

Figure 3.20: 3D radiation patterns of the proposed antenna with a thin PRS superstrate at different frequencies.

To demonstrate the improved characteristics of the proposed antennas, a comparative study of the proposed designs' and those of several published works is presented in Table 3-4. This data clearly shows that the proposed antenna provides good performance in terms of gain and the 3 dB gain bandwidth compared to other relevant works.

Table 3-4: Performance comparison of our proposed design with designs in the literature.

Ref. Nº	Freq. (GHz)	Max. Gain (dBi)	3dB Gain BW %	Substrate Type	Antenna element
[38]	15	14.9	9	Dielectric slab(One Layer)	Waveguide
		17.5	17.9	Dielectric slab(Two Layers)	
[86]	60	16	12.2	FSS(Two layers)	Slot antenna
[143]	13.7	16.3	10.9	FSS (Three layers)	Slot antenna
This work	**28**	**16**	**15.35**	Dielectric slab (One Layer)	DD patch Antenna
	Ka-band	**16.8**	**27**	Dielectric slab (Two Layers)	DD patch Antenna

Chapter 4 Gain and Bandwidth Enhancement Based on Tapered Superstrate

4.1 Introduction

Wireless communication systems are in high demand for future fifth generation (5G) millimeter wave (MMW) applications. Modern communication systems require compact size and light weight with good performance. The need for wide gain bandwidth has been increasing throughout the development of wireless device technology. Meeting this growing need for high bandwidth is a difficult problem in the low frequency spectrum. Therefore, researchers have begun to investigate and exploit the millimeter-wave available around 30 GHz [87]. Fabry-Pérot Cavity antennas (FPCa) have attracted significant attention as they provide high-gain performance, wide bandwidth, high efficiency, and a low-complexity feeding network [89].

In this chapter, a single unprinted dielectric tapered superstrate is proposed to improve the antenna performance in terms of gain, wideband, and sidelobe levels (SLLs). A low profile high dense dielectric DD patch antenna with a relative permittivity of 82 is used to excite the resonant cavity antenna instead of a microstrip patch. An aperture feeding slot is used to couple the DD patch. A single unprinted tapered dielectric layer is designed and placed above the DD patch antenna to enhance the antenna gain towards the broadside direction, broadening the bandwidth and reducing the side lobe levels. This dielectric layer is designed to compensate the phase along the superstrate by making the permittivity of the single slab superstrate high in the center, decreasing gradually toward the edges. Drilling holes in the dielectric substrate can alter the effective dielectric constant to match the required permittivity in each zone. This implemented antenna meets some of the MMW applications, and it provides higher flat gain, wider bandwidth, low side lobe level, and high radiation efficiency.   Beam steering is also targeted by using this proposed superstrate, as will be shown later.

4.2 High Gain of Low Profile High Dense Dielectric Patch Antenna using Tapered Dielectric Superstrate

Modern communication systems are drifting toward small sized high gain antennas and high data bit rates as solutions to accommodate the future application requirements such as 5G wireless communications. A high gain wideband low profile high dense dielectric (DD) patch antenna using a tapered dielectric superstrate is presented, designed, fabricated and tested. This antenna is

implemented to achieve high flat gain, wide bandwidth, and low side lobe levels. The proposed structure employs a square high dense dielectric (DD) patch. The radiating DD patch is coupled to a 50-ohm microstrip line through a rectangular-shaped slot etched on the common ground plane. A flat single layer of a tapered unprinted dielectric superstrate is designed and placed above the DD patch antenna at almost a half wavelength from the ground plane. The relative permittivity is maximum in the center of the superstrate, decreasing gradually toward the edges to correct the phase along the superstrate every 90°. The measured impedance bandwidth of the proposed antenna shows a 16 % bandwidth. The proposed antenna exhibits a flat gain of about 17.6 dBi, high radiation efficiency, and promising side lobe level in both planes over all the bandwidth. Also, using the tapered superstrate, the antenna beam is steered from -30° to 30° with good performance in terms of gain, and side lobe levels

4.3 Modelling and Analysis

The conventional dielectric superstrate provides a non-uniform phase and it does not support the phase compensation. However, designing a Fabry Perot cavity antenna with a tapered superstrate can compensate for the phase different paths. Therefore, the forward radiation will be enhanced and will be almost flat. The proposed antenna is designed with two reflectors which are the tapered dielectric superstrate and the ground plane, and a high dense dielectric (DD) patch antenna. The tapered superstrate is constructed from different relative permittivity materials where the effective permittivity is high in the center of the superstrate layer and decreased gradually moving toward the edge. The tapered superstrate is also known as a partially reflective surface (PRS) used as a transmitting window which allows partial transmission of the electromagnetic wave. As well-known principle from the Fabry-Perot cavity (FPCA) design is that the incident waves transmit through the dielectric superstrate and are then reflected by the ground plate. A conventional superstrate provides a non-uniform phase distribution along the superstrate layer, which affects the gain enhancement. Therefore, a tapered superstrate is needed; a superstrate with the ability to correct the phase to be almost uniform. The proposed tapered superstrate is designed to assure that the phase variation along the tapered superstrate is between 0 and 90° instead of between 0 and 180°. Thus, almost all the transmission of the electromagnetic wave through the proposed tapered superstrate is in phase. The tapered superstrate, designed from four different relative permittivities, can compensate the phase every 90°. Therefore, the reflection will vary along the composite

51

superstrate layer so that the reflection is high at the center of the antenna (low transmission) and low at the antenna edges (high transmission). As a result, the antenna gain is increased considerably, the gain bandwidth is enhanced, and the side lobe levels are improved as well. The proposed superstrate should be placed at a half-wavelength from the ground plane in this design, as explained by the Fresnel concept [141].

Much better results could be achieved by making the transition in the relative permittivity move smoothly from 10.2 to 2.2. However, this will result in several rings with different permittivity and with very small radii, making the antenna fabrication extremely difficult. Instead, the antenna dimensions are carefully designed, and the antenna materials are chosen with care. Acid is used to remove the copper instead of a machined step to achieve better results.

4.4 Tapered Superstrate Design
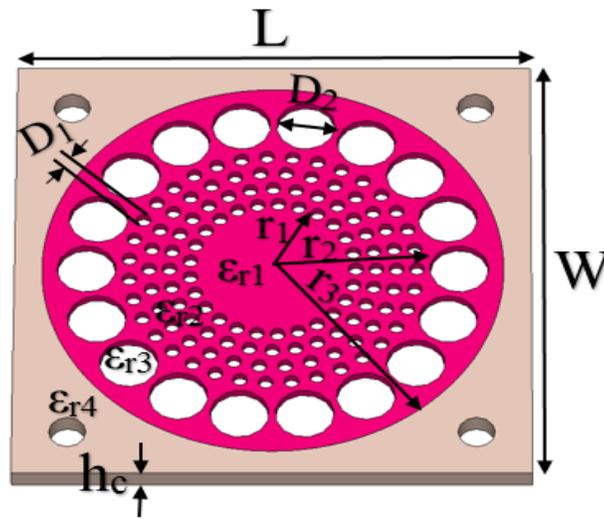
Figure 4.1: The geometry of the proposed tapered superstrate.

A tapered superstrate is proposed and designed to correct the phase, as illustrated in Fig. 4.1. This tapered superstrate is designed according to the following procedure. The thickness of the tapered superstrate h_c is determined based on equation (4.1) [141].

$$h_c = \frac{3\lambda_0}{P\left(\sqrt{\varepsilon_r} - \sqrt{\varepsilon_{min}}\right)} \qquad (4.1)$$

where λ_o is the free space wavelength at 28 GHz, ε_r and ε_{min} are the maximum and minimum permittivity of the superstrate and P is the phase correction value, determined by 360°/P; for 90° phase correction, P= 4. After selecting both the maximum and minimum relative permittivities, which are 10.2 and 2.2 in this design, the superstrate thickness is calculated and found to be 4.2 mm. The rest of the relative permittivities can be obtained depending upon the superstrate thickness and P, according to equation (4.2) [141]:

$$ h_c = \frac{\lambda_0}{P\left(\sqrt{\varepsilon_i} - \sqrt{\varepsilon_{i-1}}\right)} \quad , i = 2,3 \dots \quad (4.2) $$

where ε_i is the minimum dielectric constant, which is equal to 2.2. Equation (4.3) [141] can be used to calculate the radius r_i of each relative permittivity of the proposed superstrate.

$$ r_i = \sqrt{\left(2d\frac{\lambda_0}{P}i + \left(\frac{\lambda_0}{P}i\right)^2\right)} \quad , i = 1,2, \dots \quad (4.3) $$

The requires radius r_i, and ε_{eff} of each zone are shown in Table 4-1.

Table 4-1: The required radius and permittivites.

i	radius (mm)	ε_{eff}
1	5.5	10.2
2	8.66	7.46
3	11.4	4.44
4	15	2.2

A flat single layer dielectric substrate is used to construct the proposed superstrate, a Rogers RT3010 with relative permittivity 10.2. Next, holes are drilled to alter the effective dielectric constant of each zone to match the required relative permittivities. The hole diameters, which are shown in table II, can be calculated from Equation (4.4) [138].

$$\varepsilon_{eff} = \varepsilon_r \left(1 - \frac{\pi}{2} \left(\frac{D}{D+g} \right)^2 \right) + \frac{\pi}{2} \left(\frac{D}{D+g} \right)^2 \qquad (4.4)$$

Where D is the hole diameter and g is the distance gap between holes.

4.5 Dense Dielectric Patch Antenna Design with Tapered Superstrate

The geometry of a single square DD patch antenna with composite superstrate is shown in Fig. 4.2. The square DD patch (permittivity of 82) antenna is designed on a Rogers Duroid 6002 substrate (top layer) with thickness h_l=20 mil, (εr=2.94 and tanδ=0.0009). The bottom substrate is a Rogers RT 3010 with the same thickness of the top substrate. A 50 Ω microstrip line is printed on the bottom side of the bottom substrate with dimensions of L_f and W_f. The coupling slot in the common ground plane between the two layers has a length of Ls and width Ws. The tapered superstrate covers the DD patch antenna at an air gap height of d. The photograph of the antenna prototype is illustrated in Fig. 4.3 and the optimized parameters are listed in Table 4-2.
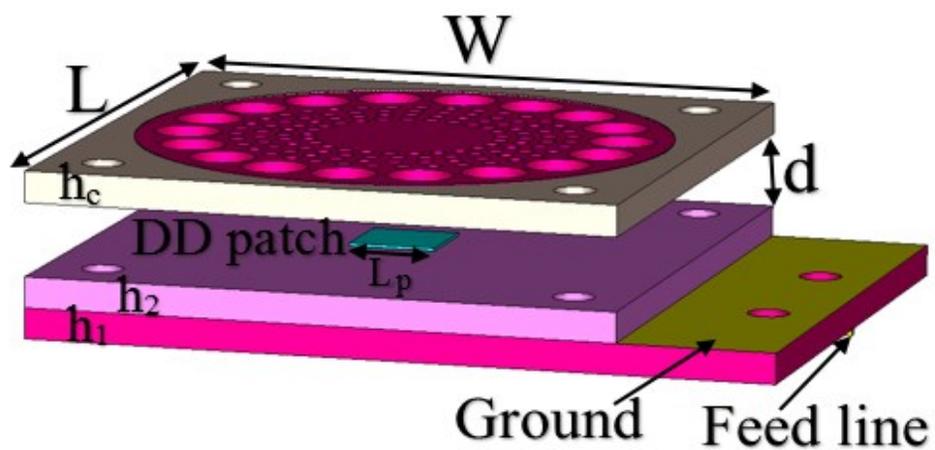
Figure 4.2: Geometry of the proposed antenna: side view.
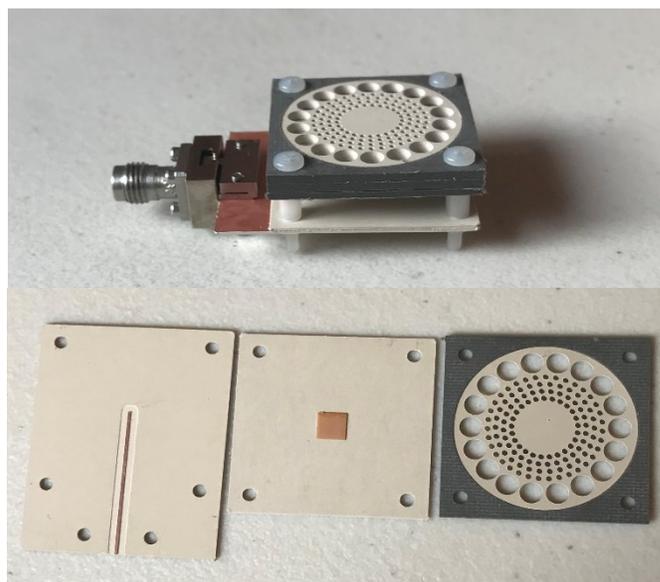
Figure 4.3: A photograph of the proposed antenna prototype.

Table 4-2: The optimized parameters of the proposed antenna.

Parameter	Values (mm)	Parameter	Values(mm)
L_p	4.1	W_f	0.39
H_p	0.15	L_s	2.75
L	25	W_s	0.22
W	25	h_c	4.2
h_1	0.508	d	5
h_2	0.508	D_1	0.75
L_f	20.1	D_2	1.6

4.5.1 Antenna Results

Low profile square DD patch antenna with a single layer unprinted composite superstrate is fabricated and tested. Fig. 4.4 shows the simulated and measured reflection coefficient of the proposed antenna. They exhibit a wider bandwidth of 16 % from 26.25 GHz to 30.75 GHz. The measured antenna gain is depicted in Fig. 4.5. The frequency shift between the simulated and measured results is a result of altering the permittivity (ε_r) of all dielectric layer's manufacture rated value (at 10 GHz) to a different value at MMW range. [139].
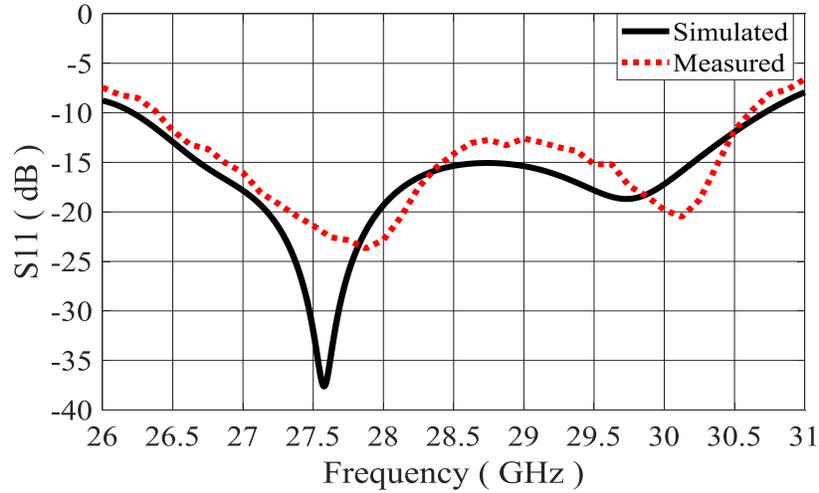
Figure 4.4: Simulated and measured reflection coefficient of the proposed antenna.
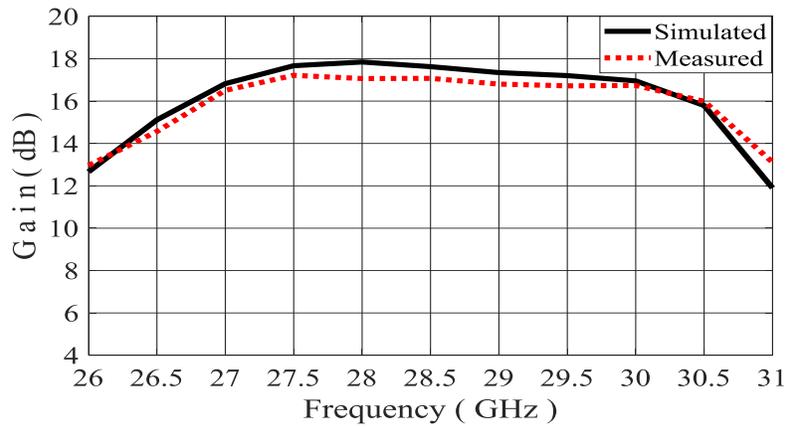
Figure 4.5: Measured and simulated gain of the implemented antenna.

Fig. 4.6 shows the E- and H-plane simulated and measured radiation patterns of the square DD patch antenna with the proposed single layer composite superstrate at 27, 28.5, and 30 GHz, indicating that the antenna provides good radiation patterns and promised side lobe levels (SLLs). The SLLs are -20, -21, and -17 dB in the E-plane, and -20, -17, and -16 dB in the H-plane at 27, 28.5, and 30 GHz respectively.
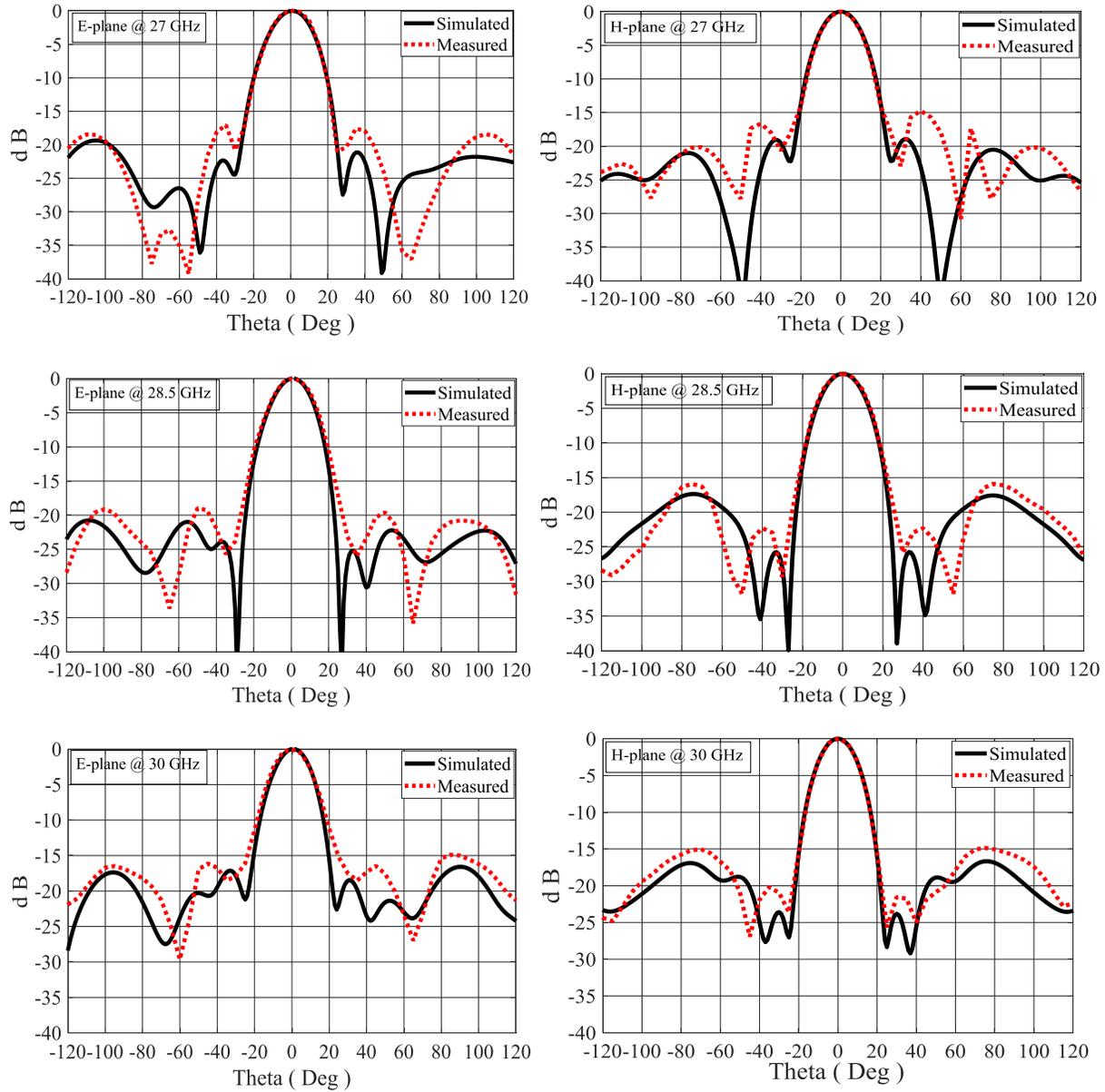
Figure 4.6:   Measured and simulated E and H-plane radiation patterns of the proposed antenna at different frequencies.

To demonstrate the improved characteristics of the proposed antennas, a comparative study of the proposed designs' and those of several published works is presented in Table 4-3. This data clearly shows that the proposed antenna provides good performance in terms of gain and the 3 dB gain bandwidth compared to other relevant works.

Table 4-3: Performance comparison of our proposed design with designs in the literature.

Ref. Nº	Freq. (GHz)	Max. Gain (dBi)	3dB Gain BW %	Substrate Type	Antenna element
[91]	28	17.78	9	FSS(one layer)	DD patch Antenna
	28	15.4	15.5		
[93]	28	16	15.4	Dielectric superstrate	DD patch Array
[86]	60	16	12.2	FSS(Two layers)	Slot antenna
[109]	30	15	10	FSS (one layer)	DRA
This work	28	17.6	16	Tapered Superstrate	DD patch Array

4.6 Beam Switching using Tapered Superstrate

The proposed structure is depicted in Fig. 4.7. This configuration is inspired by an earlier design presented in this work. It shows the proposed tapered superstrate as the PRS is applied over three high DD patches to realize the beam switching. The radiated element patches are symmetrically positioned in the centre of the tapered superstrate along the x-axis, where the distance between each two of them is S which is 1.4 mm. The lateral dimensions of the antenna are the same as the antenna geometry described above in this work. The photograph of the proposed beam switching antenna is illustrated in Fig. 4.8.
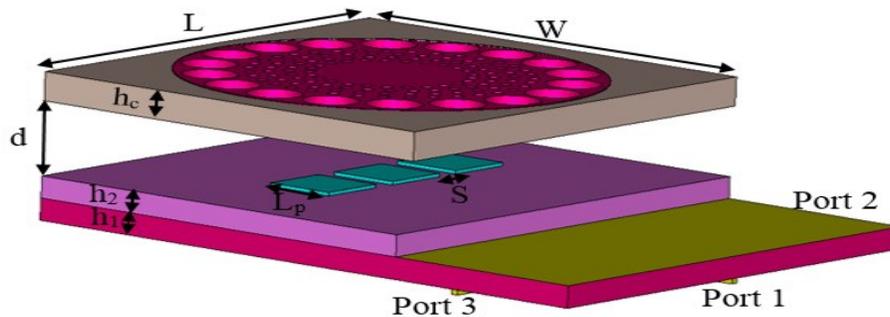
Figure 4.7: Side view of the proposed antenna with three ports for beam tilting.
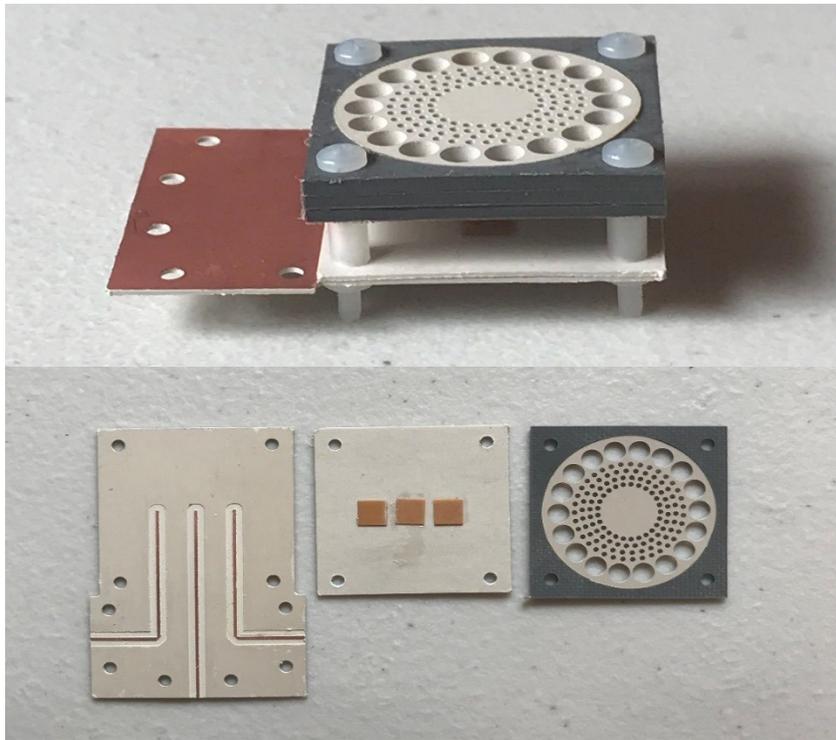
Figure 4.8: Photograph of the proposed antenna with tapered superstrate for a beam tilting antenna.

The radiated source patch moves along the x-axis plane from Sp = -7 mm from the antenna's center to Sp= 7 mm with a uniform step of 3.5 mm, as shown in Fig. 4.9. The antenna beam is steered without using a phase shifter from -30° to 30° with variable gain. Several beams are obtained in the H-plane radiation pattern, as shown in Fig. 4.10.
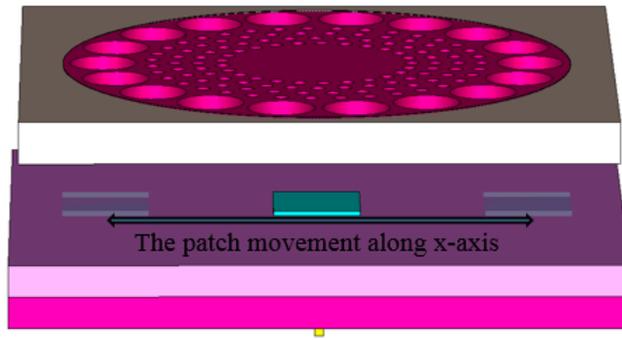
Figure 4.9: Different positions to the radiated source (the DD patch) along the x-axis.
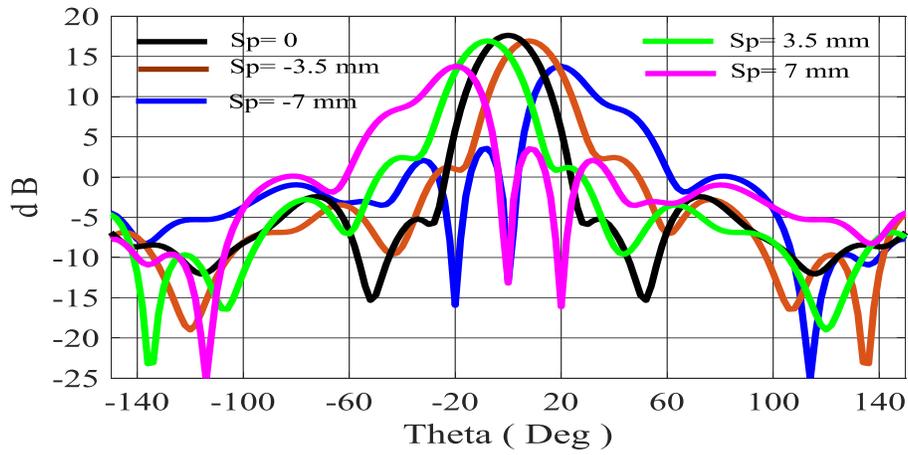
(a)
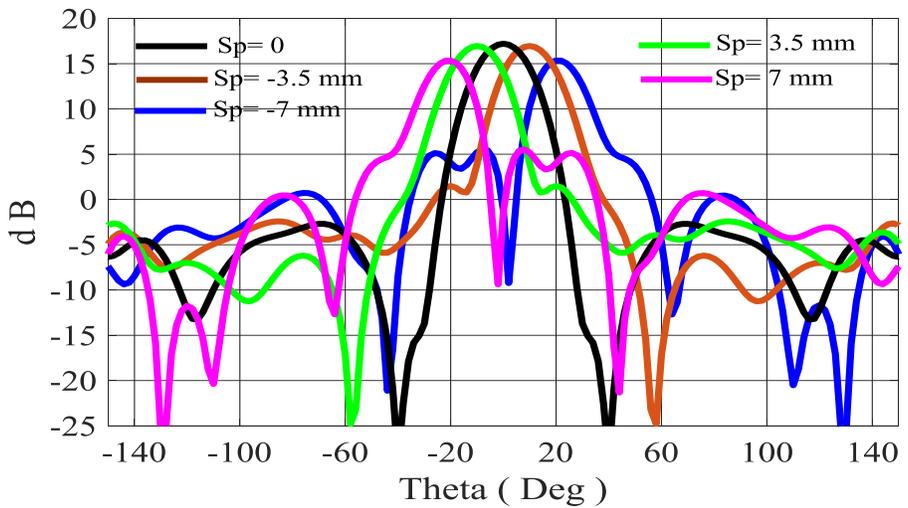
(b)

Figure 4.10: Several beams due to the DD patch movement along the x-axis at 28.5 GHz (a), and 29.5 GHz (b).

61

Based on the results achieved by moving the radiated source along the x-axis, the positions of the three patches are chosen to ensure that the beam remains within the 3 dB less of the broadside gain when port 1 is on, and the rest of ports are off. Each patch is excited by a slot etched on the common ground plane. A 50-Ω microstrip line is printed on the bottom side of the bottom substrate with dimensions of L_f and W_f under each patch. When port 1 is excited, the other two ports are terminated by 50-Ω matching loads to absorb the energy received by the corresponding patches; the same action occurs when port 2 or port 3 are excited. When port 1 is excited, the maximum gain in the broadside direction is 16.7 dBi. The gain is dropped by at least 1 dBi when the parasitic patches are added, due to the coupling between the patches. When port 2, port 3, port 1 with port 2, and port 1 with port 3 are excited, four beams at different angles are achieved. As a result, a directive beam of the antenna is steered from -20° to 20° in the H-plane radiation pattern, as depicted in Fig. 4.11.
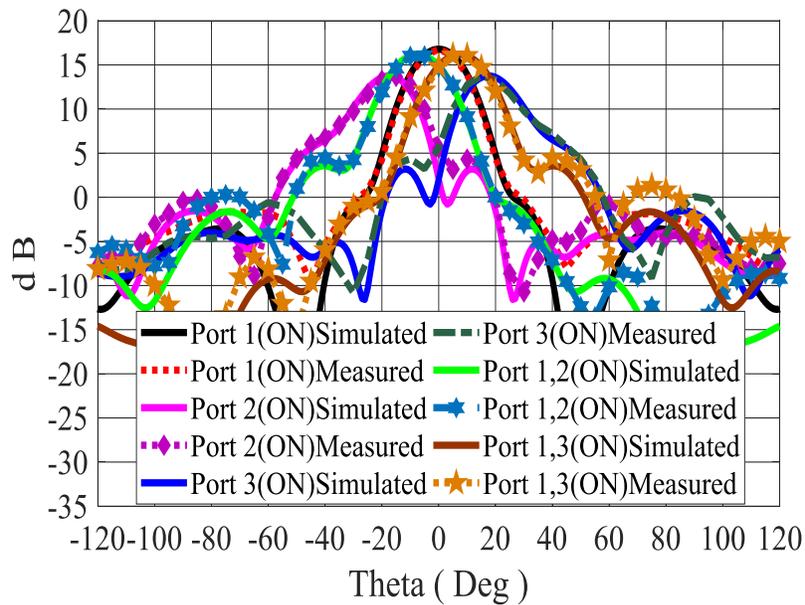
Figure 4.11: Simulated and Measured H-plane radiation patterns.

Chapter 5 Gain and Wideband Enhancement Based on FSS Superstrate

5.1 Introduction

Future wireless communication systems are strongly needed wider bandwidth, higher speeds, and low latency. Developers of the next generation of communication systems (5G) have selected the millimeter wave (MMW) band for its ability to provide all of the next generation's requirements. High gain wideband antennas capable of working in the MMW spectrum are also required [80]. Due to the high attenuation in the atmosphere and the low output power of MMW solid state sources, MMW applications require antennas with high gain in order to compensate for the expected losses [104].

This chapter presents a highly reflective unit cell (PRS superstrate) to cover the DD patch antenna and thereby enhance the gain. A positive reflection phase unit cell is also investigated to expand the 3-dB gain bandwidth. A highly reflective unit cell is modified to create a positive reflection phase and used as a superstrate. These measures improve the antenna's 3-dB gain bandwidth while maintaining its high gain characteristic.

5.2 Design Methodology

The design methodology of this proposed antenna is similar to the one stated in section 3.3. Two single-layer partially reflective surfaces are designed to improve the antenna characteristics based on FSS technology. The first PRS unit cell design begins with selecting the substrate material, which is RT/ 5880 with a thickness of 30 mils, chosen for it has low losses. The FSS's shape is then designed on the bottom of the substrate. The boundary conditions are applied, and the result is a highly reflective PRS unit cell. The second PRS unit cell design follows the same design procedure, but a microstrip line is added on the top of the PRS unit cell along with E-field direction. This line plays a significant role to extend the reflection phase of the proposed unit cell.

5.3 The Fabry-Pérot Cavity Antenna combined with an FSS Superstrate

The working mechanism of the FPC antenna is discussed in section 1.6 and section 2.3. They describe how antennas are designed of three significant parts: the radiator, the ground plane, and the PRS. In the proposed antenna, two types of PRS unit cells are added to improve the antenna performance in terms of the antenna gain and bandwidth. The first unit cell is designed to provide

a high reflection magnitude with a reflection phase that decreases with the frequency within the operating band. The second PRS unit cell is designed based on the positive reflection phase as well as a high reflection magnitude. Based on the theory of the FPC antenna [28], the antenna can achieve a good radiation performance when equations (5.1), (5.2), and (5.3) are satisfied. The working modes of a Fabry-Pérot Cavity antenna can be extended by tuning the reflection phase of the PRS.

5.4 High Gain and Wideband High Dense Dielectric Patch Antenna with an FSS Superstrate

Gain and bandwidth enhancement of a low profile, linearly polarized square dense dielectric patch antenna using a frequency selective surface (FSS) superstrate layer is proposed. A high dense dielectric patch antenna is utilized as a radiating element instead of a metallic patch to realize several significant advantages, including low profile, wide bandwidth, and high radiation efficiency. The implemented antenna is excited by an aperture-coupled feeding technique. The antenna gain is enhanced by using a highly-reflective FSS superstrate layer, for an antenna gain enhancement of 11 dB. The implemented antenna acquired a measured gain of about 17.78 dBi at 28 GHz with a 9% bandwidth, and radiation efficiency of 90%. In addition, the bandwidth of the proposed antenna is improved by using two printed sided unit cell to provide positive phase gradient over the desired frequency range. The antenna impedance bandwidth is broadened, and the measured impedance matching S11 has a 15.54 % bandwidth instead of only 9% while maintaining a high gain characteristic of about 15.4 dBi. The implemented antenna presents good radiation performance with good agreement between the measured and simulated results. The proposed antenna is a very good candidate for MMW wireless communications thanks to its attractive advantages such as low profile, low cost, light weight, small size, and ease of implementation.

5.4.1 Antenna Design

The geometry and the prototype of a single square DD patch antenna with the FSS superstrate layer are illustrated in Fig. 5.1. The square DD patch, with a relative permittivity of 82, has a very low profile with a length Lp=4.5 mm, and a height Hp=0.15 mm. The DD patch is designed on a Rogers Duriod 6002 (ε_r=2.94 and tanδ=0.0009) substrate (top layer) with thickness h_1=20 mil. The bottom substrate is a Rogers RT 3010 (ε_r=10.2 and tanδ=0.0023) with the same thickness as the top substrate. The two substrates have the same length and width (L=W=32 mm). A 50 Ω microstrip line is located

on the bottom side of the bottom substrate, with L_f=16 mm and W_f=0.39 mm. The aperture coupling feed method is used to excite the DD patch antenna. The coupling slot on the common ground plane between the two layers has a length L_S=3.571 mm and width W_S=0.2 mm. An FSS of 7×7 cells is implemented on the bottom side of the superstrate dielectric layer, which has a relative permittivity of 2.2 and thickness h_S =0.787 mm. The FSS superstrate is applied over the DD patch antenna at an air gap of d=5.35 mm.
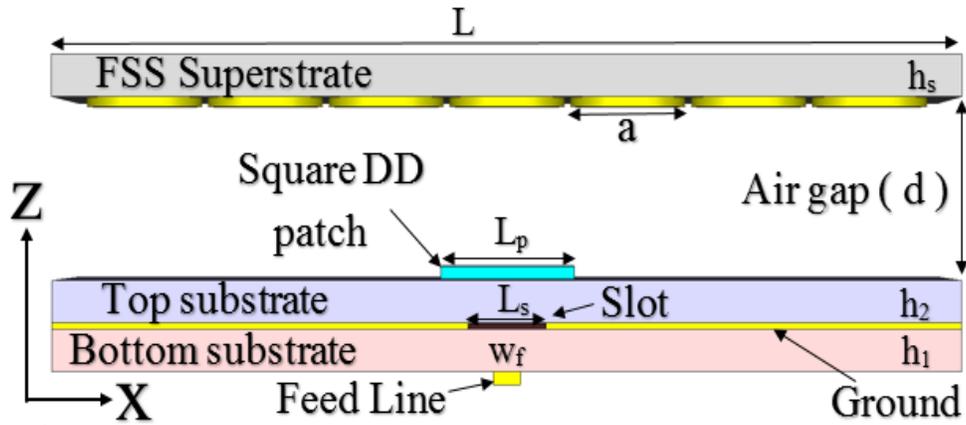
(a)
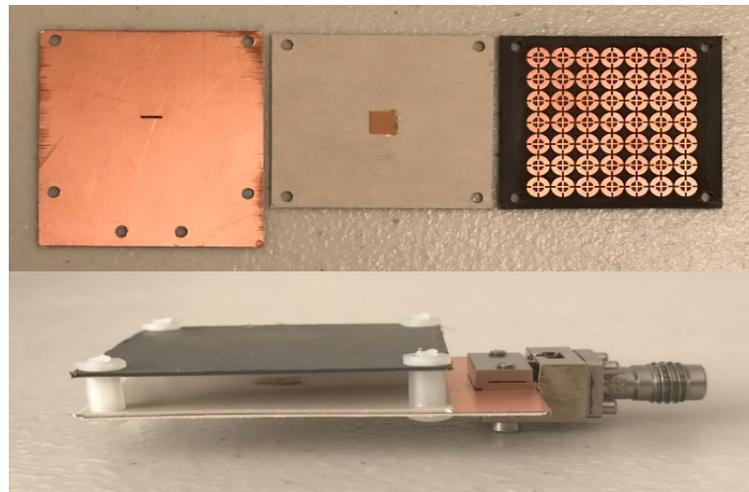
(b)

Figure 5.1: The geometry of the proposed antenna (a), and the prototype of the fabricated antenna (b) [91].

5.4.2 Highly Reflective Unit Cell Design
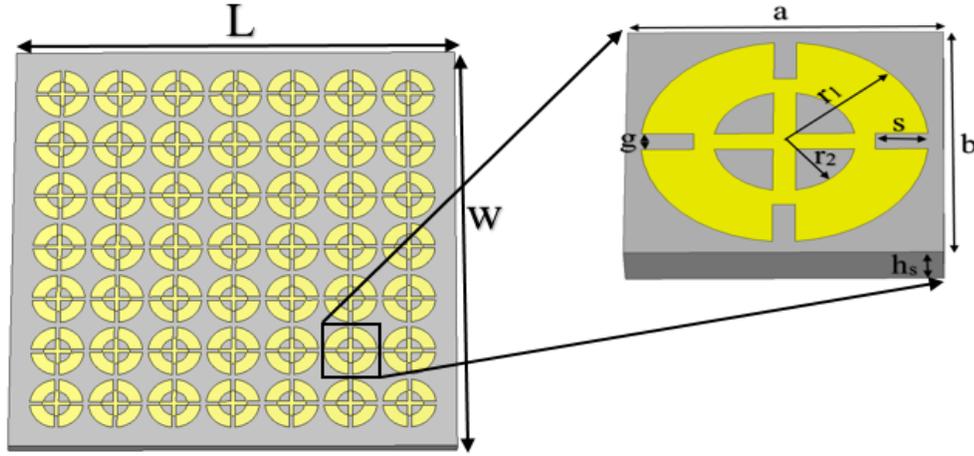
Figure 5.2:   Bottom side of the FSS superstrate, and the geometry of the proposed unit cell [91].

The implemented unit cell was designed and studied. The geometry of the FSS utilized as the superstrate layer is depicted in Fig. 5.2. It was implemented on a Rogers duroid 5880 (ε_r=2.2 and tanδ=0.0009) with thickness h=0.787 mm. The final dimensions of the proposed unit cell are: a = 4 mm, b = 4 mm, h_s = 0.787 mm, r_1 = 1.9 mm, r_2 = 0.94 mm, s = 0.77 mm, and g = 0.3 mm. The FSS unit cell characteristics vs. frequency are shown in Fig. 5.3. They indicate that the DD patch gain can be enhanced if the FSS reflection magnitude increases to unity. Therefore, the requirements of a flat reflection phase and high reflection magnitude should be targeted in order to have an FSS superstrate with good performance. The directivity D can be obtained from the magnitude of the reflection coefficient $|\Gamma_{FSS}|$ in the broadside direction $(\theta = 0)$, as given below [142]:

$$D = 10 \log\left(\frac{1 + |\Gamma_{FSS}|}{1 - |\Gamma_{FSS}|}\right) \tag{5.1}$$

Equation (5.1) shows that the directivity increases significantly as the magnitude of the reflection coefficient increases. Therefore, in order to achieve high gain performance, a high reflection magnitude should be achieved within the design frequency. The superstrate of a set of highly reflective FSS unit cells acts as a lens, allowing a high reflection magnitude to be achieved inside the antenna's resonant cavity and thus obtain a high gain for the antenna.
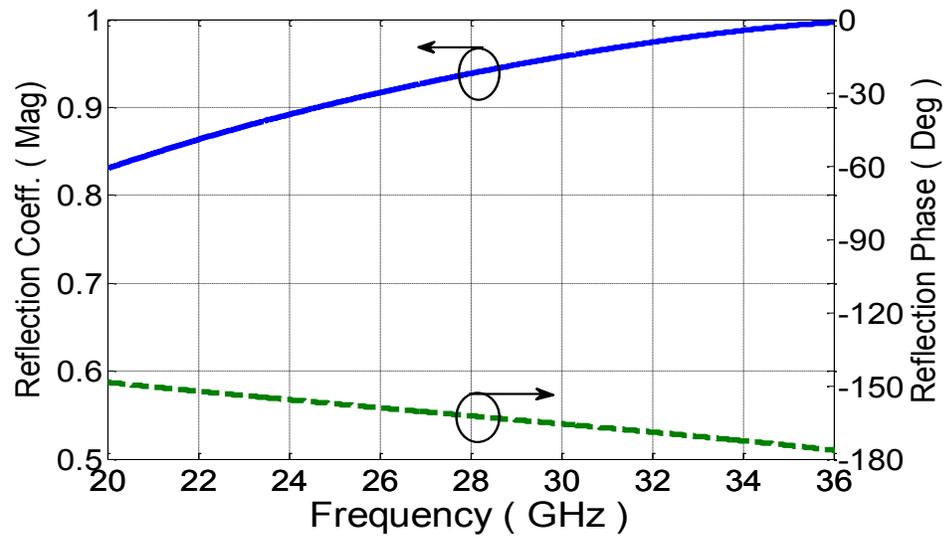
Figure 5.3: Performance of the proposed unit cell [91].

To validate the simulated results, a DD patch antenna with a highly reflective superstrate was fabricated and measured. The implemented antenna was studied and simulated using the CST full-wave electromagnetic simulation tool. Fig. 5.4 shows the measured and the simulated return losses of the proposed antenna, with an impedance matching bandwidth of around 9%. It can be seen that there is quite a discrepancy between the measured and the simulated results, even though they do follow the same pattern. The relative permittivity for all dielectric layers is given at 10 GHz in the manufacture's data sheet. Accordingly, the value of εr is altered at the MMW bands and may cause a shift in the design frequency [6], [19]. This antenna's high measured gain of about 17.78 dBi at 28 GHz and radiation efficiency of almost 90% are shown in Fig. 5.5.
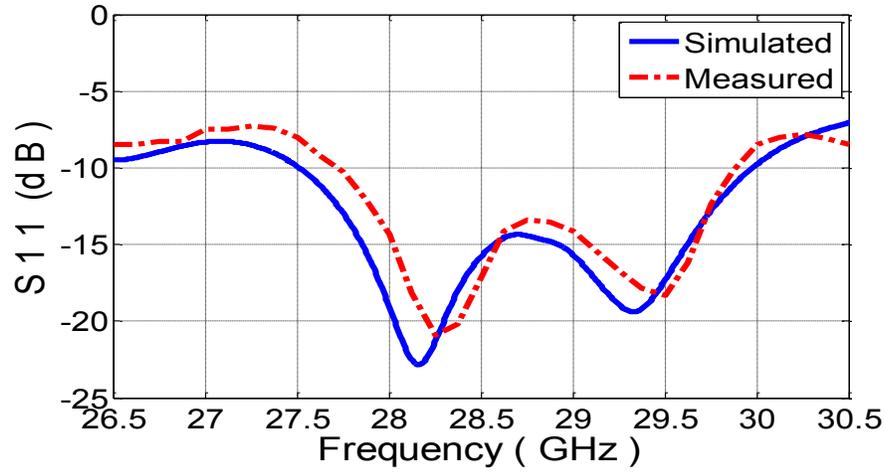
Figure 5.4: Reflection coefficient of the DD patch antenna with a positive reflection phase unit cell [91].
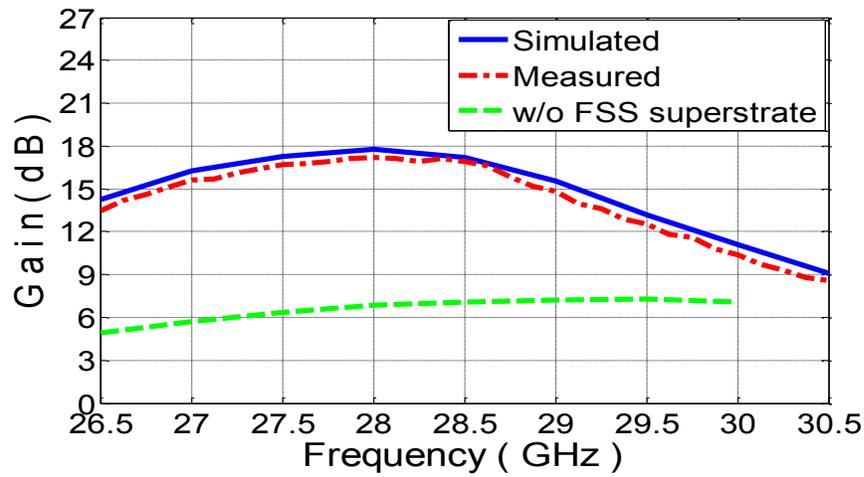
(a)
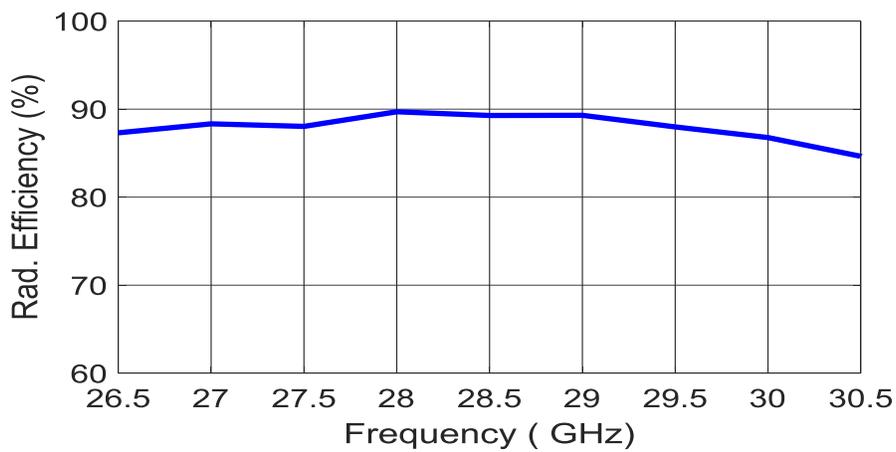
(b)

Figure 5.5: Simulated and measured gain (a), and simulated radiation efficiency (b) of the proposed antenna [91].

Fig. 5.6 shows the E- and H-plane simulated and measured radiation patterns of the proposed square DD patch antenna with a highly reflective superstrate at 28 GHz and at 29 GHz, indicating that the antenna provides good radiation patterns and low side lobe levels (SLLs). The SLLs are below -15 dB at 28 GHz (the design frequency) and then increase somewhat as the frequency is increased to 29 GHz.
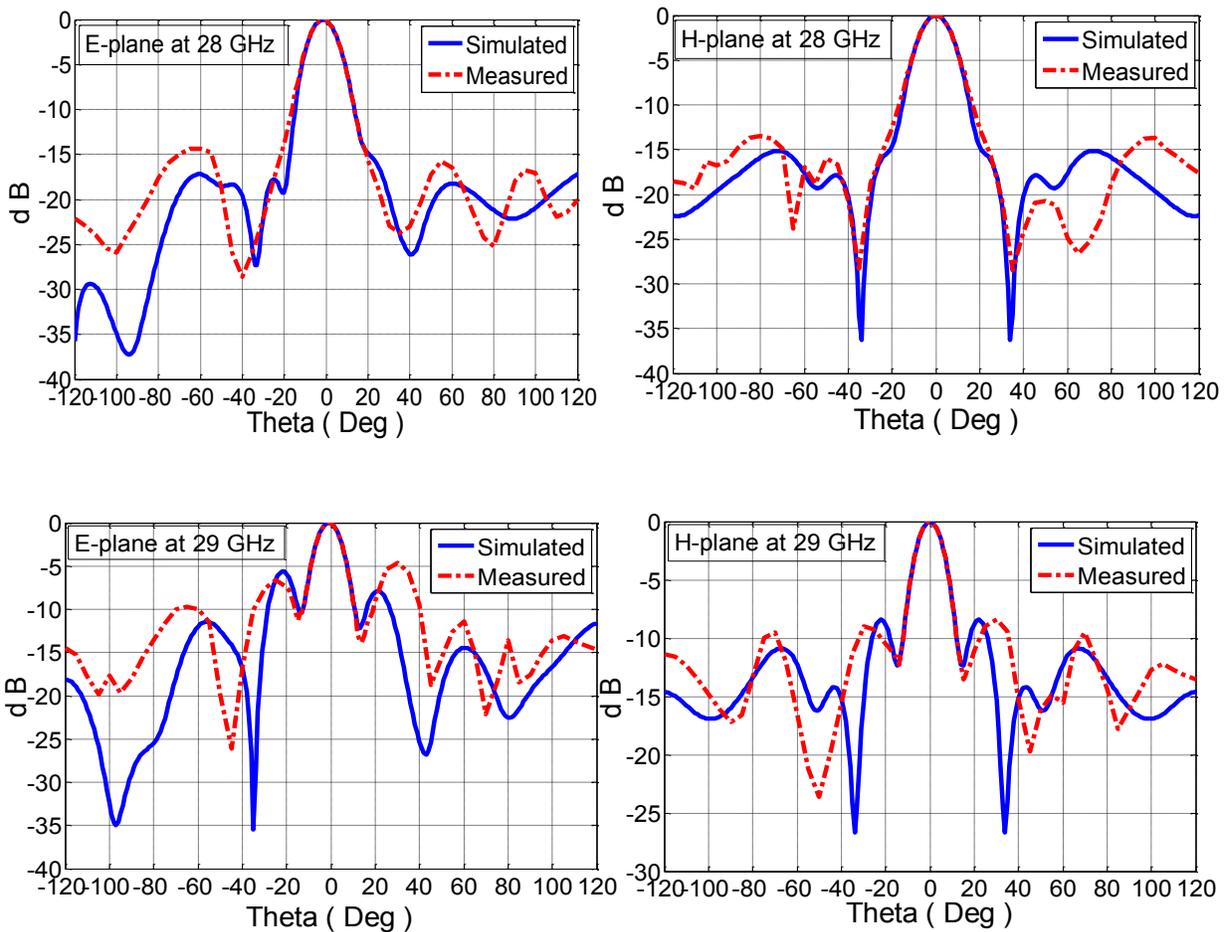
Figure 5.6: E- and H-plane radiation patterns of the proposed antenna at 28 GHz and 29 GHz [91].

5.5 Design of a Unit Cell with a Positive Phase Gradient
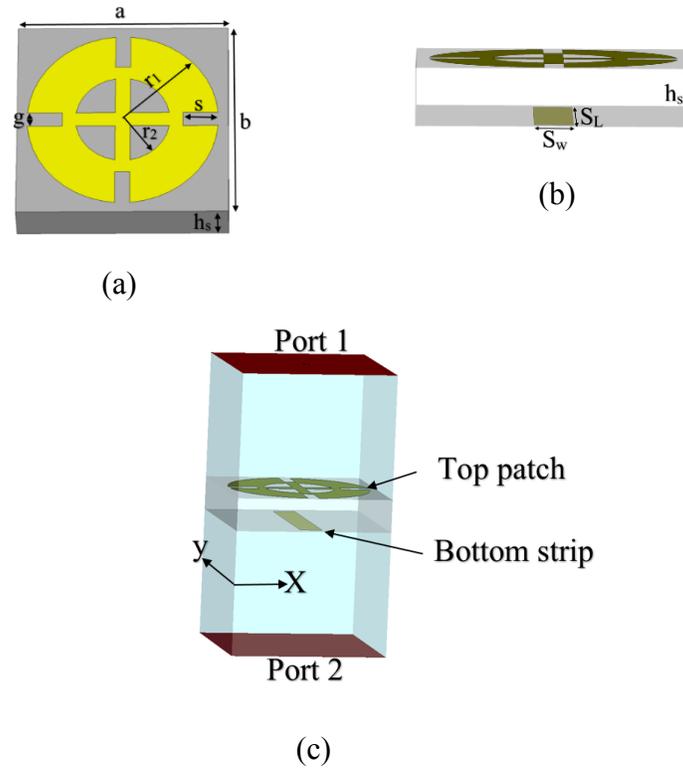
Figure 5.7: Geometry of the proposed unit cell: (a) top view, (b) side view, and (c) characterization model of the unit cell [91].

Since the DD patch antenna with a highly reflective FSS superstrate provided only a 9% bandwidth improvement, a new unit cell is proposed to broaden the antenna bandwidth while maintaining the high gain. This section presents the design procedure of a unit cell that provides a positive reflection phase gradient to be utilized as a superstrate of the high DD patch antenna. Adding a strip on the bottom side of the FSS along with E-field direction plays a significant role in changing the permittivity of the FSS substrate to extend the reflection phase.

In general, a partially reflective surface (PRS) can be defined as periodic arrays of metallic unit cells printed on either one or both sides of a dielectric material. The FSS superstrate is usually applied at a distance d of about half a wavelength (the air gap) above the antenna source; the high DD patch antenna in this design. Multiple reflections are generated between the PRS surface and the ground plane. These lead to constructive interference and enhance the gain of the antenna towards the

broadside direction when the air gap between the FSS superstrate and the ground plane is equal to d [86]:

$$d = \frac{\lambda}{2} * \left(\frac{\Phi}{2\pi} + 0.5\right) + N * \left(\frac{\lambda}{2}\right) \qquad (5.2)$$

where Φ is the reflection phase of the PRS, λ is the free space wavelength, and N is the mode order. Equation (5.2) can be rewritten in the following form to give the optimum phase where the PRS and the ground plane are assumed to be infinite and the air gap distance d=5.7 mm:

$$\Phi = \frac{4\pi d}{c} * f - (2N - 1)\pi \qquad (5.3)$$

Equation (5.3) reveals how a higher gain can be achieved by obtaining a positive reflection phase gradient Φ over the entire desired operating frequency. Both of the unit cells are designed and simulated using the CST full-wave electromagnetic simulation tool. Boundary conditions are applied to the four side walls of the unit cells, as shown in Fig. 5.7(c). Normal incidence is applied, and the incident electric field is polarized along the direction of the bottom strip.

The unit cell is designed to generate a positive phase gradient. This requires a two-sided printed unit cell, as shown in Fig. 5.7. The bottom side of the unit cell is almost the same as that of the highly reflective unit cell utilized above. The top part is the strip line designed to be parallel with the E-field to create a positive reflection phase gradient. The positive reflection phase unit cell is printed on a Rogers RT/duroid 5880 ($\varepsilon r = 2.2$ and $\tan\delta = 0.0009$) substrate with a thickness of 0.31 mil and a periodicity of p = 3.78 mm. A full-wave electromagnetic simulation tool (CST Microwave Studio) was used to design the proposed unit cell. After optimization, the final dimensions of the two-sided printed unit cell were obtained: a = 3.78 mm, b = 3.78 mm, h_S = 0.787 mm, r_1 = 1.71 mm, r_2 = 0.85 mm, s = 0.69 mm, g = 0.27 mm, S_w = 0.54 mm, S_L = 3.15 mm for the bottom. Fig. 5.8 shows the phase and magnitude of the reflection coefficient of the unit cell when the plane wave is incident normally on the bottom side of the unit cell.
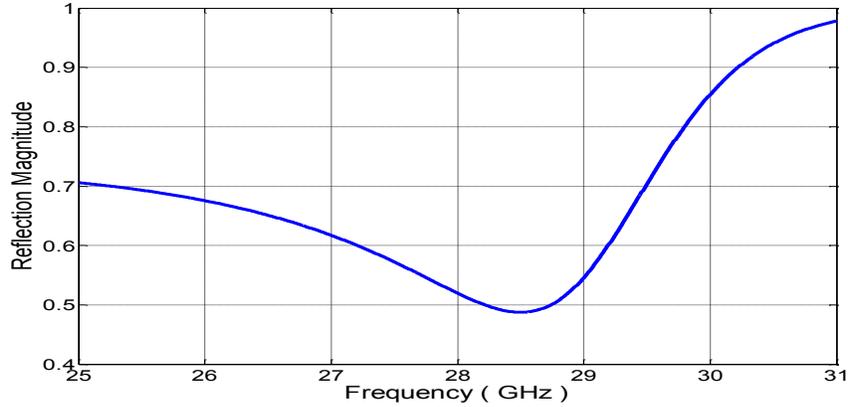
(a)
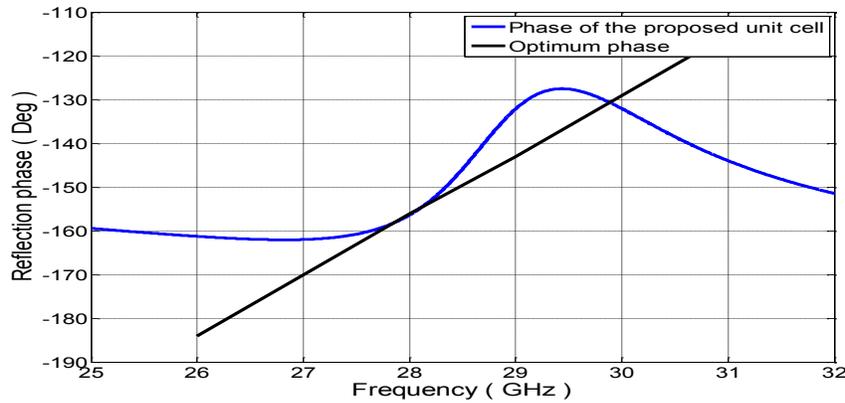
(b)

Figure 5.8: The magnitude (a), and reflection phase (b) of the proposed unit cell [91].

As shown in Fig. 5.8, the proposed unit cell produces a phase that closely resembles the optimum phase in its positive gradient within the operating frequency. A parametric study was conducted to evaluate the effect of certain design parameters, such as S_L and S_w, on the unit cell performance. Figs. 5.9 and 5.10 clearly show that both S_L and S_w have an impact on the phase gradient and on the reflection coefficient. Both the reflection magnitude and phase of the proposed unit cell are shifted toward lower frequencies as S_L is increased, and vice versa. As S_L increases, the reflection magnitude decreases, moving away from the designed frequency band. This results in a low gain antenna with a disrupted bandwidth, while a high reflection magnitude with positive phase gradient is required to achieve a high gain antenna with wide bandwidth. The parameter S_w has little impact on the unit cell's performance.
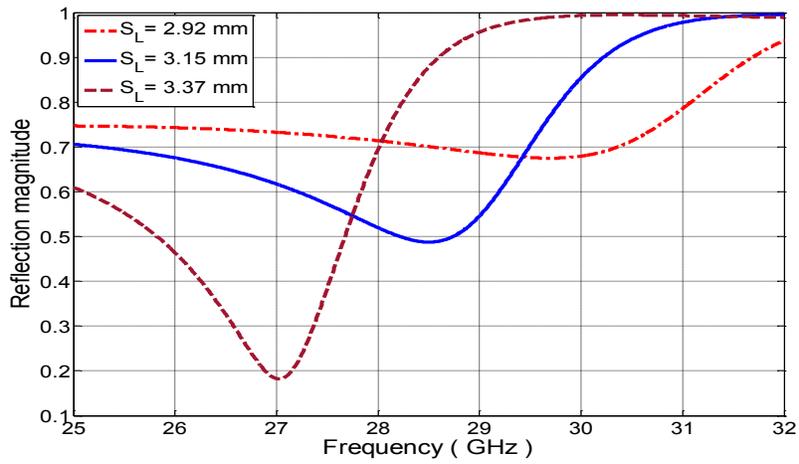
(a)
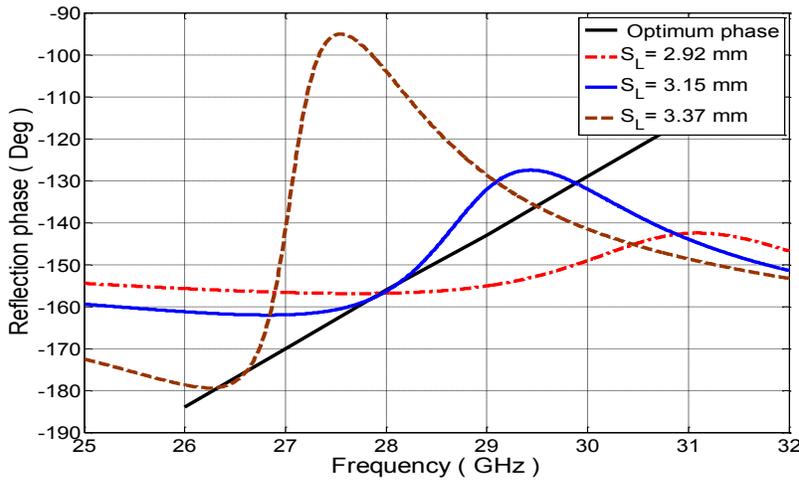
(b)

Figure 5.9: Effect of the S_L parameter on the unit cell performance: reflection magnitude (a), and reflection phase (b) [91].
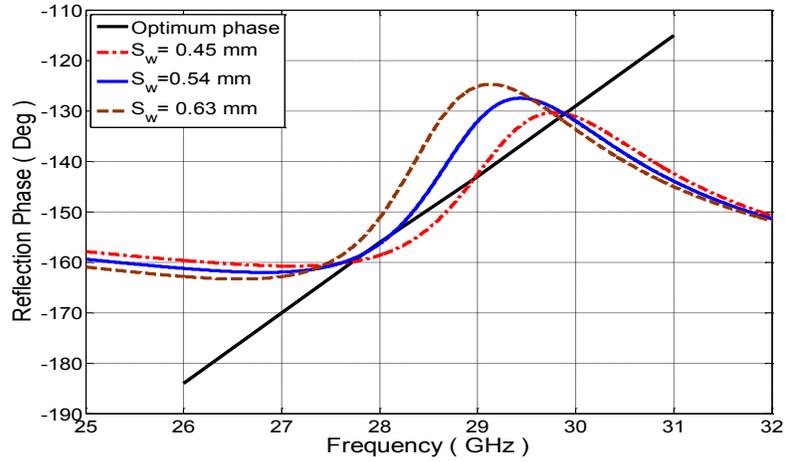
(a)
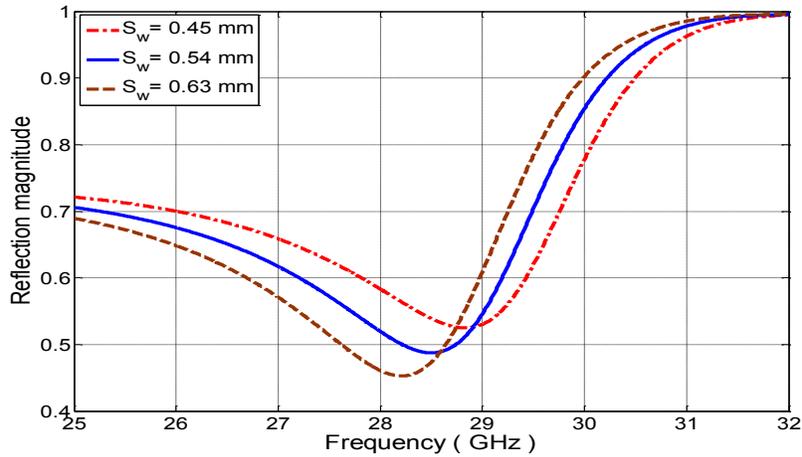
(b)

Figure 5.10:   Effect of the S_w parameter on the unit cell performance: reflection magnitude (a), and reflection phase (b) [91].

5.5.1 Antenna Performance

To verify the simulated results, a square DD patch antenna with an FSS superstrate based on the positive reflection phase gradient was fabricated and tested, as depicted in Fig. 5.11.
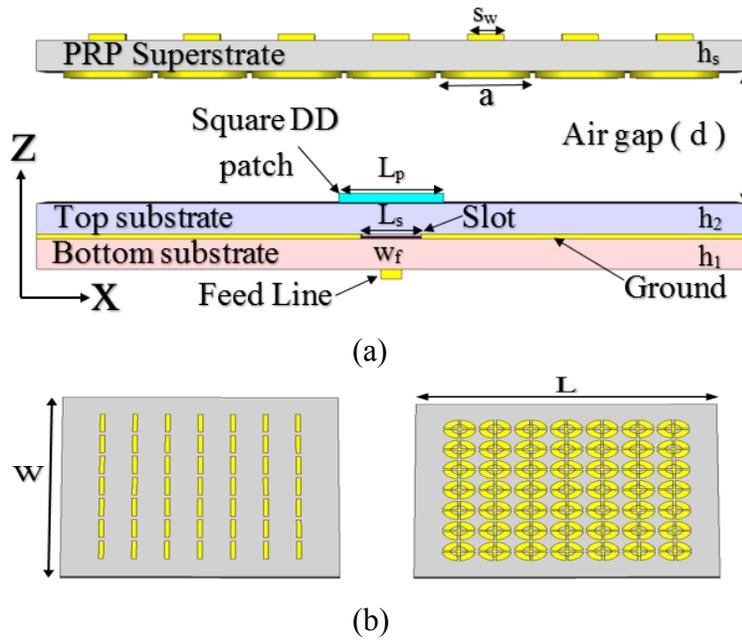
Figure 5.11: Geometry of the proposed antenna with PRP unit cells: (a) side view, (b) top and bottom of the superstrate [91].

The simulated and measured return losses of the proposed antenna are shown in Fig. 5.12. These exhibit a 15.54 % wider bandwidth compared to the 9 % bandwidth for the DD patch with a highly reflective unit cell superstrate. The simulated and measured gain together with the simulated radiation efficiency of the proposed antenna are plotted in Fig. 5.13. The results show a good agreement between the measured and the simulated antenna gain. An almost 14 dBi gain was obtained over the operating band, where the maximum gain is about 15.4 dBi at 29 GHz. The simulated radiation efficiency of the antenna is about 90% over the whole bandwidth. There are some antenna parameters that could affect the antenna performance, such as the air gap d. It was found that d has a significant effect on the antenna resonance and less effect on the antenna gain. As d increases the resonance frequency is shifted down and vice versa. The E- field distribution of the DD patch antenna with a positive phase gradient superstrate is illustrated in Fig. 5.14.
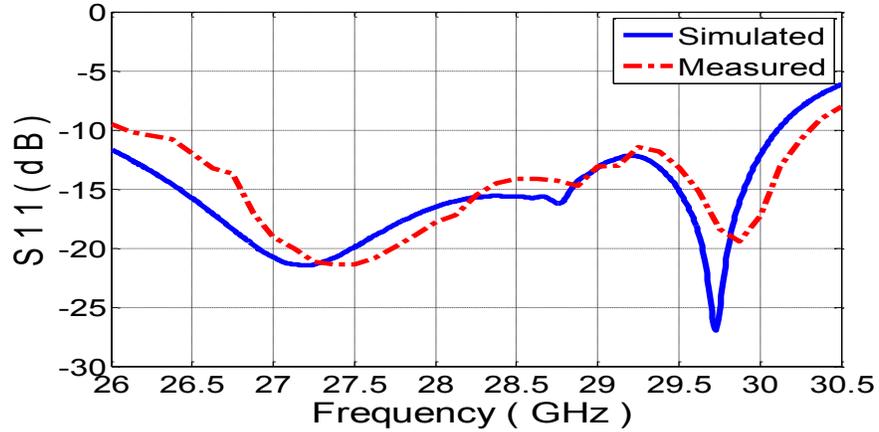
Figure 5.12:   Reflection coefficient of the DD patch antenna with a positive reflection phase superstrate [91].
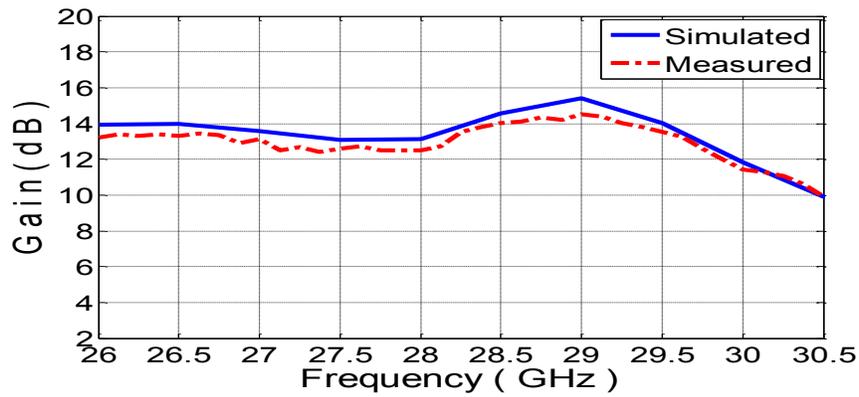
(a)
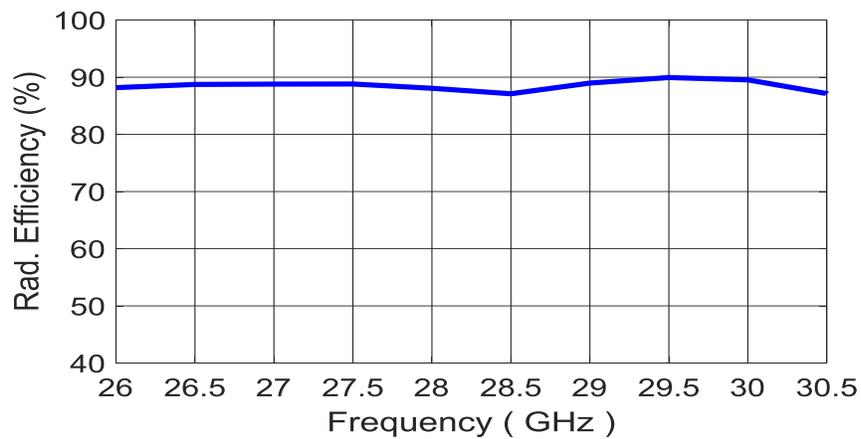
(b)

Figure 5.13: Gain (a) and radiation efficiency (b) of the DD patch antenna with a positive phase gradient unit cell [91].

(a)   (b)
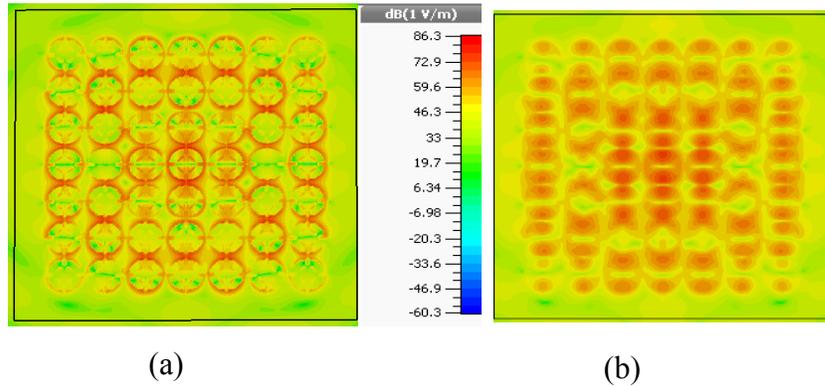
Figure 5.14: E-field distribution of the DD patch antenna with a positive phase at 28 GHz: Bottom of the superstrate (a), and top of the superstrate (b) [91].

Fig. 5.15 shows the simulated and measured radiation patterns of the proposed square DD patch antenna with a positive phase gradient superstrate at 26, 27, 28, and 29 GHz. A good agreement is obtained between the measured and the simulated results. Therefore, the side lobe levels can be assumed to be better (overall) at all frequencies within the antenna band, except for the E-plane at 29 GHz and 30 GHz (not shown here). These exceptions are due to the multiple reflections that become greater at higher frequencies.
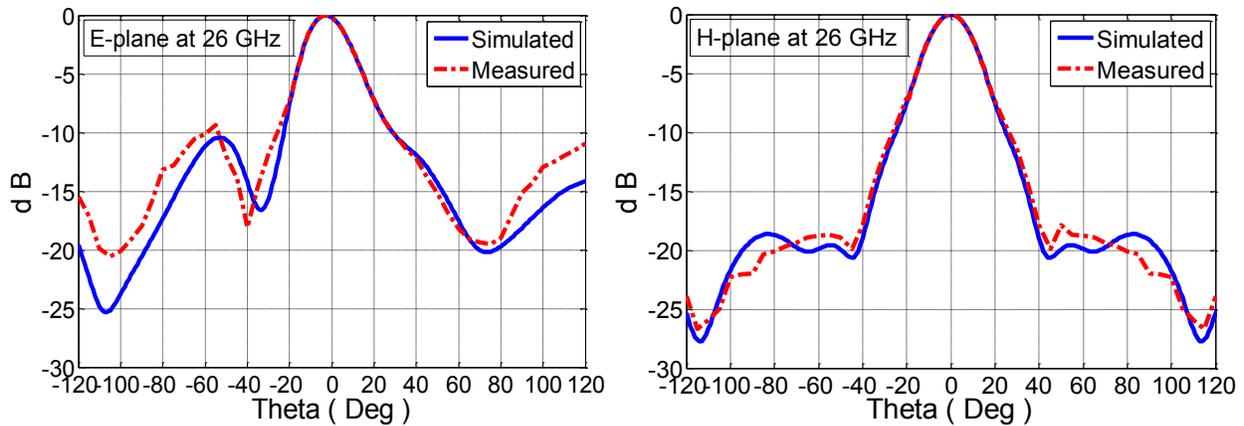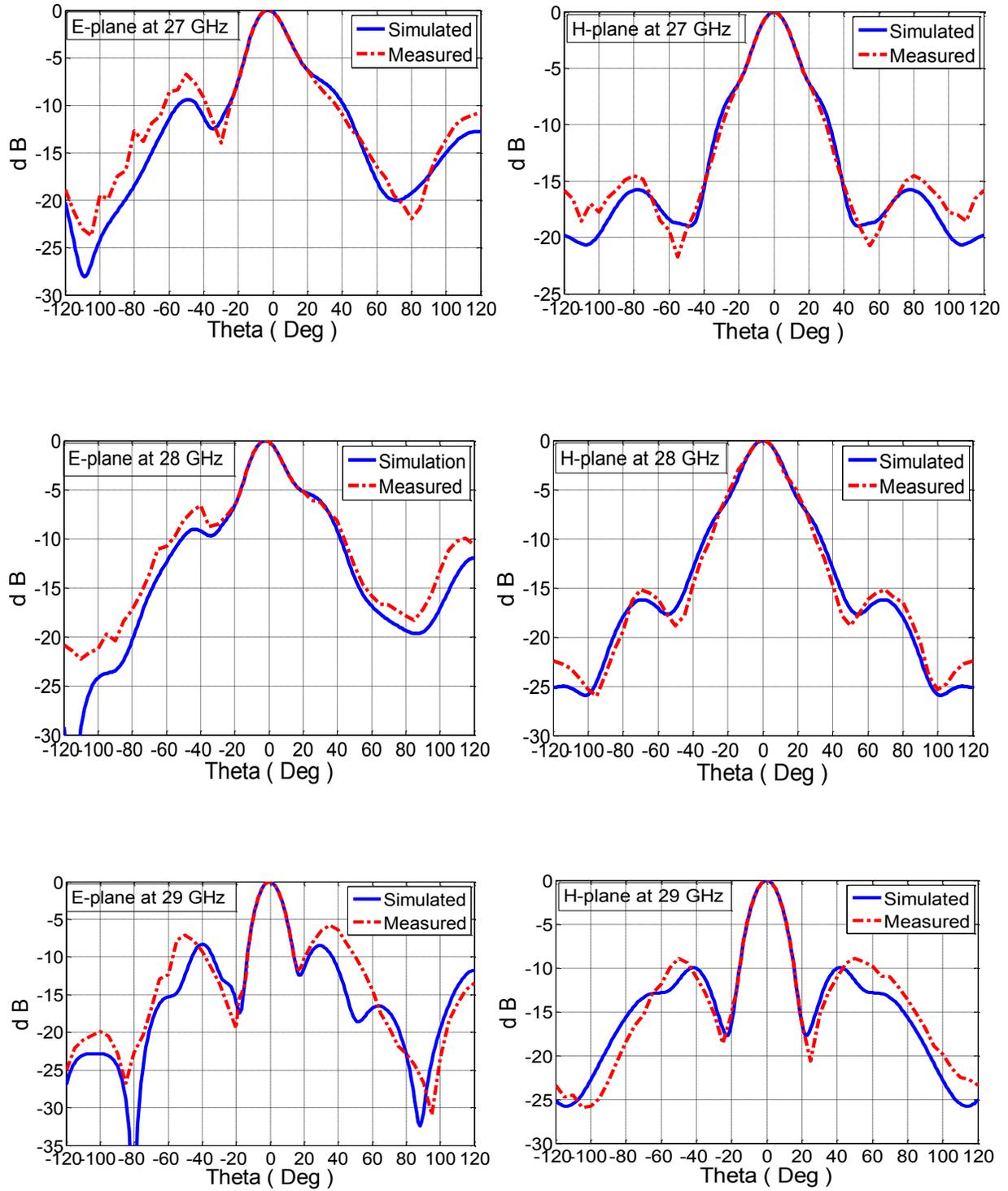
Figure 5.15: E- and H-plane radiation pattern of the DD patch with a positive phase superstrate at four different frequencies [91].

Table 5-1 compares the proposed designs to several published works, highlighting the improved performance of the proposed antenna. The proposed antenna provides a good performance in terms of gain and 3-dB gain bandwidth compared to other relevant works. Fig. 5.16 is a photograph of the proposed antenna prototype.
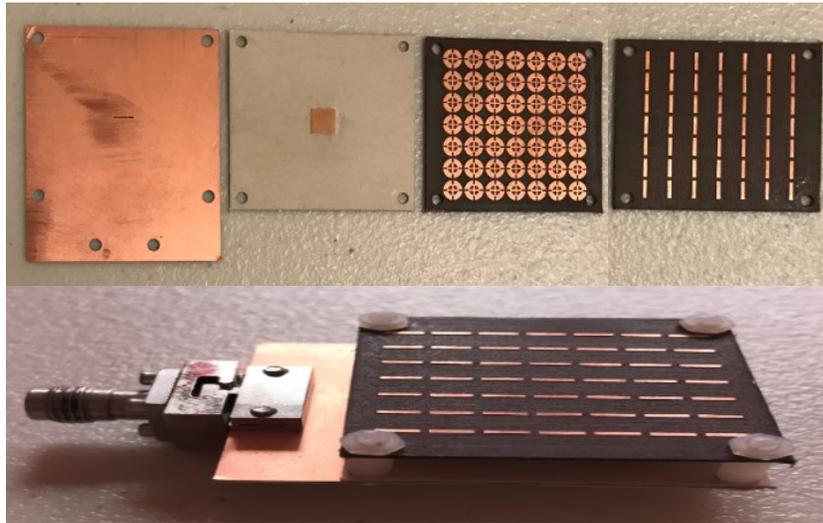
Figure 5.16: The prototype of the proposed antenna [91].

Table 5-1: Performance comparison of our proposed design with designs in the literature.

Ref. Nº	Freq. (GHz)	Max. Gain (dBi)	3dB Gain BW %	Substrate Type	Antenna element
[109]	30	15	10	FSS (one layer)	DRA
[86]	60	16	12.2	FSS(Two layers)	Slot antenna
[143]	13.7	16.3	10.9	FSS (Three layers)	Slot antenna
This work	**28**	**17.78**	**9**	FSS(highly reflective, one layer)	DD patch Antenna
	28	**15.4**	**15.5**	FSS (Positive phase gradient, one layer)	DD patch Antenna

Chapter 6 Millimetre Wave SIW Slotted Cavity Antenna

6.1 Introduction

The demand for low profile high gain antennas continues to climb. This demand is a driving force in research and development in communication technology and in the development of the next generation of wireless communication (5G) [144]. Slot antennas have become the most widely used antennas in millimeter-wave communication, thanks to their desirable characteristics such as low profile, high gain, and conformability to planar or curved surfaces [145].

Recently, the substrate integrated waveguide (SIW) concept has been more widely used than the conventional waveguide approach in antenna design. It offers many attractive advantages including the possibility to integrate all of the components on the same substrate, low insertion loss, and a low profile [146]. At millimeter-wave (MMW) frequencies, high gain antennas are required to overcome the signal attenuation due to oxygen molecules' absorption [77]. To compensate for these losses, some approaches to increase the antenna gain at the ka band have been developed [147, 148].

This chapter presents a low-profile high gain slotted SIW cavity antenna. The antenna is designed based on SIW technology with a substrate layer using a higher-order mode (TE_{440}) operating at 28 GHz. The TE_{440} mode is generated by exciting the cavity with a coaxial probe to distribute the energy and avoid using a lossy feed network. The proposed antenna offers high gain and high radiation efficiency with compact size and a simple feed. This chapter also presents a circularly-polarized (CP) substrate integrated waveguide (SIW) cavity antenna. A linearly polarized (LP) SIW cavity antenna is loaded with a linear-to-circular polarization converter, producing a high gain circularly-polarized SIW cavity antenna. The proposed antenna is designed to fulfill the requirements of future wireless communication for short range applications. These requirements include a high gain, high radiation efficiency, low side-lobe levels, easy of fabrication and a low profile.

6.2 High Gain LP/CP of an SIW Cavity Antenna based on a High Order Mode and a Linear-to-Circular Polarization Converter

A high gain low profile linearly-polarized Substrate Integrated Waveguide (SIW) cavity antenna is proposed using a TE440 high order mode. This antenna is simply excited by a coaxial probe. A linear-to-circular converter is then utilized to achieve circular polarization (CP), resulting in a circularly polarized SIW cavity antenna. This low profile, lightweight antenna offers both left- and right-hand circular polarization. The implemented antenna exhibits a measured gain of almost 16 dBi and radiation efficiency of about 96 % with good measured return loss. Its measured axial ratio is slightly less than 1.6 dB, and the antenna shows a good performance radiation pattern. The measured and simulated results show a good agreement. This antenna is considered as an appropriate candidate for use in future fifth-generation (5G) wireless systems.

6.2.1 Linearly-polarized SIW Cavity Antenna Design

(a)   (b)
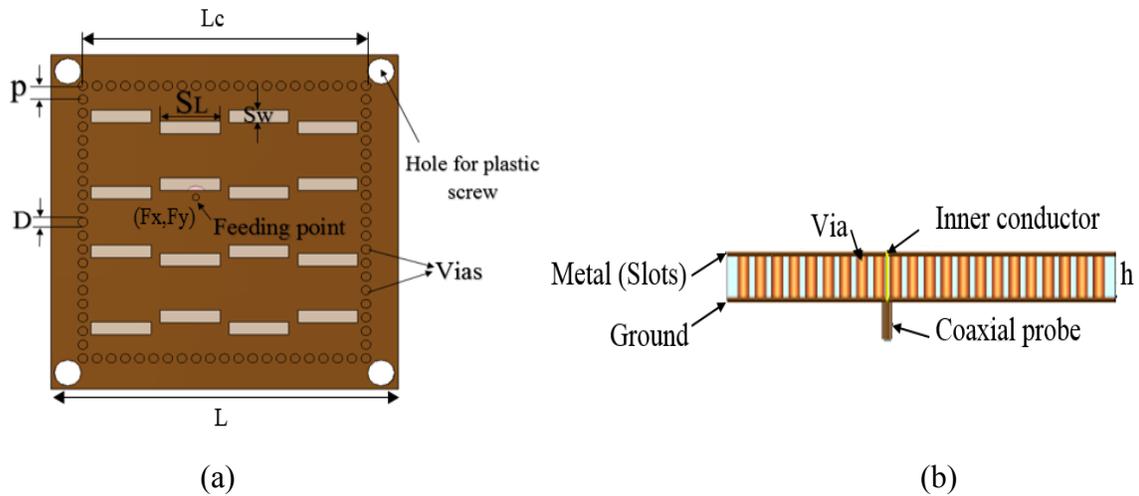
Figure 6.1: Geometry of the proposed antenna: (a) top view; (b) side view [71].

A compact square cavity antenna with SIW vias and length L was designed and implemented on a single substrate as shown in Fig. 6.1. The four side walls of the cavity are constructed from a number of metallic vias with a diameter of D and spacing of P. The square cavity was implemented using an RT/Duroid 5880 substrate with thickness h= 0.508 mm (ε_r = 2.2, tanδ = 0.0009). Probe feeding was used to excite the cavity and at the point (F_x, F_y). The outer conductor of the coaxial probe is connected to the bottom metal, which is the ground, and the inner conductor is connected to the top metal surface of the cavity.

The simulated structure shows 4×4 slots etched on the top of the cavity with length S_L and width S_W. These sub array slots are spaced at a half-waveguide wavelength, which introduces a 180° change of phase and to add another 180° the slots are placed alternatively to the opposite sides of the centerline resulting in in-phase radiation by the slots. This configuration thus provides a broadside radiation pattern for this slotted cavity antenna. The optimized parameters are listed in Table 6-1.

Table 6-1: The optimized parameters of the Linearly-polarized SIW cavity antenna.

Parameters	L_C	L	P	D	S_L	S_w	F_x	F_y
Value (mm)	22.9	23.15	1.04	0.7	4.44	0.97	-2.12	1.9

6.2.1.1 Simulated Results

The proposed antenna was studied and simulated using the CST and HFSS software packages. The antenna's reflection coefficient is depicted in Fig. 6.2. It can be observed that the return loss (S_{11} < -10dB) is reasonable with a bandwidth of almost 4.6%. Fig. 6.3 shows the antenna's gain and the radiation efficiency, indicating that the gain is as high as 16.4 dBi (achieved at 28 GHz) in the middle of the band. Moreover, it is clear that the radiation efficiency is about 98%
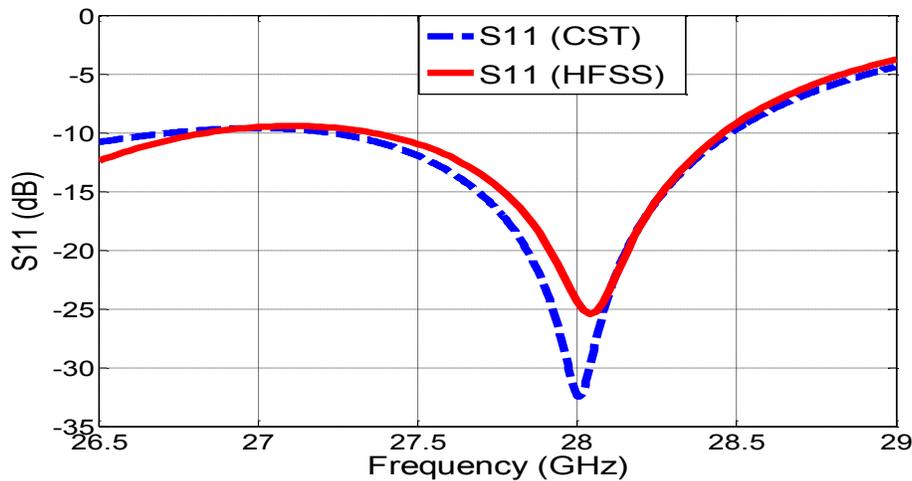
Figure 6.2: Simulated reflection coefficient of the LP SIW cavity antenna [71].
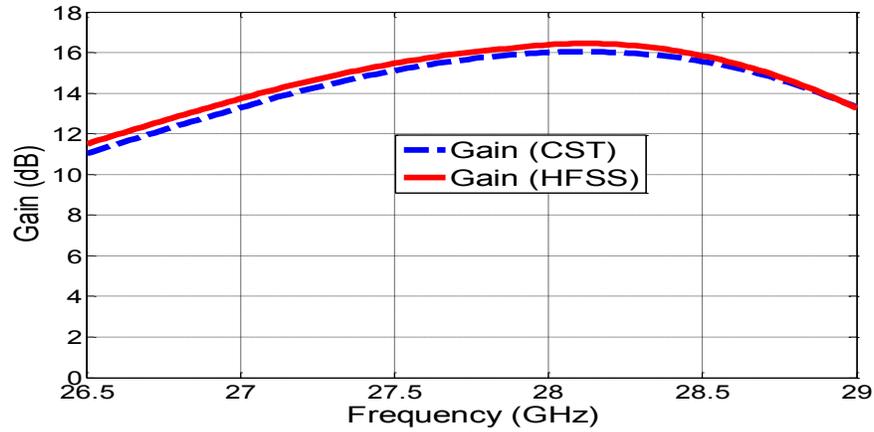
(a)
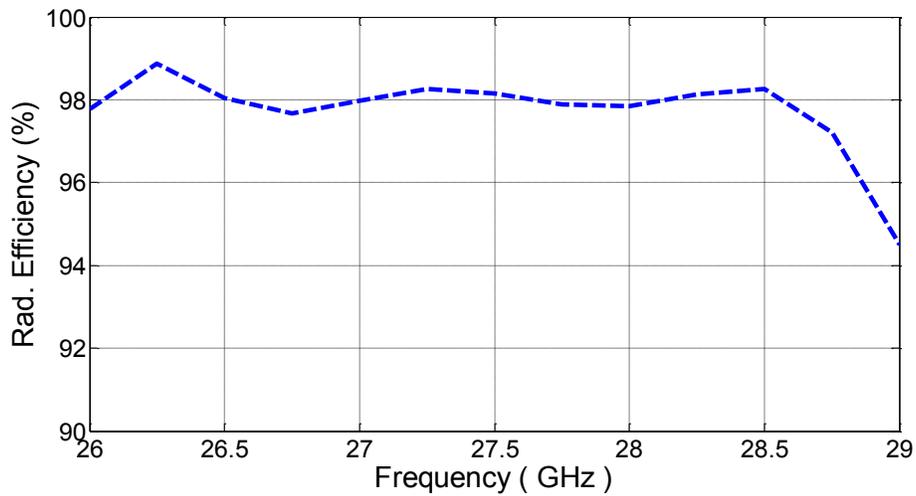
(b)

Figure 6.3: Simulated gain (a), and radiation efficiency (b) of the LP SIW cavity antenna [71].

The LP SIW cavity antenna's E- and H-plane radiation patterns are shown in Fig. 6.4. It can be observed that the E-plane beamwidth and the H-plane beamwidth are almost the same. The sidelobe levels (SLLs) in the E-plane are < -14 dB, whereas in the H-plane they are < - 17dB at 28 GHz. There is an obvious agreement between the CST and HFSS results for both the E- and the H-plane.
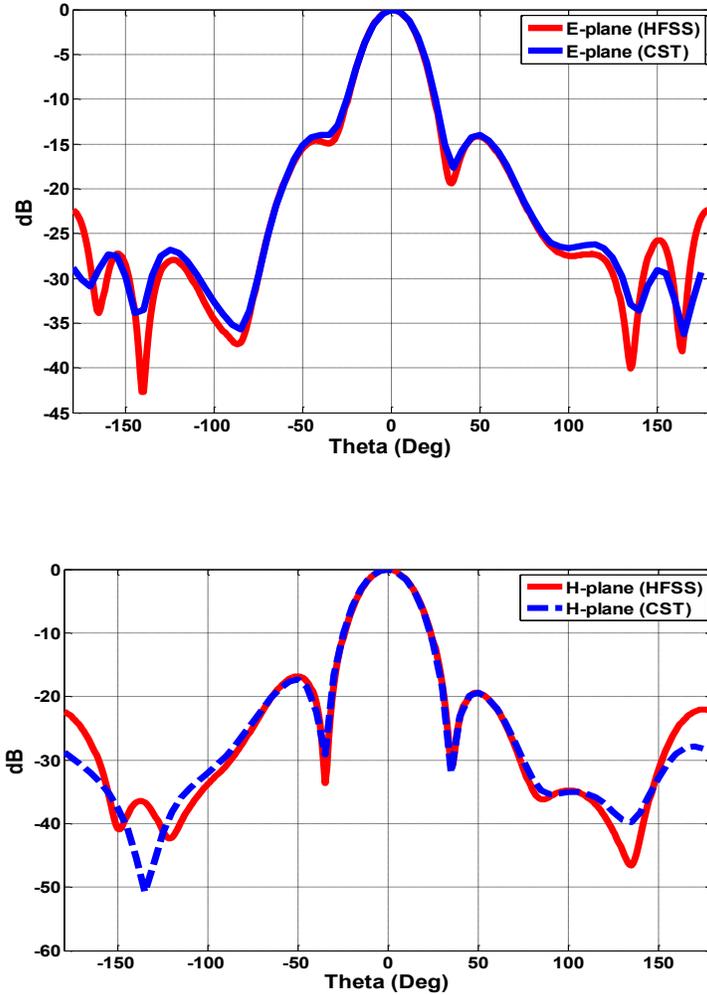
Figure 6.4: The E- and H-plane radiation patterns of the LP SIW cavity antenna [71].

6.2.2 Circularly-polarized SIW Cavity Antenna Design

Wireless communication systems are in high demand for potential fifth generation (5G) millimeter-wave (MMW) applications. Low profile, high gain, compact, and circularly-polarized antennas are strongly required in millimeter wave systems [4]. At the MMW frequency band, air attenuation occurs due to the absorption of oxygen molecules. High gain antennas are therefore are required to overcome signal attenuation. At 30 GHz, a circularly polarized antenna is very attractive for its ability to suppress multipath interference and to reduce polarization mismatch [149]. A number of studies have focused on realizing circular polarization with high gain performance [123]-[126].
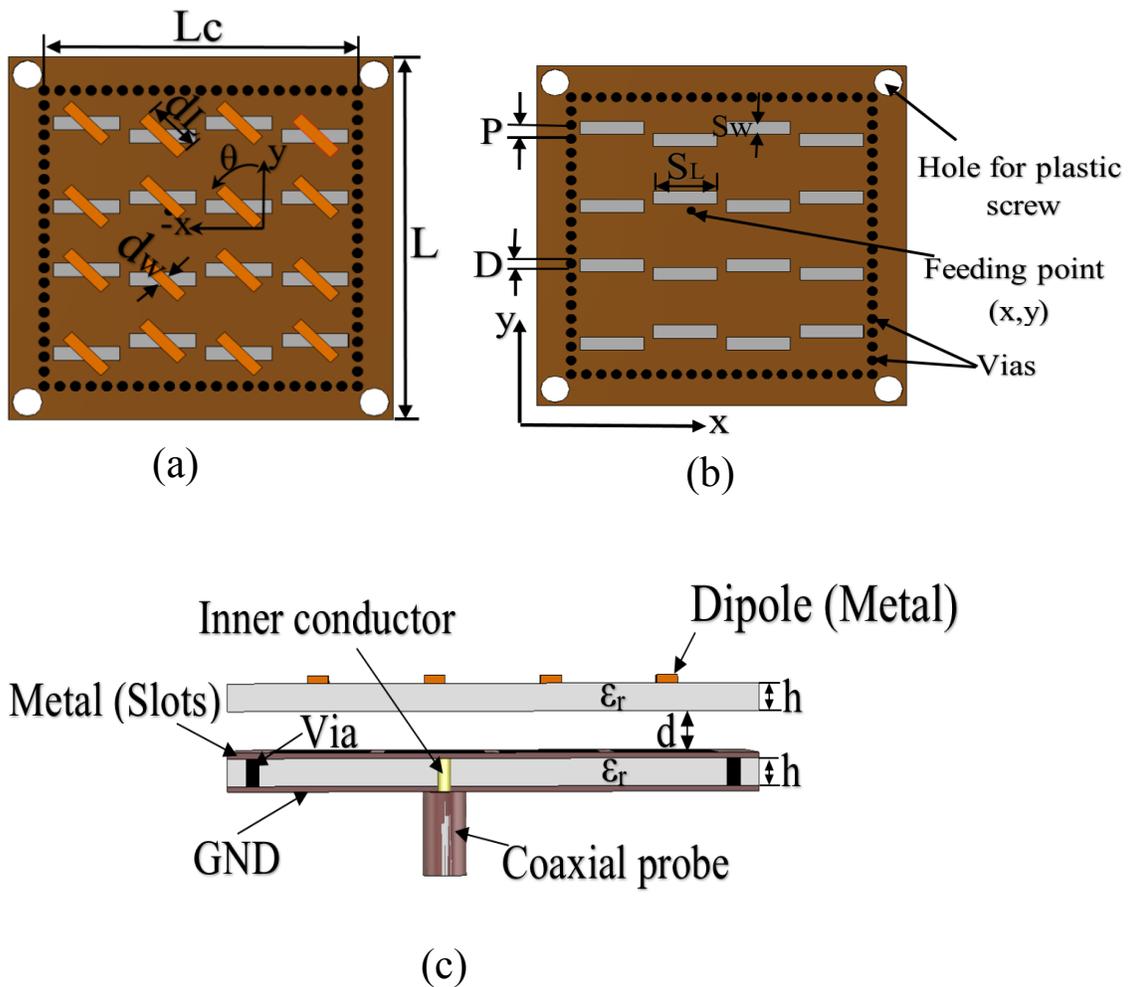
Figure 6.5: Geometry of the proposed CP SIW cavity antenna: (a) top view of the converter, (b) top view of the slotted SIW cavity, and (c) side view [71].

Fig. 6.5 shows the structure of the proposed high gain circularly-polarized slotted SIW cavity antenna. The planar bottom layer square cavity is constructed by metallic via arrays with a diameter of D and spacing of P with total length Lc on a Rogers//Duroid 5880 substrate with thickness h= 20 mils (ε_r = 2.2, tanδ = 0.0009). The polarization converter's top layer has a number of dipoles on the top side of a second substrate with the same specifications as the cavity substrate. A feeding probe located at the point (x=-2.12, y=1.9) is used to excite the cavity. Simulated using CST Microwave Studio simulator, the structure shows electric field distribution for the TE$_{440}$ mode at 28 GHz inside the SIW cavity. The 4×4 standing wave electric peaks distributed inside the SIW

85

cavity are illustrated in Fig. 6.6. Based on these peaks, 4×4 slots are cut on the top metal plate of the cavity, where each slot is placed above each standing wave peak. The E-field distributed in the two adjacent standing waves are out of phase. Therefore, the distance between each two slots in each sub-array is a half-waveguide wavelength, introducing a 180º phase change, and placed alternately on the other side of the center line. As a result, the antenna can radiate in-phase in broadside direction.
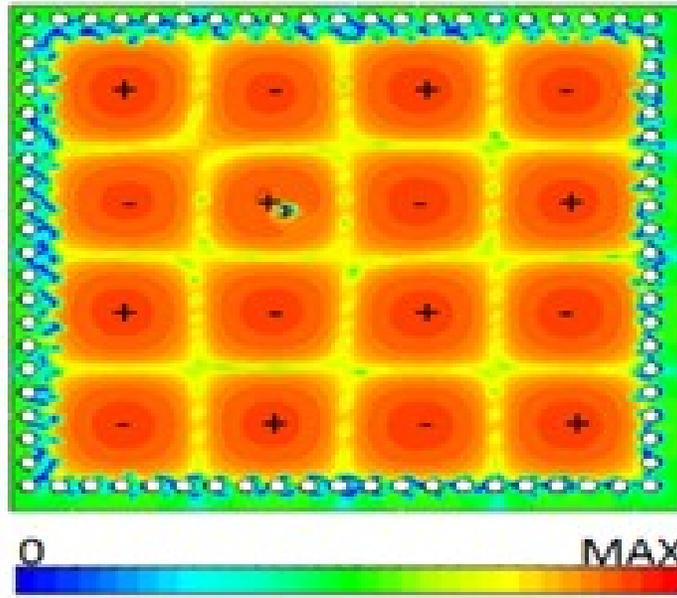
Figure 6.6: Distribution of the magnitude of the E-field for the TE440 mode at 28 GHz inside the CP SIW cavity [71].

The circularly-polarized SIW slotted cavity antenna is achieved by adding a substrate layer with the same specifications as the dipoles above the slotted cavity, separated by an air gap (d=1mm). The number of dipoles is the same as the number of slots, and each dipole is placed directly above a slot. Since the antenna radiates right hand circularly-polarized, left hand circularly-polarized waves can be achieved by rotating the upper substrate with its dipoles by 90º, known as a linear-to-circular polarization converter. The optimized parameters are listed in Table 6-2.

Table 6-2: The optimized parameters of the circularly-polarized SIW cavity antenna.

Parameter	Values (mm)
L_c	20.9
P	1.04
D	0.7
d_L	3.54
d_w	0.9
S_L	4.44
S_w	0.97
d	1

Fig. 6.7 shows the top and bottom views of the fabricated prototypes. Plastic screws and foam material are used to maintain 1 mm spacing between the antenna and the converter.
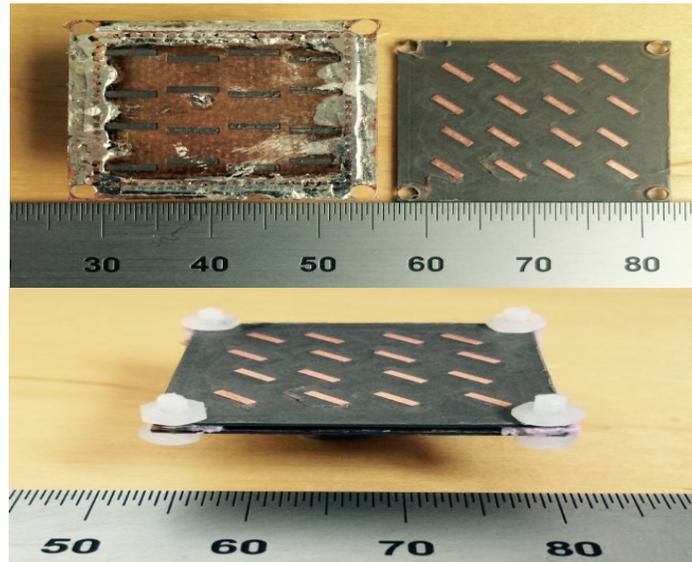
Figure 6.7: Prototype of the fabricated CP SIW cavity antenna. (a) Top of the antenna and convertor, and (b) side view [71].

6.2.2.1 Parametric Study

A parametric study was conducted to study the effect of some of the significant parameters of the implemented CP SIW cavity antenna using CST Microwave Studio. As shown in Fig. 6.8, the distance d between the antenna and the converter has some effect on the antenna resonance frequency. Dipole length d_L has an enormous influence on the axial ratio and a small effect on the antenna impedance matching. As can be seen from Fig. 6.9, resonance frequency decreases with increasing d_L and vice versa, as well as, the axial ratio. The dipole width d_W has a minor effect on the antenna axial ratio and on the antenna input impedance. Furthermore, altering the above-mentioned parameters has a minor effect on the gain of the proposed antenna, which was kept close to 16 dBi.

6.2.2.2 Simulated and Measured Results

The proposed CP SIW cavity antenna was fabricated and tested. Fig. 6.10 shows the measured and simulated reflection coefficient of the proposed antenna. It can be seen that the antenna has a good return loss (S11 < -10dB) with about 4.6% bandwidth.

(a)   (b)
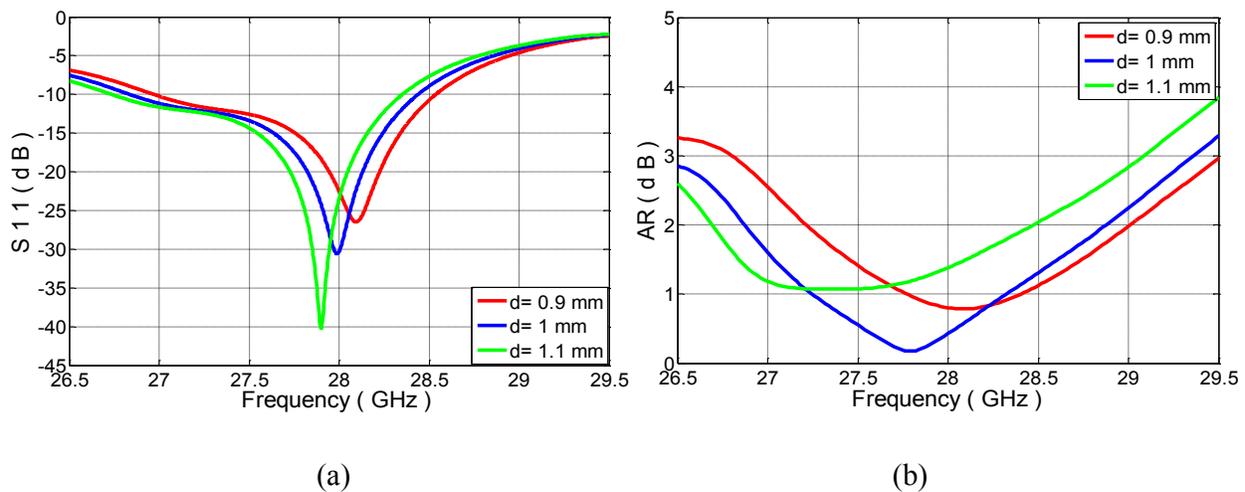
Figure 6.8: Simulated return loss (a) and axial ratio (b) of the proposed CP SIW cavity antenna considering the effect of varying the distance between the antenna and converter [71].
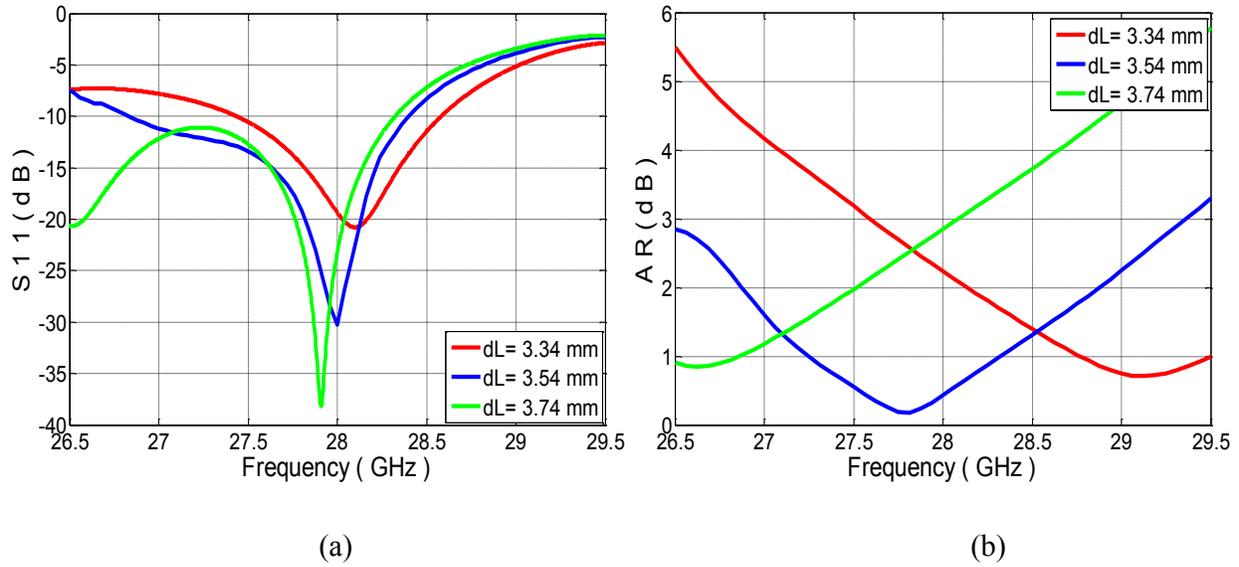
Figure 6.9: Simulated return loss (a) and axial ratio (b) of the proposed CP SIW cavity antenna considering the effect of varying the dipole length [71].
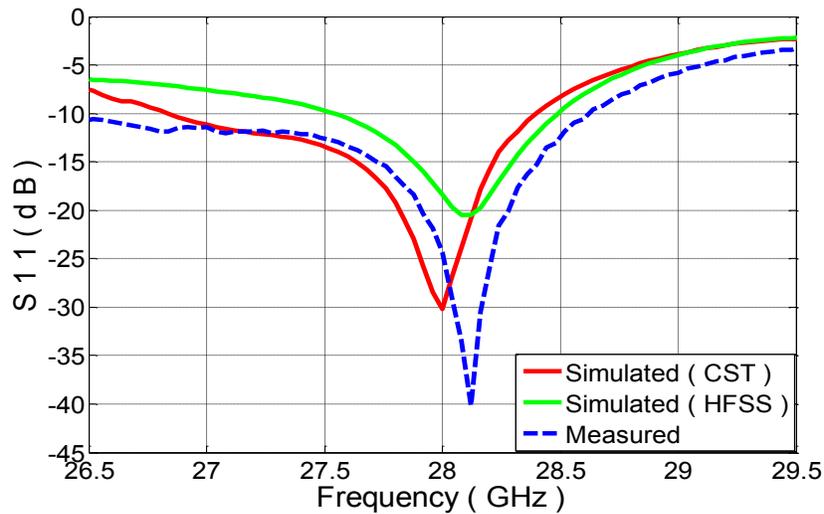
Figure 6.10: Simulated and measured reflection coefficient of the proposed CP SIW cavity antenna [71].

The simulated and measured gain and axial ratio of the implemented antenna are depicted in Fig. 6.11. As can be seen, the measured and simulated results of the antenna gain are in very good agreement. The peak gain value is about 16 dBi. The measured axial ratio (AR) bandwidth shows better performance compared to the simulated results. As shown in both Figs. 6.10 and 6.11b, there is a similar frequency shift in the resonance frequency of the CST and HFSS results. Moreover, the axial ratio is kept within the range between 1.3 dB to 1.6 dB.

89
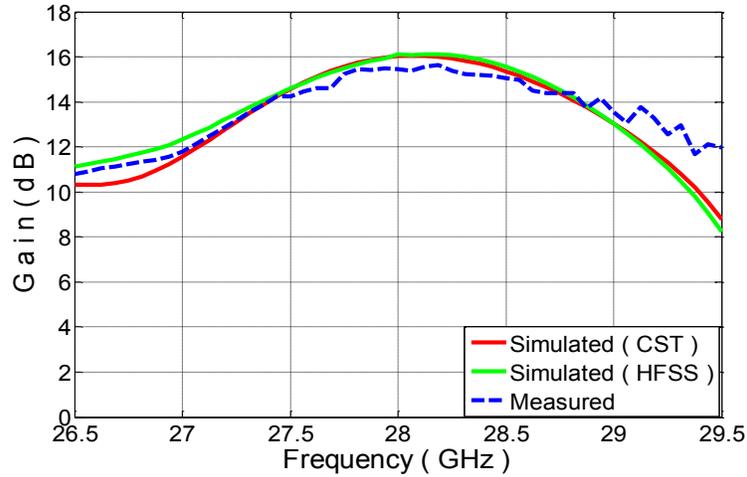
(a)
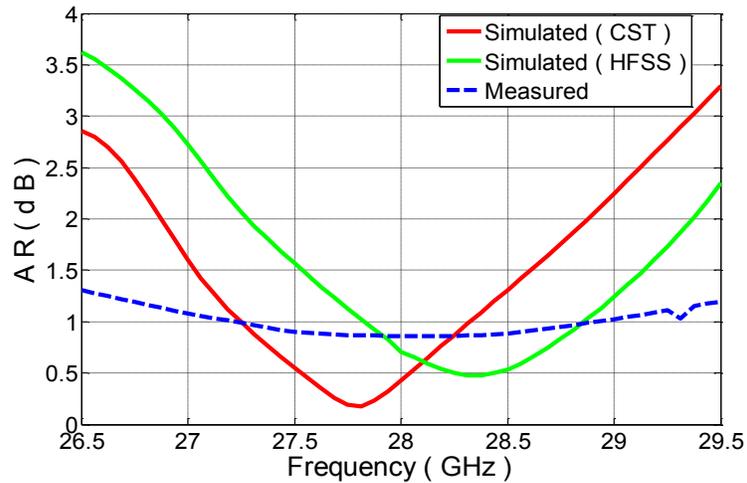
(b)

Figure 6.11: Simulated and measured gain (a) and axial ratio (b) of the CP SIW cavity antenna [71].

Fig. 6.12 shows the measured and simulated E- and H-plane patterns of the proposed antenna. The measured sidelobe level (SLL) at 28 GHz in the E-plane is < -14 dB, and it is < - 16 dB the H-plane.   Both values are close to the simulated results. The level of cross polarization of the proposed antenna is less than -23 dB. It can be concluded that the proposed CP SIW cavity antenna has a good radiation pattern and that there is a good agreement between the measured and simulated results. From Fig. 6.12 there is obviously a near symmetry in the antenna E-plane pattern because of the symmetry of the proposed antenna structure.
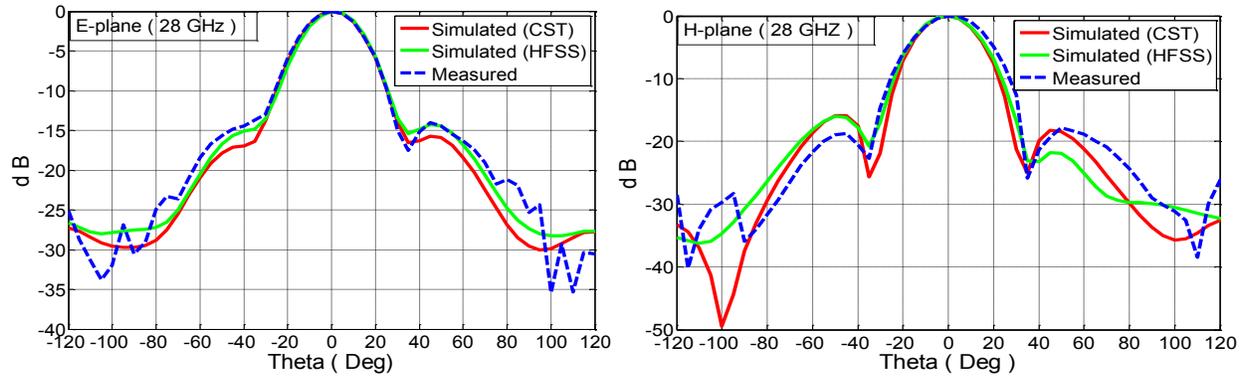
Figure 6.12: Radiation pattern of the proposed CP SIW cavity antenna [71].

Chapter 7 Conclusion and Future work

7.1 Conclusion

At millimeter-wave (MMW) frequencies, the losses associated with wireless links and systems are significant and must be overcome when designing high-performance wireless systems. A high-gain antenna is required to compensate for the overall loss in MMW wireless communication systems.

The Fabry-Pérot Cavity (FPC) antenna has been introduced as an antenna that is capable of providing a high gain and wide bandwidth using different types of superstrates. FPC antennas have attracted the attention of researchers due to its several attractive features and been determined to be a suitable candidate for communication system applications. The Highly-Directive Fabry-Pérot-type antenna is a good solution for obtaining a high gain and a wide bandwidth that can address the multiple challenges of high losses at the millimeter wave spectrum and   limited bandwidth, neither of which is acceptable for future wireless communications. Some of the attractive characteristics that distinguish FPC antennas are their low profile, planar configuration, and ease of fabrication. Fabry-Pérot cavity antennas based on partially reflective surfaces (PRSs) which act as lenses are investigated in this thesis to fulfill the growing demand for broadband high-gain antennas.

Chapter 2 provides a literature review and a brief history of Fabry-Pérot cavity antennas along with different practical applications.

A high gain broadband 2×2 square high dense dielectric patch antenna is implemented in chapter 3. The antenna gain and bandwidth are enhanced using two different partially-reflective surfaces: a single-layer perforated superstrate and a superstrate composed of two thin perforated layers. The latter, a partially reflective surface (PRS) of two thin perforated dielectric substrate layers, was designed to create a positive reflection phase gradient with high reflection magnitude. Both superstrates are applied over the DD patch antenna array, and both antenna designs exhibit good performance. The first design has a 3 dB gain bandwidth of about 15.35% and antenna gain of 16 dBi, and the second design has a 3 dB gain bandwidth of about 27 % and a high simulated gain of 16.8 dBi. At all operating frequency bands, the proposed antennas have a good radiation performance with SLL values in both the E- and the H-planes.

In Chapter 4, a tapered unprinted dielectric superstrate covering a square high dense dielectric patch antenna is simulated, fabricated, and tested. The permittivity is altered to be high in the superstrate's center and low at the edges to compensate the phase along the superstrate. The antenna exhibits a 3 dB gain bandwidth of about 16%. An almost flat high measured gain of 17.6 dBi and simulated radiation efficiency of close to 92% are achieved. The antenna gain and radiation efficiency are almost flat over the antenna's bandwidth. The proposed antenna has a good radiation performance with promised SLL values in the E- and the H-planes. Furthermore, the antenna beam is steered from -30º to 30º using the proposed tapered superstrate, with good performance in terms of gain and side lobe levels.

In Chapter 5, a linearly polarized low-profile square dense dielectric (DD) patch antenna with gain and bandwidth enhancement using a frequency selective surface (FSS) superstrate layer is presented. Two different FSS superstrates are utilized to enhance the gain and bandwidth. The DD patch antenna is covered by a set of highly reflective planar unit cells, realizing a gain enhancement of 11 dBi. The implemented antenna acquired a measured gain of about 17.78 dBi at 28 GHz with a 9% bandwidth. In addition, a superstrate layer of a positive reflection phase unit cells was designed to improve the antenna bandwidth. Using this superstrate resulted in a 6% bandwidth enhancement.

Chapter 6 introduced MMW high gain low profile linearly- and circularly-polarized slotted cavity antennas based on SIW technology. The CP cavity antenna has a good return loss, axial ratio, and high gain of 16 dBi. Furthermore, the proposed antenna has a good radiation performance with SLLs of less than -14 dB in the E-plane and less than -16 dB in the H-plane. A simple converter allows this antenna to switch between linear and circular polarization. The measured and simulated results are in very good agreement.

7.2 Future Work

The recommendations and suggestions for future work can be summarized as follows:
A high gain dual band antenna can be achieved using a single layer reflection-type surface based on the frequency selective surface (FSS) technology. Its configuration has a log periodic shape, and it can enhance the antenna gain at two different frequency bands. Another approach for the type of antenna is to utilize this unit cell, thereby broadening the antenna bandwidth and enhancing

the gain. A multi-layer dielectric superstrate with different dielectric constants placed directly above each other can also be used to realize a high gain dual band of FPC antenna.

The gain of a linearly-polarized SIW cavity antenna can be enhanced by utilizing a unit cell based on FSS technology to act as an FSS superstrate and cover all of the antenna slots.

References

[1] M. Sun, Z. N. Chen and X. Qing, "Gain Enhancement of 60-GHz Antipodal Tapered Slot Antenna Using Zero-Index Metamaterial,"IEEE Transactions on Antennas and Propagation, vol. 61, no. 4, pp. 1741-1746, April 2013.

[2] T. S. Rappaport et al., "Millimeter Wave Mobile Communications for 5G Cellular: It Will Work! ," IEEE Access, vol. 1, no., pp. 335-349, 2013.

[3] J. G. Andrews et al., ''What will 5G be?'' IEEE J. Sel. Areas Commun., vol. 32, no. 6, pp. 1065–1082, Jun. 2014.

[4] A. Ghosh et al., "Millimeter-Wave Enhanced Local Area Systems: A High-Data-Rate Approach for Future Wireless Networks," IEEE Journal on Selected Areas in Communications, vol. 32, no. 6, pp. 1152-1163, June 2014.

[5] F. Rusek et al., "Scaling Up MIMO: Opportunities and Challenges with Very Large Arrays," in IEEE Signal Processing Magazine, vol. 30, no. 1, pp. 40-60, Jan. 2013.

[6] K. C. Huang, D. J. Edwards, "Millimeter-Wave Antennas for Gigabit Wireless Communications," John Wiley & Sons Ltd, 2008.

[7] Jaco du Preez, Saurabh Sinha, Millimeter-Wave Antennas: Configuration and Applications, 2016.

[8] E. E. Altshuler and R. A. Marr, "A comparison of experimental and theoretical values of atmospheric absorption at the longer millimeter wavelengths," IEEE Transactions on Antennas and Propagation, vol. 36, no. 10, pp. 1471-1480, Oct. 1988.

[9] Y. Niu, Y. Li, D. Jin, L. Su, and A. V. Vasilakos, "A Survey of Millimeter Wave (mm-Wave) Communications for 5G: Opportunities and Challenges," Computer science-Networking and Internet Architecture, 2015.

[10] P. Pirinen, "A brief overview of 5G research activities," 1st International Conference on 5G for Ubiquitous Connectivity, Akaslompolo, 2014, pp. 17-22.

[11] K. Chandra, R. V. Prasad, B. Quang, and I. G. M. M. Niemegeers, "CogCell: cognitive interplay between 60 GHz picocells and 2.4/5 GHz hotspots in the 5G era," IEEE Communications Magazine, vol. 53, no. 7, pp. 118-125, July 2015.

[12] T. S. Rappaport, G. R. MacCartney, M. K. Samimi and S. Sun, "Wideband Millimeter-Wave Propagation Measurements and Channel Models for Future Wireless Communication System Design," IEEE Transactions on Communications, vol. 63, no. 9, pp. 3029-3056, Sept. 2015.

[13] T. Nakamura, A. Benjebbour, Y. Kishiyama, S. Suyama, and T. Imai, "5G radio access: Requirements, Concept and experimental trials," IEICE Trans. Commun., vol. E98-B, no.8, pp.1397-1406, Aug. 2015.

[14] S. Mattisson, "Overview of 5G requirements and future wireless networks," ESSCIRC 2017 - 43rd IEEE European Solid-State Circuits Conference, Leuven, 2017, pp. 1-6.

[15] Kei Sakaguchi, Thomas Haustein, Sergio Barbarossa, Emilio Calvanese, Antonio Clemente, Giuesppe Destino, Aamo Parssinen, Ilgyu Kim, Heesang, Chung Junhyeong Kim, et al., "Where. When, and how mm-wave is used in 5g and beyond" IEICE transaction, 2017.

[16] S. Hur *et al.*, "Proposal on Millimeter-Wave Channel Modeling for 5G Cellular System," IEEE Journal of Selected Topics in Signal Processing, vol. 10, no. 3, pp. 454-469, April 2016.

[17] G. Stuber, Principles of Mobile Communication, 3rd ed. Springer, 2011.

[18] S. Rangan, T. S. Rappaport and E. Erkip, "Millimeter-Wave Cellular Wireless Networks: Potentials and Challenges," Proceedings of the IEEE, vol. 102, no. 3, pp. 366-385, March 2014.

[19] G. Stuber, Principles of Mobile Communication, 3rd ed. Springer, 2011.

[20] R. W. Heath, N. González-Prelcic, S. Rangan, W. Roh, and A. M. Sayeed, "An Overview of Signal Processing Techniques for Millimeter Wave MIMO Systems," IEEE Journal of Selected Topics in Signal Processing, vol. 10, no. 3, pp. 436-453, April 2016.

[21] S. Long, M. McAllister and Liang Shen, "The resonant cylindrical dielectric cavity antenna," IEEE Transactions on Antennas and Propagation, vol. 31, no. 3, pp. 406-412, May 1983.

[22] Q. Lai, C. Fumeaux, W. Hong and R. Vahldieck, "60 GHz Aperture-Coupled Dielectric Resonator Antennas Fed by a Half-Mode Substrate Integrated Waveguide," IEEE Transactions on Antennas and Propagation, vol. 58, no. 6, pp. 1856-1864, June 2010.

[23] W. M. Abdel-Wahab and S. Safavi-Naeini, "Improvement of aperture coupling in SIW-fed DRA using embedded metallic posts," Proceedings of the 2012 IEEE International Symposium on Antennas and Propagation, Chicago, IL, 2012, pp. 1-2.

[24] H. W. Lai, K. M. Luk, and K. W. Leung, "Dense Dielectric Patch Antenna—A New Kind of Low-Profile Antenna Element for Wireless Communications," IEEE Transactions on Antennas and Propagation, vol. 61, no. 8, pp. 4239-4245, Aug. 2013.

[25] Y. Li and K. M. Luk, "A 60-GHz Dense Dielectric Patch Antenna Array," IEEE Transactions on Antennas and Propagation, vol. 62, no. 2, pp. 960-963, Feb. 2014.

[26] C. A. Balanis, Antenna Theory: Analysis and Design, 3rd ed. Hoboken, NJ: Wiley, 2005.

[27] Kwon TS, Lee JG, Lee JH. The gain estimation of a fabry perot cavity (FPC) antenna with finite dimension. J Electromagn Eng Sci. 2017;17(4):241-243

[28] G. V. Trentini, "Partially reflecting sheet arrays," IRE Transactions on Antennas and Propagation, vol. 4, no. 4, pp. 666-671, October 1956.

[29] S. Cai, Q. Wang, Z. Wang and Y. Zhai, "Design of an FSS Waveguide Filter at 8.05 GHz," 2008 IEEE MTT-S International Microwave Workshop Series on Art of Miniaturizing RF and Microwave Passive Components, Chengdu, 2008, pp. 173-175.

[30] F. Qin et al., "A Triband Low-Profile High-Gain Planar Antenna Using Fabry–Perot Cavity," IEEE Transactions on Antennas and Propagation, vol. 65, no. 5, pp. 2683-2688, May 2017.

[31] Y. Chen, K. Lin, H. Su, H. Lin, and T. Pu, "A high-gain directive superstrate antenna for 60-GHz applications," 2014 International Symposium on Antennas and Propagation Conference Proceedings, Kaohsiung, 2014, pp. 339-340.

[32] Y. Ma, W. Wu, Y. Yuan, W. Yuan, and N. Yuan, "A High-Selective Frequency Selective Surface with Hybrid Unit Cells," IEEE Access.

[33] K. W. Leung, W. C. Wong, K. M. Luk, and E. K. N. Yung, "Circular-polarized dielectric resonator antenna excited by dual conformal strips," Electron. Lett., vol. 36, no. 6, pp. 484–486, 2000.

[34] N. Ghassemi, W. Ke, S. Claude, Z. Xiupu, and J. Bornemann, "Low-cost and high-efficient w-band substrate integrated waveguide antenna array made of printed circuit board process," IEEE Trans. Antennas Propag, vol. 60, pp. 1648-1653, 2012.

[35] Y. Sugio, T. Makimoto, S. Nishimura, and H. Nakanishi, "analysis for gain enhancement of multiple reflection line antenna with dielectric plates" Trans. IECE, Jan. 1981, PP. 80-112.

[36] D. R. Jackson and N. G. Alexopoulos, "Gain enhancement methods for printed circuit antennas," IEEE Transactions on Antennas and Propagation 33 (9), 976–987 (1985).

[37] H. Boutayeb and A. C. Tarot, "Internally excited Fabry-Perot type cavity: power normalization and directivity evaluation," Antenna & Wireless Propagation Letters 5, 159–162 (2006).

[38] M. A. Al-Tarifi, D. E. Anagnostou, A. K. Amert, and K. W. Whites, "Bandwidth enhancement of the resonant cavity antenna by using two dielectric superstrates," IEEE Trans. Antennas Propag., vol. 61, no. 4, pp. 1898–1908, Apr. 2013.

[39] M. Thevenot, C. Cheype, A. Reineix, and B. Jecko, "Directive photonic-bandgap antennas," IEEE Transaction on Antennas and Propagation 47 (11), 2115–2122 (1999).

[40] M. Thévenot, J. Drouet, R. Chantalat, et al., Improvements for the EBG Resonator antenna, EurCap2006 (2006).

[41] R. Gardelli, M. Albani, and F. Capolino, "Array thinning by using antennas in a Fabry-Perot cavity for gain enhancement," IEEE Transactions on Antennas and Propagation 54 (7), 1979–1990 (2006).

[42] B. P. Chacko, G. Augustin, T. A. Denidni," A high-gain antenna based on zero-index metamaterial Superstrate," IEEE Antennas and Propagation Society International Symposium (APSURSI), Page(s): 122 - 123, July 2013.

[43] L. Ji, P. Qin, and Y. J. Guo, "Wideband Fabry-Perot Cavity Antenna With a Shaped Ground Plane," in *IEEE Access*, vol. 6, pp. 2291-2297, 2018.

[44] K. Kanjanasit and C. Wang, "A Wideband Resonant Cavity Antenna Assembled Using a Micromachined CPW Fed Patch Source and a Two-Layer Metamaterial Superstrate," IEEE Transactions on Components, Packaging and Manufacturing Technology.

[45] M. Akbari, S. Gupta, and A. R. Sebak, "High gain circularly-polarized Fabry-Perot dielectric resonator antenna for MMW applications," 2016 IEEE International Symposium on Antennas and Propagation (APSURSI), Fajardo, 2016, pp. 545-546.

[46] M. L. Abdelghani, H. Attia and T. A. Denidni, "Dual- and Wideband Fabry–Pérot Resonator Antenna for WLAN Applications," in *IEEE Antennas and Wireless Propagation Letters*, vol. 16, pp. 473-476, 2017.

[47] A. A. Kishk, A. Ittipiboon, Y. M. M. Antar and M. Cuhaci, "Slot excitation of the dielectric disk radiator," IEEE Transactions on Antennas and Propagation, vol. 43, no. 2, pp. 198-201, Feb. 1995.

[48] Y. Sugio, T. Makimoto, S. Nishimura, and H. Nakanishi, "analysis for gain enhancement of multiple reflection line antenna with dielectric plates" Trans. IECE, Jan. 1981, PP. 80-112.

[49] M. Thèvenot, A. Reineix, and B. Jecko, "A dielectric photonic parabolic reflector," Microwave Opt. Technol. Lett., vol. 21, no. 6, pp. 411–414, Jun. 1999.

[50] F. Zhu, Q. Lin, S. He, J. Hu, and Z. Ying, "A high directivity patch antenna using a PBG cover together with a PBG substrate," in Proc. 6th Int. Symp. Antennas, Propag. EM Theory, Nov. 2003, pp. 92–95.

[51] A. Weily, K. Esselle, T. Bird, and B. Sanders, "Dual resonator 1-D EBG antenna with slot array feed for improved radiation bandwidth," IET Microwaves, Antennas & Propagation, vol. 1, no. 1, pp. 198–203, 2007.

[52] H. Yang and N. Alexopoulos, "Gain enhancement methods for printed circuit antennas through multiple superstrates," IEEE Transactions on Antennas and Propagation, vol. 35, no. 7, pp. 860-863, July 1987.

[53] I. Ocket, A. Phommahaxay, H. A. C. Tilmans, J. B. Mills and B. Nauwelaers, "Millimeter wave micromachined cavity resonators on MCM-D: Oscillator-resonator co-design and packaging considerations," 2009 IEEE MTT-S International Microwave Symposium Digest, Boston, MA, 2009, pp.

[54] G. Marconi and C.S. Franklin, "Reflector for Use in Wireless Telegraphy and Telephony," US Patent 1,301,473, April 1919.

[55] J. Hirokawa, M. Ando and N. Goto, "Waveguide-fed parallel plate slot array antenna," IEEE Transactions on Antennas and Propagation, vol. 40, no. 2, pp. 218-223, Feb. 1992.

[56] B. A. Munk, "Frequency Selective Surfaces: Theory and Design," Wiley-Interscience, 2005.

[57] J.C. Vardaxoglou, "Frequency Selective Surfaces Analysis and Design," John Wiley, 1997.

[58] V. D. Agrawal, and F.A. Pelow, "Design of a Dischroic Cassegrain Subreflector", IEEE Trans. Antennas Propag., AP-27, no. 4, pp.466-473, July 1979.

[59] H. D. Griffiths, A. M. Vernon, and K. Milne, "Planar Phase Shifting Structures for Steerable DBS Antennas," Proc. 6th International Conference on Antennas and Propagation (ICAP 89), 1989, pp. 45-49.

[60] F. C. Seman, R. Cahill, V. F. Fusco, and G. Goussetis, "Design of a Salisbury Screen Absorber Using Frequency Selective Surfaces to Improve Bandwidth and Angular Stability Performance," IET Microw. Antennas Propag., vol. 5, no. 2, pp. 149-156, Jan. 2011.

[61] J. Romeu, and Y. Rahmat-Samii, "Fractal FSS: A Novel Dual-Band Frequency Selective Surface," IEEE Trans. Antennas and Propag. Vol. 48, no. 7, pp. 1097-1105, July 2000.

[62] T. K. Wu, \Frequency-selective surface and grid array," Wiley, New York, 1995.

[63] B.A. Munk, \Frequency-selective surfaces: Theory and design," Wiley, New York, 2000.

[64] E. A. Parker, "The Gentleman's Guide to Frequency Selective Surfaces," 17th Q.M.W Antenna Symposium, April, pp. 1–18, 1991.

[65] N. Marcuvitz, Waveguide Handbook. IET, 1951.

[66] D. Jackson and A. Oliner, "A leaky-wave analysis of the high-gain printed antenna configuration," IEEE Transaction on Antennas and Propagation, vol. 36, no. 7, pp. 905–910, July 1998.

[67] A. P. Feresidis and J. C. Vardaxoglou, "High gain planar antenna using optimized partially reflecting surfaces," IEEE Proceedings on Microwaves, Antennas and Propagation, vol. 148, no. 6, pp. 345–350, 2001.

[68] C. Cheype, C. Serier, M. Thevenot, T. Monediere, A. Reineix and B. Jecko, "An electromagnetic bandgap resonator antenna," IEEE Transactions on Antennas and Propagation, vol. 50, no. 9, pp. 1285-1290, Sept. 2002.

[69] B. A. Zeb, R. M. Hashmi, K. P. Esselle and Y. Ge, "The use of reflection and transmission models to design wideband and dual-band Fabry-Perot cavity antennas (invited paper)," 2013 International Symposium on Electromagnetic Theory, Hiroshima, 2013, pp. 1084-1087.

[70] C. A. Balanis, "Advanced Engineering Electromagnetics," Second edition, John Wiley& Sons, Inc., 2012.

[71] M. Asaadi; A. R. Sebak, "High Gain Low Profile Circularly Polarized Slotted SIW Cavity Antenna for MMW Applications," IEEE Antennas and Wireless Propagation Letters, vol.PP, no.99, pp.1-1.

[72] J. K. Plourde and Chung-Li Ren, "Application of Dielectric Resonators in Microwave Components," IEEE Transactions on Microwave Theory and Techniques, vol. 29, no. 8, pp. 754-770, Aug 1981.

[73] Y. Li and K. M. Luk, "Wideband Perforated Dense Dielectric Patch Antenna Array for Millimeter-Wave Applications," IEEE Transactions on Antennas and Propagation, vol. 63, no. 8, pp. 3780-3786, Aug. 2015.

[74] Q. Lai, G. Almpanis, C. Fumeaux, H. Benedickter, and R. Vahldieck, "Comparison of the Radiation Efficiency for the Dielectric Resonator Antenna and the Microstrip Antenna at Ka Band," IEEE Transactions on Antennas and Propagation, vol. 56, no. 11, pp. 3589-3592, Nov. 2008.

[75] A. A. Kishk, M. R. Zunoubi, and D. Kajfez, "A numerical study of a dielectric disk antenna above grounded dielectric substrate," IEEE Transactions on Antennas and Propagation, vol. 41, no. 6, pp. 813-821, June 1993.

[76] A. Foroozesh and L. Shafai, "Effects of Artificial Magnetic Conductors in the Design of Low-Profile High-Gain Planar Antennas with High-Permittivity Dielectric Superstrate," IEEE Antennas and Wireless Propagation Letters, vol. 8, pp. 10-13, 2009.

[77] O. M. Haraz, A. Elboushi, S. A. Alshebeili and A. Sebak, "Dense Dielectric Patch Array Antenna with Improved Radiation Characteristics Using EBG Ground Structure and Dielectric Superstrate for Future 5G Cellular Networks," IEEE Access, vol. 2, pp. 909-913, 2014.

[78] Z. Liu, W. Zhang, D. Fu, Y. Gu, and Z. Ge, "Broadband Fabry-Perot resonator printed antennas using FSS superstrate with dissimilar size."Microw. Opt. Technol. Lett, vol. 50, no. 6, pp. 1623-1627,2008.

[79] A. Pirhadi, H. Bahrami and J. Nasri, "Wideband High Directive Aperture Coupled Microstrip Antenna Design by Using a FSS Superstrate Layer," IEEE Transactions on Antennas and Propagation, vol. 60, no. 4, pp. 2101-2106, April 2012.

[80] H. Vettikalladi, O. Lafond and M. Himdi, "High-Efficient and High-Gain Superstrate Antenna for 60-GHz Indoor Communication," IEEE Antennas and Wireless Propagation Letters, vol. 8, no., pp. 1422-1425, 2009.

[81] J. H. Kim, C. H. Ahn and J. K. Bang, "Antenna Gain Enhancement Using a Holey Superstrate," IEEE Transactions on Antennas and Propagation, vol. 64, no. 3, pp. 1164-1167, March 2016.

[82] F. Kaymaram and L. Shafai, "Enhancement of microstrip antenna directivity using double-superstrate configurations," Canadian Journal of Electrical and Computer Engineering, vol. 32, no. 2, pp. 77-82, Spring 2007.

[83] M. A. Al-Tarifi, D. E. Anagnostou, A. K. Amert and K. W. Whites, "Bandwidth Enhancement of the Resonant Cavity Antenna by Using Two Dielectric Superstrates," IEEE Transactions on Antennas and Propagation, vol. 61, no. 4, pp. 1898-1908, April 2013.

[84] R. M. Hashmi, B. A. Zeb and K. P. Esselle, "Wideband High-Gain EBG Resonator Antennas With Small Footprints and All-Dielectric Superstructures," IEEE Transactions on Antennas and Propagation, vol. 62, no. 6, pp. 2970-2977, June 2014.

[85] K. Konstantinidis, A. P. Feresidis and P. S. Hall, "Multilayer Partially Reflective Surfaces for Broadband Fabry-Perot Cavity Antennas," IEEE Transactions on Antennas and Propagation, vol. 62, no. 7, pp. 3474-3481, July 2014.

[86] H. Attia, M. L. Abdelghani and T. A. Denidni, "Wideband and High-Gain Millimeter-Wave Antenna Based on FSS Fabry–Perot Cavity," IEEE Transactions on Antennas and Propagation, vol. 65, no. 10, pp. 5589-5594, Oct. 2017.

[87] Goel, Soni; Kamal, Ashmita; Choudhary, Priyanka," Bandwidth Enhancement Using Stacked Configuration in Microstrip Antenna Array for Millimeter Wave Applications," IUP Journal of Telecommunications. Feb2016, Vol. 8 Issue 1, p38-46. 9p.

[88] M. M. M. Ali, S. I. Shams, and A. Sebak, "Low Loss and Ultra Flat Rectangular Waveguide Harmonic Coupler," IEEE Access, vol. 6, pp. 38736-38744, 2018.

[89] L. Ji, P. Qin, and Y. J. Guo, "Wideband Fabry-Perot Cavity Antenna with a Shaped Ground Plane," IEEE Access, vol. 6, pp. 2291-2297, 2018.

[90] A. A. Kishk, H. A. Auda and B. C. Ahn, "Accurate prediction of radiation patterns of dielectric resonator antennas," Electronics Letters, vol. 23, no. 25, pp. 1374-1375, December 3, 1987.

[91] M. Asaadi, I. Afifi and A. Sebak, "High Gain and Wideband High Dense Dielectric Patch Antenna Using FSS Superstrate for Millimeter-Wave Applications," IEEE Access, vol. 6, pp. 38243-38250, 2018.

[92] A. R. Weily, L. Horvath, K. P. Esselle, B. C. Sanders and T. S. Bird, "A planar resonator antenna based on a woodpile EBG material," IEEE Transactions on Antennas and Propagation, vol. 53, no. 1, pp. 216-223, Jan. 2005.

[93] M. Asaadi and A. Sebak, "Gain and Bandwidth Enhancement of 2×2 Square Dense Dielectric Patch Antenna Array Using a Holey Superstrate," IEEE Antennas and Wireless Propagation Letters, vol. 16, pp. 1808-1811, 2017.

[94] J. B. Muldavin and G. M. Rebeiz, "Millimeter-wave tapered-slot antennas on synthesized low permittivity substrates," IEEE Transactions on Antennas and Propagation, vol. 47, no. 8, pp. 1276-1280, Aug 1999.

[95] M. Chryssomallis, "Smart antennas," IEEE Antennas Propag. Mag., vol. 42, no. 43, pp. 129–136, 2000.

[96] G. Cerri, R. D. Leo, V. M. Primiani, C. Monteverde, and P. Russo, "Design and prototyping of a switching beam disc antenna for wideband communications," IEEE Trans. Antennas Propag., vol. 54, no. 12, pp. 3721–3726, 2006.

[97] J. Kim, M. Kim, and R. Mittra, "Scan capability of Fabry Perot cavity (FPC) antennas with array feeds," in Proc. IEEE-APS, 2012, pp. 1–2.

[98] A. A. Kishk, "Enhanced gain of scanning DRA array," 2016 10th European Conference on Antennas and Propagation (EuCAP), Davos, 2016, pp. 1-3.

[99] A. Ourir, S. N. Burokur, and A. de Lustrac, "Phase-varying metamaterial for compact steerable directive antennas," Electron. Lett., vol. 43, no. 9, pp. 493–494, Apr. 2007.

[100] A. Ourir, S. N. Burokur, and A. de Lustrac, "Electronic beam steering of an active metamaterial-based directive subwavelength cavity," in Proc. 2nd Eur. Conf. Antennas Propag., Edinburgh, U.K., Nov. 2007, pp. 1–4.

[101] T. Debogovic and J. Perruisseau-Carrier, "Array-fed partially reflective surface antenna with independent scanning and beamwidth dynamic control," IEEE Trans. Antenna Propag., vol. 62, no. 1, pp. 446–449, Jan. 2014.

[102] L. Ji, Y. J. Guo, P. Qin, S. Gong, and R. Mittra, "A Reconfigurable Partially Reflective Surface (PRS) Antenna for Beam Steering," IEEE Transactions on Antennas and Propagation, vol. 63, no. 6, pp. 2387-2395, June 2015.

[103] B. P. Chacko, G. Augustin and T. A. Denidni, "Tilted-beam MPA with broad-useful bandwidth," IET Microwaves, Antennas & Propagation, vol. 11, no. 4, pp. 471-476, 18 3 2017.

[104] A. Vosoogh, P. S. Kildal and V. Vassilev, "Wideband and High-Gain Corporate-Fed Gap Waveguide Slot Array Antenna with ETSI Class II Radiation Pattern in V-Band," IEEE Transactions on Antennas and Propagation, vol. 65, no. 4, pp. 1823-1831, April 2017.

[105] A. K. Singh, M. P. Abegaonkar and S. K. Koul, "High-Gain and High-Aperture-Efficiency Cavity Resonator Antenna Using Metamaterial Superstrate," IEEE Antennas and Wireless Propagation Letters, vol. 16, pp. 2388-2391, 2017.

[106] M. J. Al-Hasan, T. A. Denidni and A. R. Sebak, "Millimeter-Wave EBG-Based Aperture-Coupled Dielectric Resonator Antenna," IEEE Transactions on Antennas and Propagation, vol. 61, no. 8, pp. 4354-4357, Aug. 2013.

[107] Y. Jia, Y. Liu, H. Wang, K. Li and S. Gong, "Low-RCS, High-Gain, and Wideband Mushroom Antenna," IEEE Antennas and Wireless Propagation Letters, vol. 14, pp. 277-280, 2015.

[108] B. P. Chacko, G. Augustin and T. A. Denidni, "FPC Antennas: C-band point-to-point communication systems," IEEE Antennas and Propagation Magazine, vol. 58, no. 1, pp. 56-64, Feb. 2016.

[109] M. Akbari, S. Gupta, M. Farahani, A. R. Sebak and T. A. Denidni, "Gain Enhancement of Circularly Polarized Dielectric Resonator Antenna Based on FSS Superstrate for MMW Applications," IEEE Transactions on Antennas and Propagation, vol. 64, no. 12, pp. 5542-5546, Dec. 2016.

[110] A. R. Weily, T. S. Bird and Y. J. Guo, "A Reconfigurable High-Gain Partially Reflecting Surface Antenna," in IEEE Transactions on Antennas and Propagation, vol. 56, no. 11, pp. 3382-3390, Nov. 2008.

[111] A. R. Weily, K. P. Esselle, T. S. Bird and B. C. Sanders, "Dual resonator 1-D EBG antenna with slot array feed for improved radiation bandwidth," IET Microwaves, Antennas & Propagation, vol. 1, no. 1, pp. 198-203, February 2007.

[112] C. Mateo-Segura, A. P. Feresidis and G. Goussetis, "Highly directive 2-D leaky wave antennas based on double-layer meta-surfaces," Proc. EuCAP, Apr. 2010, pp. 1-5.

[113] D. Abbou, T. P. Vuong, R. Touhami, F. Ferrero, D. Hamzaoui and M. C. E. Yagoub, "High-Gain Wideband Partially Reflecting Surface Antenna for 60 GHz Systems," IEEE Antennas and Wireless Propagation Letters, vol. 16, pp. 2704-2707, 2017.

[114] R. Lian, Z. Tang and Y. Yin, "Design of a Broadband Polarization-Reconfigurable Fabry–Perot Resonator Antenna," IEEE Antennas and Wireless Propagation Letters, vol. 17, no. 1, pp. 122-125, Jan. 2018.

[115] M. J. Hill, R. W. Ziolkowski, J. Papapolymerou, "A High-Q Reconfigurable Planar EBG Cavity Resonator," IEEE Microw. Wireless Compon. Lett., vol. 11, no. 6, Dec. 2001.

[116] Y. Cassivi, L. Perregrini, K. Wu, G. Conciauro, "Low-Cost and High-Q Millimeter-Wave Resonator Using Substrate Integrated Waveguide Technique," European Microwave Conference, 2002. 32nd, pp. 1-4, Oct. 2002.

[117] I. Ocket, A. Phommahaxay, H. A. C. Tilmans, J. B. Mills and B. Nauwelaers, "Millimeter wave micromachined cavity resonators on MCM-D: Oscillator-resonator co-design and packaging considerations," 2009 IEEE MTT-S International Microwave Symposium Digest, Boston, MA, 2009, pp.

[118] S. S. Sekretarov, D. M. Vavriv and L. V. Shevtsova, "Slotted Waveguide Antenna Arrays for Airborne Radars," 18-th INTERNATIONAL CONFERENCE ON MICROWAVES, RADAR AND WIRELESS COMMUNICATIONS, Vilnius, Lithuania, 2010, pp. 1-4.

[119] T.-S. Horng and N. G. Alexopoulos, "Corporate feed design for microstrip arrays," IEEE Trans. Antennas Propag., vol. 41, no. 12, pp. 1615–1624, Dec. 1993.

[120] A. Elboushi and A. Sebak, "High-gain hybrid microstrip/conical horn antenna for MMW applications," IEEE Antennas Wireless Propag. Lett., vol. 11, pp. 129–132, Jan. 2012.

[121] A. Perron, T. A. Denidni, and A.-R. Sebak, "High-gain hybrid dielectric resonator antenna for millimeter-wave applications: Design and implementation," IEEE Trans. Antennas Propag., vol. 57, no. 10, pp. 2882– 2892, Oct. 2009.

[122] Y. Lang, S. Qu, and J. Chen, "Wideband Circularly Polarized Substrate Integrated Cavity-Backed Antenna Array," IEEE Antennas and Wireless Propagation Letters, vol. 13, pp. 1513-1516, 2014.

[123] H. Sun, Y. X. Guo and Z. Wang, "60-GHz Circularly Polarized U-Slot Patch Antenna Array on LTCC," IEEE Transactions on Antennas and Propagation, vol. 61, no. 1, pp. 430-435, Jan. 2013.

[124] A. B. Guntupalli and K. Wu, "60-GHz Circularly Polarized Antenna Array Made in Low-Cost Fabrication Process," IEEE Antennas and Wireless Propagation Letters, vol. 13, no. , pp. 864-867, 2014.

[125] T. Zhang, Y. Zhang, L. Cao, W. Hong, and K. Wu, "Single-Layer Wideband Circularly Polarized Patch Antennas for Q-Band Applications," IEEE Transactions on Antennas and Propagation, vol. 63, no. 1, pp. 409-414, Jan. 2015.

[126] Y. Li, Z. N. Chen, X. Qing, Z. Zhang, J. Xu, and Z. Feng, "Axial Ratio Bandwidth Enhancement of 60-GHz Substrate Integrated Waveguide-Fed Circularly Polarized LTCC Antenna Array," IEEE Transactions on Antennas and Propagation, vol. 60, no. 10, pp. 4619-4626, Oct. 2012.

[127] H. S. Lee and M. S. Lee, "A study on the enhancement of gain and axial ratio bandwidth of the multilayer CP-DRA," Circuits and Systems for Communications (ECCSC), 2010 5th European Conference on, Belgrade, 2010, pp. 248-252.

[128] C. Liu, Y. X. Guo, X. Bao and S. Q. Xiao, "60-GHz LTCC Integrated Circularly Polarized Helical Antenna Array," IEEE Transactions on Antennas and Propagation, vol. 60, no. 3, pp. 1329-1335, March 2012.

[129] J. W. Baik, T. H. Lee, S. Pyo, S. M. Han, J. Jeong, and Y. S. Kim, "Broadband Circularly Polarized Crossed Dipole With Parasitic Loop Resonators and Its Arrays," IEEE Transactions on Antennas and Propagation, vol. 59, no. 1, pp. 80-88, Jan. 2011.

[130] Y. Lang, S. W. Qu, and J. X. Chen, "Wideband Circularly Polarized Substrate Integrated Cavity-Backed Antenna Array," IEEE Antennas and Wireless Propagation Letters, vol. 13, no., pp. 1513-1516, 2014.

[131] A. Elboushi, O. M. Haraz, and A. Sebak, "Circularly-polarized SIW slot antenna for MMW applications," 2013 IEEE Antennas and Propagation Society International Symposium (APSURSI), Orlando, FL, 2013, pp. 648-649.

[132] K. S. Min, J. Hirokawa, K. Sakurai, M. Ando, and N. Goto, "Single-layer dipole array for linear-to-circular polarisation conversion of slotted waveguide array," IEE Proceedings - Microwaves, Antennas and Propagation, vol. 143, no. 3, pp. 211-216, Jun 1996.

[133] Wangwang Han; Feng Yang; Jun Ouyang; Peng Yang, "Low-Cost Wideband and High-Gain Slotted Cavity Antenna Using High-Order Modes for Millimeter-Wave Application," Antennas and Propagation, IEEE Transactions on, vol.63, no.11, pp.4624-4631, Nov. 2015.

[134] A. Ip and D. R. Jackson, "Radiation from cylindrical leaky waves," IEEE Trans. Antennas Propag., vol. 38, pp. 482-488, Apr. 1990.

[135] Taek-Sun Kwon, Jae-Gon Lee, Jeong-Hae Lee," The Gain Estimation of a Fabry-Perot Cavity (FPC) Antenna with a Finite Dimension," Journal of Electromagnetic Engineering and Science 2017;17(4):241-243.

[136] T. Zhao, D. R. Jackson, and J. T. Williams, "2-D periodic leaky-wave Antennas-part II: slot design," IEEE Trans. Antennas Propag., vol. 53, pp. 3515-3524, Nov. 2005.

[137] D. R. Jackson, A. A. Oliner, and A. Ip, "Leaky-wave propagation and radiation for a narrow beam multiple-layer structure," IEEE Trans. Antennas Propag., vol. 41, pp. 344-348, Mar. 1993.

[138] J. B. Muldavin and G. M. Rebeiz, "Millimeter-wave tapered-slot antennas on synthesized low permittivity substrates," IEEE Transactions on Antennas and Propagation, vol. 47, no. 8, pp. 1276-1280, Aug 1999.

[139] A. Elboushi, O. Haraz, and A. Sebak, High Gain Circularly Polarized Slot-Coupled Antenna for Millimeter Wave Applications, Microwave Opt Technol Lett 56 (2014) 2522-2526.

[140] S. Wang, A. P. Feresidis, G. Goussetis and J. C. Vardaxoglou, "High-gain subwavelength resonant cavity antennas based on metamaterial ground planes," IEE Proceedings - Microwaves, Antennas and Propagation, vol. 153, no. 1, pp. 1-6, 6 Feb. 2006.

[141] H. D. Hristov, Fresnel Zones in Wireless Links, Zone Plate Lenses and Antennas. London, U.K.: Artech House, 2000.

[142] A. Foroozesh and L. Shafai, "Investigation Into the Effects of the Patch-Type FSS Superstrate on the High-Gain Cavity Resonance Antenna Design," IEEE Transactions on Antennas and Propagation, vol. 58, no. 2, pp. 258-270, Feb. 2010.

[143] K. Konstantinidis, A. P. Feresidis and P. S. Hall, "Broadband Sub-Wavelength Profile High-Gain Antennas Based on Multi-Layer Metasurfaces," IEEE Transactions on Antennas and Propagation, vol. 63, no. 1, pp. 423-427, Jan. 2015.

[144] Ashraf, N.; Haraz, O.; Ashraf, M.A.; Alshebeili, S., "28/38-GHz dual band millimeter wave SIW array antenna with EBG structures for 5G applications," in Information and Communication Technology Research (ICTRC), 2015 International Conference on, vol., no., pp.5-8, 17-19 May 2015.

[145] Guo Qing Luo; Zhi Fang Hu; Lin Xi Dong; Ling Ling Sun, "Planar Slot Antenna Backed by Substrate Integrated Waveguide Cavity," Antennas and Wireless Propagation Letters, IEEE, vol.7, no., pp.236-239, 2008.

[146] Bozzi, M.; Georgiadis, A.; Wu, K., "Review of substrate-integrated waveguide circuits and antennas," in Microwaves, Antennas & Propagation, IET, vol.5, no.8, pp.909-920, June 6 2011.

[147] Zhangfeng Li; Haitao Xu; Guoqiang Zhao; Yafen Ge; Houjun Sun, "A substrate integrated waveguide slot array antenna at Ka-band," Microwave and Millimeter Wave Technology (ICMMT), 2012 International Conference on, vol.3, no., pp.1-4, 5-8 May 2012.

[148] Elboushi, A.; Sebak, A.R., "High gain hybrid DRA / horn antenna for MMW applications," in Antennas and Propagation Society International Symposium (APSURSI), 2014 IEEE, vol., no., pp.1968-1969.

[149] Elboushi, A.; Haraz, O.M.; Sebak, A.; Denidni, T., "A new circularly polarized high gain DRA millimeter-wave antenna," Antennas and Propagation Society International Symposium (APSURSI), 2010 IEEE, vol., no., pp.1-4, 11-17 July 2010.